UC Riverside

UC Riverside Electronic Theses and Dissertations

Title

Benchmark Dose-Response Modeling Approaches to Integrate Toxicogenomics Into Quantitative Risk Assessment

Permalink

https://escholarship.org/uc/item/3w1833xx

Author

Bhat, Virunya S.

Publication Date

2014

Peer reviewed|Thesis/dissertation

eScholarship.org Powered by the California Digital Library
University of California

UNIVERSITY OF CALIFORNIA
RIVERSIDE

Benchmark Dose-Response Modeling Approaches to Integrate Toxicogenomics Into Quantitative Risk Assessment

A Dissertation submitted in partial satisfaction
of the requirements for the degree of

Doctor of Philosophy

in

Environmental Toxicology

by

Virunya S. Bhat

June 2014

Dissertation Committee:
Dr. David Eastmond, Chairperson
Dr. Jay Gan
Dr. Carl Cranor

Copyright by
Virunya S. Bhat
2014

The Dissertation of Virunya S. Bhat is approved by

_____

_____

_____

Committee Chairperson

University of California, Riverside

Acknowledgements

This journey, in ways unimaginable and oftentimes surreal, has spanned two decades. Reminiscent of risk assessment, filled with uncertainty and risk, I've fortunately been aided by a countless contingency of family, friends and mentors that never doubted, but instead helped pave the way. Your unwavering love, encouragement, and wisdom have meant the world to me and carried me through. Words could never express how proud, honored and eternally grateful I am to journey onward with all of you.

In this dissertation, I am grateful for the expertise from the co-authors listed in each publication who contributed to the research that forms Chapters 1 and 2. *Chapter 1 is a pre-copy-editing, author-produced version of an article accepted for publication in* Toxicological Sciences *following peer review. The definitive publisher-authenticated version* **Virunya S. Bhat, Susan D. Hester, Stephen Nesnow, and David A. Eastmond. Concordance of Transcriptional and Apical Benchmark Dose Levels for Conazole-Induced Liver Effects in Mice *Toxicol. Sci. (2013) 136 (1): 205-215*** *is available online at: http://toxsci.oxfordjournals.org/content/136/1/205.abstract?sid=85614fb0-9b71-4039-a198-37717a848005*.

Chapter 2 is a pre-copy-editing, author-produced version of an article accepted for publication in Toxicological Sciences *following peer review. The definitive publisher-*

authenticated version **David R. Geter, Virunya S. Bhat, B. Bhaskar Gollapudi, Radkakrishna Sura, and Susan D. Hester. Dose-Response Modeling of Early Molecular and Cellular Key Events in the CAR-Mediated Hepatocarcinogenesis Pathway** ***Toxicol. Sci. (2014) 138 (2): 425-445.*** *is available online at:* http://toxsci.oxfordjournals.org/content/138/2/425.abstract

For the diuron research that forms Chapter 3 of this dissertation, I am grateful for the expertise and contributions from Drs. Susan Hester, Charles Wood, João Lauro V. de Camargo, and David Eastmond.

Dedication

To Kiran and Ravi

and

Happy Birthday Neel and Deven

ABSTRACT OF THE DISSERTATION

Benchmark Dose-Response Modeling Approaches to Integrate Toxicogenomics Into Quantitative Risk Assessment

by

Virunya S. Bhat

Doctor of Philosophy, Graduate Program in Environmental Toxicology
University of California, Riverside, June 2014
Dr. David A. Eastmond, Chairperson

The 21st century vision for toxicity testing and risk assessment is to become more efficient at evaluating a broader range of chemicals with minimal animal testing. The objective of this research was to determine if short-term global gene expression profiling can be used to inform potency and chemical mode of action (MOA) determinations and thus collectively serve as a strategy to prioritize future or data-poor chemicals for further evaluation. Dose-response modeling was used to estimate low-dose potency for activation or repression of key genes and pathways, and these transcriptional benchmark dose (BMD_T) estimates were compared to benchmark dose estimates for more traditional toxicological (i.e., apical) responses (BMD_A) at the cellular or tissue level which were observed after the same exposure duration. These BMD_T and BMD_A were also compared to BMD_A for the ultimate adverse outcome that might traditionally serve as the basis of

quantitative risk assessment. The case studies included (1) liver gene expression at 30 days for conazole antifungal agents, some of which are hepatocarcinogens in mice, (2) liver gene expression at 2 and 7 days for phenobarbital, a prototype nongenotoxic rodent hepatocarcinogen that activates the constitutive androstane receptor (CAR), and (3) urinary bladder gene expression at 7 days and 20 weeks for diuron, a substituted urea pesticide associated with urinary bladder cytotoxicity and tumorigenesis in rats. BMD_T and BMD_A estimates are particularly useful in informing threshold dose-response and risk assessment approaches for nongenotoxic carcinogens. Our studies showed that BMD_T estimates for key genes and pathways were highly concordant and thus phenotypically anchored to BMD_A for target tissue responses observed after the same exposure duration. Our short-term BMD_T were also consistent with potency estimates for the tumorigenic outcome or precursor key events such as hyperplasia. In conclusion, this research demonstrated the utility of short-term global gene expression profiling for informing potency with respect to MOA determinations and quantitative risk assessment of long-term exposures. Further, these case studies encompassed multiple rodent species, target tissues, MOA, and exposure durations ranging from 2 days to 20 weeks, thus demonstrating the potential utility of this approach as a chemical testing and prioritization strategy.

TABLE OF CONTENTS

ABSTRACT OF THE DISSERTATION vii

TABLE OF CONTENTS ix

List of Figures xi

List of Tables xii

INTRODUCTION 1

CHAPTER 1 10

Abstract 10

Introduction 12

Materials and Methods 15

Results 21

Discussion 27

Figures and Tables 35

CHAPTER 2 43

Abstract 43

Introduction 45

Materials and Methods 47

Results 50

Discussion 55

Figures and Tables 60

CHAPTER 3 64
Abstract 64
Introduction 66
Materials and Methods 69
Results 77
Discussion 86
Figures and Tables 92
GENERAL CONCLUSIONS 101
REFERENCES 105
Appendix A: Chapter 1 Supplementary Data 120
Appendix B: Chapter 2 Supplementary Data 131
Appendix C: Chapter 3 Supplementary Data 162

List of Figures

Figure 1.1. Range of transcriptional benchmark dose estimates.....35

Figure 1.2. Direct concordance of benchmark dose estimates for Cyp2b10 gene transcription and protein measurements at 30 days.....36

Figure 1.3. 30-d transcriptional benchmark dose estimates for some genes mirrored the tumorigenic potency gradient.....37

Figure 2.1. Most significant cellular pathways at 2 days according to sex.....60

Figure 2.2. Range of transcriptional BMD levels (mg/kg-day) for selected pathways significantly altered in both sexes at 2 days.....61

Figure 3.1. Apical benchmark dose levels in urinary bladder of male rats fed diuron for 20 weeks.....92

Figure 3.2. Range of pathway transcriptional benchmark dose levels (BMD_T) in the urinary bladder of male rats fed diuron for 20 weeks.....93

Figure 3.3. Range of pathway transcriptional benchmark dose levels (BMD_T) in the urinary bladder of male rats fed diuron for 7 days.....94

List of Tables

Table 1.1. Dose-responsive probe sets and their associated pathways at 30 days a 38

Table 1.2. Direct gene (transcriptional) and apical BMDL dose-response concordance at 30 days [a] 39

Table 1.3. 30-day transcriptional and 30-day apical benchmark dose estimates 40

Table 1.4. Liver tumor incidence used for benchmark dose modeling 41

Table 1.5. Comparison of 30-day and chronic benchmark dose estimates.....42

Table 2.1. Pathway-level transcriptional benchmark dose estimates in male and female CD-1 mice exposed to phenobarbital in the diet for 2 or 7 days[1] 62

Table 2.2. Benchmark dose estimates for apical and biomarker endpoints in male and female CD-1 mice exposed to phenobarbital in the diet for 2 or 7 days. 63

Table 3.1. Urothelial lesion incidence in male rats considered for benchmark dose modeling [1] 95

Table 3.2. Apical benchmark dose (BMD_A) results in the urinary bladder at 20 weeks and 2 years 96

Table 3.3. Most significant canonical pathways at 20 weeks 97

Table 3.4 Pathway transcriptional benchmark dose summary at 20 weeks.....98

Table 3.5. Most significant canonical pathways at 7 days.....99

Table 3.6. Pathway transcriptional benchmark dose summary at 7 days 100

Table A.1. Normalized fold change (FC) in signal intensity with increasing dose for the 48 dose-responsive probes. [a] 120

Table A.2. Transcriptional benchmark dose estimates ($BMDL_T$) for the 48 dose-responsive probes[a] 127
Table A.3. Best-fit models for increased mean relative liver weight at 30 days 130
Table B.1. Xenobiotic metabolism pathway transcriptional benchmark dose summary in male mice at 2 and 7 days 131
Table B.2. Xenobiotic metabolism pathway transcriptional benchmark dose summary in female mice at 2 and 7 days 134
Table B.3. PXR/RXR pathway transcriptional benchmark dose summary in male mice at 2 and 7 days.....137
Table B.4. PXR/RXR pathway transcriptional benchmark dose summary in female mice at 2 and 7 days 139
Table B.5. Protein ubiquitination pathway transcriptional benchmark dose summary in male mice at 2 and 7 days 141
Table B.6. Protein ubiquitination pathway transcriptional benchmark dose summary in female mice at 2 and 7 days 144
Table B.7. Eif2 signaling pathway transcriptional benchmark dose summary in male mice at 2 and 7 days 148
Table B.8. Eif2 signaling pathway transcriptional benchmark dose summary in female mice at 2 and 7 days 150
Table B.9. Cell-cycle control of chromosomal replication pathway transcriptional benchmark dose summary in male mice at 2 and 7 days 152

Table B.10. Cell-cycle control of chromosomal replication pathway transcriptional benchmark dose summary in female mice at 2 and 7 days.....153
Table B.11. Role of Brca1 in DNA damage response pathway transcriptional benchmark dose summary in male mice at 2 and 7 days.....154
Table B.12. Role of Brca1 in DNA damage response pathway transcriptional benchmark dose summary in female mice at 2 and 7 days.....155
Table B.13. Cell-cycle: G2/M DNA damage checkpoint regulation pathway transcriptional benchmark dose summary in male mice at 2 and 7 days 156
Table B.14. Cell-cycle: G2/M DNA damage checkpoint regulation pathway transcriptional benchmark dose summary in female mice at 2 and 7 days.....157
Table B.15. Mitotic roles of polo-like kinases pathway transcriptional benchmark dose summary in male mice at 2 and 7 days.....158
Table B.16. Mitotic roles of polo-like kinases pathway transcriptional benchmark dose summary in female mice at 2 and 7 days.....159
Table B.17. Glutathione-mediated detoxification pathway transcriptional benchmark dose summary in male mice at 2 and 7 days.....160
Table B.18. Glutathione-mediated detoxification pathway transcriptional benchmark dose summary in female mice at 2 and 7 days.....161
Table C.1. Aryl hydrocarbon receptor (AhR) signaling pathway transcriptional benchmark dose summary in male rat bladder at 20 weeks.....162

Table C.2. Glutathione-mediated detoxification pathway transcriptional benchmark dose summary in male rat bladder at 20 weeks.....164
Table C.3. Nrf2-mediated oxidative stress response pathway transcriptional benchmark dose summary in male rat bladder at 20 weeks.....165
Table C.4. Xenobiotic metabolism pathway transcriptional benchmark dose summary in male rat bladder at 20 weeks.....167
Table C.5. CD28 signaling in T-helper cells pathway transcriptional benchmark dose summary in male rat bladder at 20weeks.....169
Table C.6. Clathrin mediated endocytosis signaling pathway transcriptional benchmark dose summary in male rat bladder at 20 weeks.....170
Table C.7. LPS/IL-1 mediated inhibition of RXR function pathway transcriptional benchmark dose summary in male rat bladder at 20 weeks.....171
Table C.8. Calcium-induced T lymphocyte apoptosis pathway transcriptional benchmark dose summary in male rat bladder at 20 weeks.....172
Table C.9. Integrin signaling pathway transcriptional benchmark dose summary in male rat bladder at 20 weeks 173
Table C.10. Nur77 signaling in T lymphocytes pathway transcriptional benchmark dose summary in male rat bladder at 20 weeks.....174
Table C.11. Inhibition of matrix metalloprotease pathway transcriptional benchmark dose summary in male rat bladder at 7 days 175

Table C.12. Nrf2-mediated oxidative stress pathway transcriptional benchmark dose summary in male rat bladder at 7 days 176
Table C.13. Hepatic fibrosis/stellate cell activation pathway transcriptional benchmark dose summary in male rat bladder at 7 days 178
Table C.14. VDR/RXR activation pathway transcriptional benchmark dose summary in male rat bladder at 7 days 180
Table C.15. Xenobiotic metabolism pathway transcriptional benchmark dose summary in male rat bladder at 7 days 181
Table C.16. Aryl-hydrocarbon signaling pathway transcriptional benchmark dose summary in male rat bladder at 7 days 183
Table C.17. Leukocyte extravasation pathway transcriptional benchmark dose summary in male rat bladder at 7 days 185
Table C.18. Acute phase response signaling pathway transcriptional benchmark dose summary in male rat bladder at 7 days 187
Table C.19. LPS/IL-1-mediated inhibition of RXR function pathway transcriptional benchmark dose summary in male rat bladder at 7 days 189
Table C.20. Atherosclerosis signaling pathway transcriptional benchmark dose summary in male rat bladder at 7 days 191
Table C.21. Glutathione-mediated detoxification pathway transcriptional benchmark dose summary in male rat bladder at 7 days 192

INTRODUCTION

The 21st century vision for toxicity testing and risk assessment is to become more efficient at evaluating a broader range of chemicals with minimal animal testing. Toxicological characterization of the approximately 80,000 chemicals in commerce using the traditional battery of toxicology studies, such as the 2-year rodent bioassay for predicting carcinogenic potential, is not economically or technologically feasible in the foreseeable future (NRC, 2007a). A chronic bioassay requires 5 years to plan, conduct, and evaluate; 860 animals; and $2–$4 million per chemical. As a result, the gold standard National Toxicology Program has conducted an average of 12 bioassays per year over the past several decades (Manuppello and Willett, 2008), resulting in approximately 580 tested chemicals to date (NTP, 2013). Coincidentally, this approximates the number of quantitative human health risk assessments (~540) available through the U.S. Environmental Protection Agency's Integrated Risk Information System (IRIS) (U.S. EPA, 2014). The backlog of untested chemicals precludes a basis for their possible regulation or for limiting their potential for human or environmental exposure. While synthetic chemicals are essential to modern life, there are limited tools available to make sustainable decisions that reduce the environmental and societal impact of chemicals while maximizing their economic value (U.S. EPA, 2011a). From a strategic and tactical viewpoint, new risk assessment approaches that integrate existing knowledge with emerging and novel

technologies will advance testing strategies and improve the utility and predictability of risk assessment methods (Dellarco *et al.*, 2010).

A series of reports by the National Academies of Sciences (NRC, 2007a,b, 2009) outlined a strategy for less reliance on animal testing and greater efficiency in risk assessment by adopting newer toxicogenomic approaches. Since gene expression changes can precede clinical or phenotypically-observable changes (i.e. apical effects), gene expression signatures after short-term chemical exposure may inform or predict adverse effects of longer-term exposures. Risk assessment toxicologists recognize that embracing these modern technologies could better serve societal public health goals, but the precedence in doing so has to date been largely qualitative in nature. Some mode of action or chemical class-based examples of the use of toxicogenomic data in risk assessment include discerning rodent liver or lung carcinogens from non-carcinogens (Auerbach *et al.*, 2010; Ellinger-Ziegelbauer *et al.*, 2008; Thomas *et al.*, 2007a), phenobarbital-like hepatocarcinogens from peroxisome proliferators (Hamadeh *et al.*, 2002a,b); and genotoxic from nongenotoxic rodent hepatocarcinogens (Fielden *et al.*, 2011; Mathijs *et al.*, 2010; Waters *et al.*, 2010). These methods are useful as initial screening or prioritization tools and to identify chemical mode of action (MOA) but offer limited insight of the relative potencies of individual chemicals and thus cannot serve as the basis for quantitative risk assessment or derivation of acceptable exposure levels. When used in conjunction with dose-response information, genomic data can also inform relative

potency for agents acting through a particular MOA. Some examples of chemical class-based potency estimates based on gene expression data include the 50% effective dose or concentration (ED_{50} or EC_{50}) for aryl hydrocarbon receptor activation by dioxin-like compounds (Kopec *et al.*, 2010) or for phthalate-induced reproductive or developmental toxicity (Hannas *et al.*, 2012; Schulpen *et al.*, 2014). There are also a multitude of chemical-specific examples of low-dose potency estimates based on transcriptional responses such as BMD_T estimates for activation or repression of key genes and pathways associated with exposure to arsenic, carbon black nanoparticles, chloroprene, dioxin, and furan (Bourdon *et al.*, 2013; Jackson *et al.*, 2014; Rowlands *et al.*, 2013; Thomas *et al.*, 2013; Yaeger *et al.*, 2013).

Quantitative risk assessment, on the other hand, uses knowledge of dose-response relationships for a sensitive adverse or "critical" effect to calculate an acceptable exposure level, such as mg/kg-day in food, mg/L in drinking water, or ppm in air. The point on the dose-response curve, usually extrapolated from the low-dose region, that serves as the basis of this risk calculation is termed the Point-of-Departure or POD (U.S. EPA, 2005; 2011b). The preferred approach to estimate a POD is to use a dose-response modeling approach such as Benchmark Dose (U.S. EPA, 2002, 2005; 2012; 2013) since it considers the entire range of the experimental data as opposed to traditional no-observed adverse effect level (NOAEL) or lowest observed adverse effect level (LOAEL) values, which are only one of the experimental dose levels, can be influenced by sample size and dose-spacing, and do

not take into consideration the slope or shape of the dose-response curve (Davis *et al.*, 2011; Thomas *et al.*, 2007b; U.S. EPA, 2012). Benchmark dose modeling involves fitting the dose-response data to a series of mathematic models to estimate the benchmark dose (BMD), which is the central tendency for the dose at which the response is elevated above background (i.e. controls) and its associated 95% lower confidence limit on the benchmark dose (BMDL).

Most quantitative risk assessments, whether for cancer or non-cancer effects, require a POD for subsequent estimation of safe or acceptable lifetime exposure levels, such as an oral or inhalation cancer slope factor, oral Reference Dose (RfD), or inhalation Reference Concentration (RfC) (U.S. EPA, 2002, 2005). Independent of a regulatory purpose, a low-dose POD is also a measure of potency that allows hazard ranking of different agents for a specific health effect (U.S. EPA, 2005). Identification of the critical effect from which the POD is estimated is facilitated by knowledge of the chemical's mode or mechanism of action and the sequence of key cellular or molecular events that, if perturbed, lead to the critical effect (U.S. EPA, 2002, 2005). Thus, adopting newer toxicogenomic data, particularly after short-term exposures, for quantitative risk assessment of chronic exposure will require dose-response and time-course information for key molecular events and knowledge of which gene expression changes quantitatively relate to phenotypically-observable toxicity endpoints that have traditionally served as the basis of chemical regulation (Ankley *et al.*, 2010; Boverhof and Zacharewski, 2006;

Edwards and Preston, 2008; Keller *et al.*, 2012; Paules, 2003; Thomas *et al.*, 2007b, 2009, 2011, 2012). Genomic signatures and predictive profiles are time-sensitive (Boverhof and Zacharewski, 2006; Paules, 2003), thus time-course and progression of gene expression changes will be as critical a consideration as dose-response for incorporating toxicogenomic data into quantitative risk assessment.

Whole-genome microarray methods provide both a discovery engine for identifying chemical MOA and an information base for MOA-based risk assessment (Edwards and Preston, 2008). There is particular interest in the use of toxicogenomic data to replace or augment dose–response assessment based on traditional apical endpoints (Chiu *et al.*, 2013). Adapted from the source code of traditional Benchmark Dose software, BMDExpress (Thomas *et al.*, 2007b, Yang *et al.*, 2007) software can accommodate whole-genome microarray data to conduct probe-level dose-response modeling in a manner analogous to traditional benchmark dose modeling of apical endpoints.

The objective of this research was to use quantitative dose-response modeling to generate low-dose transcriptional (BMD_T) and apical benchmark dose (BMD_A) levels after short-term (≤30 d) or intermediate (20 weeks) exposure to chemical agents. These BMD_T and BMD_A estimates, particularly when interpreted in conjunction, can inform potency, allow for an examination of key event concordance across dose and time, and contribute to the weight of evidence for the proposed MOA for adverse outcomes of chronic exposure.

A case study approach was selected to encompass multiple laboratory animal species (rats and mice), multiple target tissues (liver and urinary bladder) and multiple short-term exposure durations (from 2 days to 20 weeks) in order to demonstrate the broad utility of the approach. Further, the chemical agents are considered nongenotoxic carcinogens, with PB being a prototype. For nongenotoxic carcinogens, a threshold dose-response approach can be employed in quantitative cancer risk assessment when supported by MOA information (Boobis *et al.*, 2006) based on the assumption that the adverse outcome (i.e. cancer) will not occur if exposure concentrations are below levels that do not alter tumorgenic key events. When consistent with apical effects, transcriptional changes in genes and pathways can also serve as quantitative 'bioindicators' of treatment-related adverse responses (Preston, 2002). Thus, our BMD_T and BMD_A estimates are particularly useful in informing threshold dose-response approaches for nongenotoxic carcinogens.

The 3 case studies included:

(1) conazole antifungal agents – some of which are hepatocarcinogens in laboratory mice but not rats

(2) phenobarbital (PB) - a prototype constitutive androstane receptor (CAR) agonist and nongenotoxic rodent (rat and mouse) hepatocarcinogen

(3) diuron- a substituted urea herbicide associated with urinary bladder carcinogenesis in rats belied to act via a cytotoxicity-mediated MOA

Distinguishing a rodent liver tumorigen from a non-tumorigen (without long-term testing), or more so, a PB-like mode of action for liver tumors that has limited relevance to human health from other modes of chemical-specific toxicity or tumorigenicity is a risk assessment challenge that hinders efficient regulatory decisions. A number of toxicity studies with conazole pesticides have included liver gene expression and traditional (i.e. apical) toxicity endpoints to further assess mode of action and to compare to the prototypical nongenotoxic CAR agonist, PB (Allen *et al.*, 2006; Bruno *et al.*, 2009; Chen *et al.*, 2008, 2009; Goetz *et al.*, 2006; Hester *et al.*, 2006, 2012; Nesnow *et al.*, 2009, 2011a,b; Ortiz *et al.*, 2010; Peffer *et al.*, 2007; Ross and Leavitt, 2010; Ross *et al.*, 2009, 2010; Sun *et al.*, 2005; Ward *et al.*, 2006; Wolf *et al.*, 2006).

The MOA for conazole-induced hepatocellular tumors in mice is thought to be due to a non-DNA-reactive (i.e. nongenotoxic) MOA, considering the weight-of-evidence for negative *in vivo* and *in vitro* genotoxicity (Allen *et al.*, 2006; Chen *et al.*, 2009; Dewhurst and Dellarco, 2004; Nesnow, 2012; Peffer, 2011; U.S. EPA, 2006a,b). Beginning with the molecular initiating (i.e. first key) event of CAR activation, the sequence of key events has been proposed to involve hepatocyte hypertrophy, increased all-trans retinoic acid metabolism/decreased hepatic retinoic acid levels, oxidative stress, induction of mutations, altered cholesterol biosynthesis/metabolism through inhibition of Cyp51, increase in hepatic mevalonic acid levels, increased cell proliferation, suppression of apoptosis, and ultimately tumor induction (U.S. EPA, 2011c).

Phenobarbital (PB) is a widely-used sedative and anti-epileptic drug and a nongenotoxic and prototypical CAR agonist associated with liver tumors in rodents but not humans (Elcombe *et al.*, 2014; Holsapple *et al.*, 2006). The key events include CAR activation commonly measured by altered CAR-specific gene expression, increased hepatocellular proliferation, formation of altered hepatic foci, and ultimately liver tumors. Altered epigenetic changes, induction of hepatic Cyp2b enzymes, liver hypertrophy, and decreased apoptosis have been identified as associative events (Elcombe *et al.*, 2014).

Recognizing that the previous conazole and phenobarbital case studies encompassed liver gene expression in mice, rat urinary bladder tumorigenesis associated with diuron exposure was selected as the third case study to illustrate that a BMD_T and BMD_A concordance analysis can be applied to and inform the risk assessment of other animal species and target tissues as well. The key events in diuron-induced urinary bladder tumorigenesis are proposed to involve metabolic activation to toxic metabolites, mainly N-(3,4-dichlorophenyl) urea (DCPU), which are excreted and concentrated in the urine, leading to cytotoxicity, involving urothelial cell degeneration, necrosis, and cellular exfoliation, followed by sustained regenerative cell proliferation, urothelial hyperplasia, and eventually tumors (Da Rocha *et al.*, 2014).

Thus, the overall objective of this research was to determine whether BMD_T and BMD_A estimates after shorter-term exposures can inform potency and temporality for early

key events in a proposed chemical MOA. BMD_T and BMD_A estimates can also help characterize the magnitude of transcriptomic-to-phenotypic uncertainty. Each of these elements contributes to the weight-of-evidence for the proposed MOA and also has the potential to improve the efficiency of quantitative risk assessments of long-term chemical exposures.

CHAPTER 1

CONCORDANCE OF TRANSCRIPTIONAL AND APICAL BENCHMARK DOSE LEVELS FOR CONAZOLE-INDUCED LIVER EFFECTS IN MICE

Abstract

The ability to anchor chemical class-based gene expression changes to phenotypic lesions and to describe these changes as a function of dose and time informs mode of action determinations and improves quantitative risk assessments. Previous global expression profiling identified a 330-probe cluster differentially expressed and commonly responsive to 3 hepatotumorigenic conazoles (cyproconazole, epoxiconazole, propiconazole) at 30 days. Extended to 2 more conazoles (triadimefon and myclobutanil), the present assessment encompasses 4 tumorigenic and 1 non-tumorigenic conazole. Transcriptional benchmark dose levels ($BMDL_T$) were estimated for a subset of the cluster with dose-responsive behavior and a ≥ 5-fold increase or decrease in signal intensity at the highest dose. These genes primarily encompassed CAR/RXR activation, P450 metabolism, liver hypertrophy – glutathione depletion, LPS/IL-1 mediated inhibition of RXR, and NRF2-mediated oxidative stress pathways. Median $BMDL_T$ estimates from the subset were concordant (within a factor of 2.4) with apical benchmark doses ($BMDL_A$) for increased liver weight at 30 days for the 5 conazoles. The 30-day median $BMDL_T$ estimates were within one-half order of magnitude of the chronic $BMDL_A$ for hepatocellular tumors. Potency differences seen in the dose-responsive transcription of certain Phase II

metabolism, bile acid detoxification, and lipid oxidation genes mirrored each conazole's tumorigenic potency. The 30-day $BMDL_T$ corresponded to tumorigenic potency on a mg/kg-day basis with cyproconazole > epoxiconazole > propiconazole > triadimefon > myclobutanil (non-tumorigenic). These results support the utility of measuring short-term gene expression changes to inform quantitative risk assessments from long-term exposures.

Introduction

Toxicological characterization of the approximately 80,000 chemicals in commerce using the traditional battery of toxicology studies, including the rodent bioassay for predicting carcinogenicity, is not economically or technologically feasible (NRC, 2007a). A chronic bioassay requires up to 5 years and $2–$4 million per chemical (Manuppello and Willett, 2008). From a tactical standpoint, risk assessment approaches that integrate existing knowledge with emerging technologies will advance testing strategies, improve the utility and predictability of risk assessment methods, and reduce the environmental and human health impact of chemicals while maximizing their economic value (Dellarco *et al.*, 2010; U.S. EPA, 2011a).

The National Academies of Sciences (NRC, 2007a,b, 2009) proposed a strategy for reduced reliance on animal testing and greater efficiency in risk assessment by adopting newer toxicogenomic approaches. Since molecular changes precede clinical or phenotypic (i.e. apical) effects, genomic changes after short-term chemical exposure may inform longer-term effects at lower, more environmentally relevant exposures. To date, the application of more modern technologies has been largely qualitative, such as discerning rodent liver or lung carcinogens from non-carcinogens (Auerbach *et al.*, 2010; Ellinger-Ziegelbauer *et al.*, 2008; Thomas *et al.*, 2007a); phenobarbital-like from peroxisome proliferator hepatocarcinogens (Hamadeh *et al.*, 2002); and genotoxic from nongenotoxic hepatocarcinogens (Fielden *et al.*, 2011). These methods are useful screening and

prioritization tools and can also inform chemical mode of action (MOA) determinations used to assess human health relevance. When used in conjunction with dose-response information, genomic data can also inform relative potency for agents acting through a particular MOA, such as the 50% effective dose (ED_{50}) for aryl hydrocarbon receptor activation by dioxin-like compounds (Kopec *et al.*, 2010) or phthalate-induced male reproductive developmental toxicity (Hannas *et al.*, 2012).

Most quantitative cancer or non-cancer risk assessments require a low-dose point-of-departure (POD), such as a 10% effective dose (ED_{10}) for a sensitive adverse effect, to subsequently derive acceptable exposure levels. The benchmark dose (BMD) approach is the preferred method for identifying a low-dose POD since it considers the entire range of the experimental data as opposed to one of the experimental doses being identified as the no-observed or lowest-observed-adverse-effect level (NOAEL or LOAEL, respectively). The latter are influenced by sample size and dose-spacing and do not consider the slope or shape of the dose-response curve (Davis *et al.*, 2011; U.S. EPA, 2002, 2005, 2012). Further, there may be fundamental differences in the biological response (i.e., dose transitions) at different parts of the dose-response curve for lesion induction (Slikker *et al.*, 2004).

Use of genomic data from shorter-term exposures to identify critical molecular effects and a POD for quantitative risk assessment of chronic exposure will require dose-

response and time-course information for key molecular events and knowledge of how these changes quantitatively relate to apical toxicity endpoints that have traditionally served as the basis of chemical regulation (Ankley *et al.*, 2010; Edwards and Preston, 2008; Paules, 2003). Whole-genome microarray methods provide both a discovery engine for identifying early key events in a chemical MOA and an information base for MOA-based risk assessment (Edwards and Preston, 2008). The desire for genomic data to complement dose–response assessments of traditional endpoints (Chiu *et al.*, 2013) is facilitated by the BMDExpress program (Thomas *et al.*, 2007b, Yang *et al.*, 2007), which accommodates whole-genome microarray data for probe-level dose-response modeling and low-dose extrapolation.

Conazoles are a class of fungicides with agricultural and pharmaceutical applications. Some conazoles, such as cyproconazole, epoxiconazole, propiconazole and triadimefon, induce hepatocellular tumors in mice, but with varying potencies and tumor profiles (Bomhard and Hahnemann, 1986; Gerspach, 1997; Mellert, 1992; Warren *et al.*, 1988). Conversely, myclobutanil was not tumorigenic in mice (Anderson *et al.*, 1993- based on California Department of Food and Agriculture, 2000; Goldman and Harris, 1986- INCHEM, 1992 and California Dept. Food and Agriculture, 2000). Traditional toxicity endpoints could not distinguish myclobutanil from propiconazole or triadimefon after 30 days of exposure, but some aspects of their gene expression profiles were distinct (Ward *et al.*, 2006). Similarly, global expression profiling found that cyproconazole,

epoxiconazole and propiconazole had 330 differentially expressed probe sets in common after 30 days of dietary exposure at the highest (i.e. a tumorigenic) dose (Hester *et al.*, 2012). By encompassing 4 tumorigenic and 1 non-tumorigenic conazole, the present study proposed that the 330-probe high-dose signature could be extended to estimate transcriptional benchmark dose levels ($BMDL_T$) for dose-related probe sets and that this refined low-dose signature could help discern a tumorigenic from a non-tumorigenic conazole at 30 days. We also compared the dose and time-course concordance of transcriptional and apical benchmark dose levels at 30 days (i.e. phenotypic anchoring) and at 2 years to identify the magnitude of transcriptomic-to-phenotypic extrapolation uncertainty, another crucial element in toxicogenomic-driven quantitative risk assessment.

Materials and Methods

The chemical substance characterization and animal exposure protocols have been described previously (Allen *et al.*, 2006; Hester *et al.*, 2012; Nesnow *et al.*, 2009; Ward *et al.*, 2006). Briefly, these studies were comparatively designed to assess traditional liver endpoints such as liver weight, hepatic microsomal enzyme induction, and liver histopathology as well as global gene expression in the liver with Affymetrix mouse 430 2.0 whole genome arrays after 30 days of dietary exposure to 5 conazoles in male CD-1 mice, the more sensitive sex. Microarray processing and normalization procedures have been described previously using Rosetta Resolver software (Nesnow *et al.*, 2009; Hester *et*

al., 2012). The 30-day studies were conducted in the same facility (U.S. EPA National Health and Environmental Effects Research Laboratory, Research Triangle Park, NC).

Liver gene expression was assessed in 5 mice per dose for cyproconazole and epoxiconazole and 3 mice per dose for propiconazole, triadimefon and myclobutanil. Three dose levels and a concurrent control were included and the highest dose for cyproconazole (200 ppm), epoxiconazole (500 ppm) and triadimefon (1800 ppm) was the tumorigenic dose in 18-month feeding studies (Bomhard and Hahnemann, 1986; Mellert, 1992; Warren *et al.*, 1988). The highest dose for propiconazole (2500 ppm) was based on a 24-month feeding study (Hunter *et al.*, 1982). However, in order to be consistent with the chronic exposure duration for the other 4 conazoles, benchmark dose estimates for liver tumors for propiconazole in the present study were based on the observed incidences from an 18-month study in which the highest dose of 850 ppm was also tumorigenic (Gerspach, 1997). The highest dose for myclobutanil in the present study was 2000 ppm. Myclobutanil was tested at up to 2000 ppm in an 18-month feeding study and was not found to be tumorigenic (Anderson *et al.*, 1993- based on California Department of Food and Agriculture, 2000).

Transcriptional benchmark dose estimation

In the present assessment, transcriptional benchmark dose levels ($BMDL_T$) for liver gene expression were estimated with BMDExpress software (version 1.4.1, 2012) as described by Thomas *et al.* (2007b) and Yang *et al.* (2007) with some modifications. The

primary modifications were (1) rather than global gene expression, the dose-response assessment was restricted to the 330-probe differentially expressed gene (DEG) cluster proposed as a 30-day tumorigenicity signature that was previously derived from a global profile (Hester *et al.*, 2012). (2) IPA software (Ingenuity Pathway Analysis, Ingenuity® Systems, www.ingenuity.com) was used for functional annotation since the pre-configured KEGG database is no longer updated. (3) A high-dose fold change (FC) cut-off of 5 (induced or repressed) was ultimately applied based on considerations explained in the Results.

The estimated consumed dose (mg/kg-day) served as the dose metric for each conazole. Normalized linear signal intensities for each probe set were fit to Hill, power, linear (1°), and polynomial (2°) dose-response models. Each model was run assuming constant variance, and the benchmark response factor was set to 1.349 of the control group standard deviation (SD). This represents 11% change in signal intensity tail area due to allowance for a 1% change (0.5% in each tail) to occur in the absence of exposure (Thomas *et al.*, 2007b; Yang *et al.*, 2007). This 10% change in transcriptional response, either up- or down-regulated over background (i.e. controls) is intended to represent the dose at which transcription is altered above or below background and to be analogous to the 10% benchmark dose level (BMD_{10}) for quantal data, such as histopathology lesions or tumor incidence and also to "one control standard deviation" above or below the background benchmark response (BMD_{1SD}) for continuous data, such as altered liver weight or liver

enzymes (U.S. EPA, 2012). For best-fit model selection, a nested likelihood ratio test was performed on the linear and polynomial 2° models. If the more complex model provided a significantly improved fit ($p < 0.05$), the more complex model was selected. The simpler model was selected if the more complex model did not provide a significantly improved fit. Similar to apical benchmark dose guidelines (U.S. EPA, 2012), models with a global goodness-of-fit p value < 0.1 were excluded; p values of 1 indicate a perfect fit (i.e. the model's predicted response is identical to the observed response). To select the best globally-fitting model with the least complexity, the Akaike Information Criterion (AIC is $-2L + 2p$, where L is the log-likelihood at the maximum likelihood estimates [MLEs] for p estimated parameters), for the selected polynomial model was then compared with the AIC for the Hill and power models. The model with the lowest AIC was selected as the final model. In cases where the ''k'' slope parameter for the Hill model was out of bounds, the Hill model was excluded from the final selection. Unacceptable fits excluded from further analyses were probe sets with a BMD_T value greater than the highest dose or a global goodness-of-fit p value < 0.1. Descriptive statistics for each conazole were based on the lower 95% confidence limit ($BMDL_T$) of the BMD_T from the best-fitting model.

The remainder of the transcriptional dose-response analysis focused on the 330 probe sets previously reported as being commonly responsive to 3 hepatotumorigenic conazoles (cyproconazole, epoxiconazole, and propiconazole) (Hester *et al.*, 2012). Briefly, the GeneChip .cel files were normalized and statistically analyzed using Rosetta

Resolver software with ANOVA followed by application of the Benjamini-Hochberg false discovery test ($p < 0.05$). The DEG lists from the high-dose carcinogenic feed levels of cyproconazole (200 ppm), epoxiconazole (500 ppm), and propiconazole (2500 ppm) were used in a Venn analysis to identify a set of 330 probe sets common to the 3 hepatocarcinogenic conazoles. The myclobutanil and triadimefon transcriptional responses were also processed, normalized, and statistically analyzed using Rosetta Resolver software with ANOVA followed by application of the Benjamini-Hochberg false discovery test ($p < 0.05$) from .cel files described in Ward *et al.*, (2006).

In the present assessment, the 330 probe set IDs mapped to 281 unique genes based on their NCBI Entrez Gene ID; when more than one probe mapped to the same gene, the highest intensity probe was selected for dose-response analysis. Given background variability, in order to exclude non-dose-related or only modestly responsive probes, only probes with a normalized fold change (FC) in signal intensity at the high dose (i.e. the tumorigenic dose) of $\geq$ 5-fold (induced or repressed) were included in the $BMDL_T$ descriptive statistics. Dose-responsive behavior was difficult to discern when the high-dose FC was <5 (described in Results).

Apical benchmark dose estimation for liver tumors and precursor liver effects

Apical effects are clinical or morphologic effects such as increased liver weight or liver tumors that have more traditionally served as the basis of low-dose quantitative risk

assessment. Increased mean relative liver weight and pentoxyresorufin dependylase activity (PROD) at 30 days were modeled based on published data (Allen *et al.*, 2006; Hester *et al.*, 2012) using mean consumed dose (mg/kg-day) as the dose metric. The lower 95% confidence interval for the response at one control standard deviation was used to define these benchmark responses ($BMDL_{1SD}$). Liver weight was assessed in 10 to 16 mice per dose for each of the 5 conazoles and PROD was assessed in 4 mice per dose for propiconazole, triadimefon, and myclobutanil. PROD activity measures the O-dealkylation of pentoxyresorufin to resorufin *in vitro* (Lubet *et al.*, 1985) and represents Cyp2b10 protein induction mediated via activation of the xenobiotic-metabolizing nuclear receptor constitutive androstane receptor (CAR) in mice (Ross *et al.*, 2010).

The liver tumor benchmark dose ($BMDL_{10}$) was estimated for hepatocellular adenomas, carcinomas, and the combined incidence of hepatocellular adenoma or carcinoma observed in male mice, the more sensitive sex, after chronic dietary exposure for approximately 18 months to cyproconazole (Warren *et al.*, 1988 - based on Peffer, 2011 and U.S. EPA, 1990), epoxiconazole (Mellert, 1992 - based on U.S. EPA, 2001), propiconazole (Gerspach, 1997 - based on Dewhurst and Dellarco, 2004), or triadimefon (Bomhard and Hahnemann, 1986 - based on Dewhurst and Dellarco, 2004). Myclobutanil was not tumorigenic after chronic dietary exposure (Anderson *et al.*, 1993- based on California Department of Food and Agriculture, 2000). The lower 95% confidence interval of the dose estimated to result in a 10% increase in tumor incidence above background (i.e.

controls) was used to define the tumor benchmark response ($BMDL_{10}$). Thus, $BMDL_{10}$ values were not estimated when the rate at the highest dose group was less than 10%, which occurred at times when adenomas or carcinomas were evaluated separately (see Table 4). The 5 factors collectively taken into consideration for selecting the best-fit model included the global goodness-of-fit p value (must be ≥ 0.1 but highest value preferred); lowest AIC value, Chi^2 residual values of less than 2 at each dose level, visual fit (U.S. EPA, 2012), and the margin between the BMD_{10} and $BMDL_{10,}$ with a preferences for ratios < 2 (Muri *et al*., 2009). Individual animal data were not available to account for reduced survival observed for one of the 5 conazoles, propiconazole. A mortality-adjusted BMDL could be lower, recognizing that other factors, such as goodness-of-fit, also contribute to estimated BMDL levels. The best-fit $BMDL_{1SD}$ model for increased relative liver weight at 30 days and the $BMDL_{10}$ for hepatocellular tumors after chronic exposure were compared to the 30-day median $BMDL_T$ estimates for each conazole.

Results

Transcriptional benchmark dose estimates

The $BMDL_T$ values were estimated for the 330 probe sets (281 genes) that comprise the conazole hepatotumorigenicity signature at 30 days. These $BMDL_T$ values were intended to reflect the dose at which transcription is altered above or below background (i.e. controls) in an approach analogous to apical benchmark dose levels ($BMDL_A$) for traditional data. In initial studies, generally poor modeling results, such as low goodness-

of-fit p values or poor visual fits were obtained for probes having a normalized fold change (FC) in signal intensity of < 5 at the high dose. This tended to encompass probes that had modest or no change in signal intensity across increasing dose levels, particularly at the low and intermediate dose levels (**Appendix A Table A.1**). When identifying DEGs, the greatest source of variability which accounts for high false-negative (i.e. low sensitivity) rates occurs for DEGs with low intensity signals and small fold changes (Choe *et al.*, 2005). Thus, an important feature of a successful microarray analysis is to account for probe sets with low signal intensity, such as by filtering them from the analysis (Choe *et al.*, 2005). Consequently, it was concluded that dose-response behavior that would permit reliable low-dose extrapolation was not clearly discernible when the high-dose fold change (FC) was less than 5, and as a result, a FC "cut-off" for inclusion was established at 5.0. Probe sets within the 330-probe cluster with a FC < 5 at the high dose (i.e. tumorigenic dose) were excluded from further dose-response analyses.

Of the 330 probes, there were 48 probes (mapping to 45 Entrez genes) considered to have dose-responsive behavior at 30 days since they had a FC ≥ 5 at the high dose for at least one conazole (**Table 1.1**). The number of probes that had an acceptable statistical $BMDL_T$ fit ranged from 19 of 48 for myclobutanil to 38 of 48 for propiconazole (**Appendix A Table A.2**). The 48 probes primarily encompassed pathways associated with CAR/RXR activation, P450 metabolism, glutathione depletion - hepatocellular hypertrophy, LPS/IL-1 mediated inhibition of RXR function, and NRF2-mediated oxidative stress response

according to IPA Tox Lists, a pathway library based on sets of genes known to be perturbed upon compound treatment and that eventually result in measurable pathology (**Table 1.1**). Box and whisker plots illustrate the range of $BMDL_T$ estimates and suggest relatively low variability in the modeled genes for each conazole (**Figure 1.1**). More notably, the range of $BMDL_T$ estimates can inform potency for the 5 conazoles with respect to the 30-day conazole hepatotumorigenicity signature. Cyproconazole was the most potent conazole based on the lowest median $BMDL_T$ of 9 mg/kg-day and myclobutanil was the least potent, with the highest median $BMDL_T$ of 78 mg/kg-day. Myclobutanil, the non-tumorigenic conazole, also had a statistical lower outlier, which was the $BMDL_T$ of 6.9 mg/kg-day for *Cyp2b10*. Traditional subchronic toxicity endpoints could not distinguish myclobutanil from tumorigenic conazoles at 30 days, since myclobutanil is also associated with dose-related increases in liver weight, Cyp2b10 induction, increased PROD activity, hepatic cell proliferation and hepatic hypertrophy but not liver tumors in mice (Allen *et al.*, 2006; Health Canada, 2010). Thus, not all CAR-activating xenobiotics lead to rodent liver tumors and this chemical class-based $BMDL_T$ approach considered the $BMDL_T$ for *Cyp2b10* transcription at 30 days to be a distinction between a non-tumorigenic CAR agonist and 4 tumorigenic CAR agonists.

On a direct gene-to-apical outcome basis, a high degree of direct concordance was found between $BMDL_T$ estimates for *Cyp2b10* gene expression and $BMDL_A$ estimates for Cyp2b10 protein expressed as PROD activity for 3 conazoles for which data were

available, 2 tumorigenic (propiconazole and triadimefon) and the one non-tumorigenic (myclobutanil) conazole (**Figure 1.2 and Table 1.2**). CAR activation has been proposed as the molecular initiating (i.e. first key) event in a MOA sequence culminating in rodent liver tumors (U.S. EPA, 2011c). Since *Cyp2b10* is a target gene of CAR activation in mice (Ross *et al.*, 2010), we propose that our $BMDL_T$ values for *Cyp2b10* can be viewed as a measure of potency for CAR activation in mice. Further, we observed quantitative concordance, thus anchoring these $BMDL_T$ to their apical $BMDL_A$ for Cyp2b protein (via PROD measurements) at 30 days. However, the $BMDL_T$ for Cyp2b10 gene or protein alone was insufficient to distinguish myclobutanil from tumorigenic conazoles based on Table 2.

Further, with respect to phenotypically anchoring conazole-specific gene expression signatures, 30-day median $BMDL_T$ estimates from the 48-probe subset (excluding those with unacceptable fits and/or with a high-dose FC < 5) were concordant (within a factor of 2.4) with apical benchmark doses ($BMDL_A$) for increased liver weight at 30 days for the 5 conazoles (**Table 1.3 and Appendix A Table A3**). This concordance of 30-day $BMDL_T$ with the 30-day $BMDL_A$ for increased liver weight is mechanistically supported by CAR/RXR activation, P450 metabolism, and glutathione depletion - hepatocellular hypertrophy being the primary biological pathways represented in the 45 dose-related genes comprising the 30-day hepatotumorigenicity signature. Although centrilobular and panlobular hepatocellular hypertrophy, and at times cytoplasmic vacuolation, were observed after 30 days of dietary exposure to some of the conazoles

(Hester *et al.*, 2012; Allen *et al.*, 2006), benchmark dose levels were not estimated due to their steep dose-responses and small sample sizes (n=5) included for histological examination. Further, since the BMDL for incidence data is estimated at the 10% response level (U.S. EPA, 2012) and the minimum sample size that can observe a 10% response is 10 (1 out of 10 animals affected), the sample sizes of 5 would estimate BMDL values outside of the power of detection. However, the sample sizes of 10-16 were adequate for modeling liver weight, since BMDL estimates for continuous data are based on the standard deviation of the control group rather than a 10% increase (U.S. EPA, 2012).

Potency differences in the dose-responsive transcription of some genes, such as those involved in Phase II metabolism, bile acid detoxification, or lipid oxidation, including *Gstm3, Gstt3, Abcc4, Akr1b7,* and *Lcn13*, tended to mirror the tumorigenic potency gradient. For example, the $BMDL_T$ estimates for *Akr1b7* were 8, 16, and 51 mg/kg-day for cyproconazole, epoxiconazole, and propiconazole, respectively (**Figure 1.3**). Whereas, transcription of *Akr1b7* was not dose-related for the weak tumorigen, triadimefon, or the non-tumorigen, myclobutanil, based on FC values of ≤ 5 at the highest tested dose. The aldo-keto reductase *Akr1b7* gene is a common transcriptional target of the CAR and pregnane X receptor (PXR) family of xenobiotic receptors (Liu *et al.*, 2009) and plays a crucial role in bile acid metabolism and detoxification (Schmidt *et al.*, 2011). The up-regulation of Akr1b7 has been implicated in oxidative stress (Jia *et al.*, 2006; Volat *et al.*, 2012). Similarly, potency differences in the repressed transcription of the lipid oxidation

gene, lipocalin 13 (*Lcn13*) at 30 days tended to mirror the tumorigenic potency gradient. $BMDL_T$ estimates for *Lcn13* were 16, 21, 31 and 104 mg/kg-day for cyproconazole, propiconazole, triadimefon, and myclobutanil, respectively. At the highest dose, the decreases in FC values ranged from -8 to -22 for these 4 conazoles. While also repressed for epoxiconazole (FC of up to -8 at the highest dose), the $BMDL_T$ result for *Lcn13* for epoxiconazole was an unacceptable fit (i.e. BMD > highest dose) and thus excluded. Potency gradients at 30 days that mirrored tumorigenic potency were also observed for 2 un-annotated probe sets, 1443137_at and 1438068_at. These probe sets were retained in the analysis since they were considered bioindicators of dose-responsive transcription for the 5 conazoles at 30 days, while recognizing that their potential biological or functional relevance is currently unknown. The $BMDL_T$ estimates for the 1443137_at probe set were 3, 4, 9, 12, and 30 mg/kg-day for cyproconazole, epoxiconazole, propiconazole, triadimefon, and myclobutanil, respectively. Similarly $BMDL_T$ estimates for the 1438068_at probe set were 10, 30, 35, 62, and 82 mg/kg-day for the same conazoles.

Chronic apical benchmark dose estimates

Chronic apical $BMDL_{10}$ values were estimated for hepatocellular adenomas, hepatocellular carcinomas, and for the combined incidence of adenomas or carcinomas observed in male mice after chronic (i.e. 18 months) of dietary exposure for the 4 tumorigenic conazoles (cyproconazole, epoxiconazole, propiconazole, and triadimefon). The chronic study details and the incidence data used for benchmark dose modeling are

presented in **Table 4.** In addition to potency differences, the liver tumor profiles varied to some degree, as cyproconazole was primarily associated with adenomas and epoxiconazole was primarily associated with carcinomas. Triadimefon was only associated with hepatocellular adenomas.

The $BMDL_{10}$ values for hepatocellular tumors, particularly for the combined incidence of adenoma or carcinoma, suggested different potencies with cyproconazole > epoxiconazole > propiconazole > triadimefon > myclobutanil (non-tumorigenic) (**Table 1.5**). The 30-day median $BMDL_T$ estimates correctly stratified these 5 conazoles according to tumorigenic potency on a mg/kg-day basis and were within one-half order of magnitude of the chronic $BMDL_A$ for the combined incidence of hepatocellular adenoma or carcinoma, which are conventionally combined for quantitative risk assessment purposes.

Discussion

The present assessment refined the previously proposed 30-day high-dose gene signature (Hester *et al.*, 2012) by estimating low-dose transcriptional $BMDL_T$ for dose-related probes. We used this refined signature to help differentiate 4 tumorigenic conazoles from a non-tumorigenic conazole after 30 days of exposure and compare the dose and time-course concordance of $BMDL_T$ and $BMDL_A$ at 30 days (i.e. phenotypic anchoring) and at 18 months. Chemical class-based approaches to risk assessment not only foster efficiency compared to a substance-by-substance evaluation but also help identify patterns within a

category, increase confidence in the results, and contribute to the weight-of-evidence (OECD, 2007).

Since profiling global gene expression is a powerful tool to elucidate toxicant modes of action (Edwards and Preston, 2008), by focusing on the 330-probe cluster, and further reducing it to 48 probes, potentially valuable mechanistic information may have been lost from our analysis. For example, in addition to CAR activation, CYP51 inhibition has been proposed as an additional MOA and this pathway leads to altered cholesterol homeostasis (Nesnow, 2013). Cholesterol-related genes in our analysis had low intensity signals and were less dose-responsive as compared to the CAR-related genes in our analysis. Previous studies with global expression profiling have been used primarily in a qualitative fashion to improve the mechanistic understanding of liver tumor formation (reviewed by U.S. EPA, 2011c). These earlier studies lacked quantitative dose-response information and low-dose potency estimates (i.e. BMDLs) for the gene expression and apical toxicity endpoints that were assessed in parallel. Also missing from these studies was a concordance analysis of the data that could contribute to the weight-of-evidence for key events in the proposed MOA. Our studies generated quantitative dose-response information allowing both low dose potency estimates and concordance values for the data to be identified. In terms of potency and mechanism, we identified conazole-specific dose-related patterns in liver gene expression at 30 days that are consistent with early, proposed molecular and phenotypic key events in the conazole MOA pathway. As indicated above,

$BMDL_T$ values for *Cyp2b10* as a measure of potency for CAR activation alone did not correctly stratify the 5 conazoles according to tumorigenic potency. Similarly, $BMDL_{1SD}$ values for increased relative liver weight did not correctly stratify the 5 conazoles. However, our median $BMDL_T$ values for the 48-probe dose-related subset from the 30-day tumorigenicity signature correctly stratified these 5 conazoles according to tumorigenic potency. A challenge to incorporating toxicogenomic technologies into the current risk assessment paradigm has been the functional interpretation of genomic data - the linking of potentially related gene expression alterations to conventional, more well-established toxicological endpoints (Hamadeh *et al.*, 2002; Paules, 2003; Yu *et al.*, 2006).

Following CAR activation, the molecular initiating event, the first phenotypic key event in conazole hepatotumorigenicity has been proposed to be hepatic hypertrophy (U.S. EPA, 2011c). Other downstream key events such as oxidative stress, increased cell proliferation, and suppression of apoptosis ultimately contribute to tumor induction (Nesnow, 2013; U.S. EPA, 2011c). Since *Cyp2b10* is a target gene of CAR activation in mice (Ross *et al.*, 2010), we believe that our $BMDL_T$ values for *Cyp2b10* can be viewed as a quantitative measure of potency for CAR activation in mice. Further, the $BMDL_A$ for Cyp2b protein measured via PROD activity at 30 days was a quantitatively concordant apical anchor for *Cyp2b10* based on companion data for 3 conazoles (propiconazole, triadimefon, and myclobutanil). The higher median $BMDL_T$ estimate for myclobutanil compared to the tumorigenic conazoles suggests that transcription of conazole-induced

genes associated with hepatotumorigenesis at 30 days is less responsive for myclobutanil relative to the other conazoles and may help explain its lack of tumorigenicity after chronic exposure. Our class-based $BMDL_T$ dose-response approach also found that myclobutanil had the least number of probe sets (19 of 48) meeting the cut-off criteria. Together, these observations suggest that at 30 days myclobutanil can be identified as the least potent conazole with respect to potential hepatotumorigenicity relative to the other 4 conazoles. Traditional toxicity endpoints did not distinguish myclobutanil from propiconazole or triadimefon, 2 hepatotumorigenic conazoles (Allen *et al.*, 2006). In fact, our $BMDL_T$ estimates for *Cyp2b10* suggest that myclobutanil is at least as potent as propiconazole and triadimefon at activating CAR, which is possibly also reflected in increases in liver weight. Myclobutanil is also equally or more potent than triadimefon and propiconazole at inducing liver cell proliferation at 30 days, based on $BMDL_{ISD}$ estimates of 115, 118, and 158 mg/kg-day, respectively, when measured using the proliferation cell nuclear antibody (data not shown; modeled based on Allen *et al.*, 2006). $BMDL_{ISD}$ estimates were 12 and 10 mg/kg-day for liver cell proliferation at 30 days for cyproconazole and epoxiconazole, respectively, when measured using the Ki67 antibody, a more specific cell proliferation marker than proliferation cell nuclear antigen (data not shown; modeled based on Hester *et al.*, 2012). Thus, in addition to dose considerations, other factors may influence the outcome of an individual key event, and these factors may affect the likelihood of progression to the next key event or the magnitude of the ultimate response (Julien *et al.*, 2009).

As indicated above, hepatic hypertrophy is the first phenotypic key event following CAR activation (U.S. EPA, 2011c). Since increases in liver weight can be related to hepatic hypertrophy, the observation that our gene expression changes (median $BMDL_T$) correlated well to potency for induction of hepatic hypertrophy (i.e. $BMDL_A$ for increased liver weight) supports the validity of this toxicogenomic approach. The factors contributing to the lack of hepatotumorigenicity associated with myclobutanil exposure in mice are unclear, given that the proposed molecular initiating event, CAR activation (based on Cyp2b10 induction), and other early key events, such as increased liver weight, hepatocellular hypertrophy, and liver cell proliferation are indistinguishable for many conazoles. Despite this, our 30-day median $BMDL_T$ for our subset of genes correctly stratified these 5 conazoles according to tumorigenic potency (i.e. the last key event). Further, our results are the first to couple transcriptional and apical benchmark doses thereby allowing for a direct comparison of concordance and potency at low-dose exposures for key molecular and apical events across 5 members of the same class of compounds. Being less influenced by sample size and dose-spacing and informing the dose-response curve, benchmark dose levels are preferable low-dose PODs as compared to NOAEL or LOAEL values.

One of the uncertainties in the present assessment is the observation that the 30-day median $BMDL_T$ value of 9 mg/kg-day for cyproconazole was above the chronic $BMDL_A$ of 2 mg/kg-day for hepatocellular adenoma or carcinoma (combined). Time-course apical

benchmark dose modeling for proposed key events, such as hepatocyte hypertrophy and hepatocyte lipid content of marked severity at 7 days, increased liver weight and reduced serum cholesterol at 30 days, and single cell necrosis and hepatocellular tumors at 18 months, suggested $BMDL_A$ values in the range of 2 to 4 mg/kg-day for cyproconazole (data not shown). For the other 3 tumorigenic conazoles (epoxiconazole, propiconazole, and triadimefon), the 30-day median $BMDL_T$ values were below the chronic $BMDL_A$ for the combined incidence of hepatocellular adenoma or carcinoma. Nonetheless, the 4.3-fold ratio between the 30-day median $BMDL_T$ (9 mg/kg-day) and chronic $BMDL_A$ (2.1 mg/kg-day) for hepatocellular tumors for cyproconazole falls within the existing 10-fold uncertainty factor commonly used to account for extrapolation from a less-than-lifetime to a lifetime (i.e. chronic) exposure duration (U.S. EPA, 2002). Adopting the 30-day median $BMDL_T$ values directly as PODs for quantitative risk assessment of nongenotoxic carcinogens would seem to be a feasible approach for the 3 other tumorigenic conazoles (epoxiconazole, propiconazole, and triadimefon), particularly considering that other uncertainty factors, such as for interspecies and intraspecies extrapolation and database deficiencies can also be considered. Just as traditional uncertainty factor categories identify areas of uncertainty in the dose-response analysis (U.S. EPA, 2002), the incorporation of toxicogenomic data into quantitative risk assessment, particularly when extrapolating a short-term transcriptional POD to derive an acceptable exposure level for long-term exposure will be associated with some degree of uncertainty or variability. Transcriptomic-to-phenotypic extrapolation uncertainty has not been addressed in the published literature,

perhaps since characterization of uncertainty in the risk assessment process does not occur until a POD is established. Until recently, methods to estimate a low-dose POD for a critical effect at the molecular level were not available. Our approach of comparing the concordance of transcriptional and apical benchmark dose estimates could be used to inform both potency and the magnitude of transcriptomic-to-phenotypic extrapolation uncertainty. Of note, our 30-day median $BMDL_T$ values were within 10-fold of the chronic BMDL values for tumors. This approach can help prioritize chemicals for future testing and may lead to more expeditious and feasible decision-making. In traditional risk assessments based on chronic rat and mouse bioassay results, the most sensitive target organ was the liver in mice for cyproconazole, epoxiconazole, and propiconazole but for triadimefon and myclobutanil, the rat central nervous system and testes, respectively, were the most sensitive target tissues (U.S. EPA, 2000, 2006a,b,c, 2008).

In conclusion, the ability to couple transcriptional and apical dose-responses after short-term exposures is consistent with the 21st century vision for more efficient risk assessment with reduced animal testing (NRC, 2007a). Our chemical class and key event-based concordance analyses using $BMDL_T$ and $BMDL_A$ at 30 days informed low-dose potency for a class of chemicals that are believed to share a common tumorigenic MOA. While traditional toxicity endpoints could not distinguish tumorigenic from non-tumorigenic conazoles at 30 days, our median $BMDL_T$ values corresponded well to tumorigenic potency on a mg/kg-day basis with cyproconazole > epoxiconazole >

propiconazole > triadimefon > myclobutanil (non-tumorigenic) and were within one half order of magnitude of $BMDL_A$ values for liver tumors. When the magnitude of transcriptomic-to-phenotypic extrapolation uncertainty, a critical element to toxicogenomic-driven quantitative risk assessment, can be more fully characterized, a low-dose transcriptional POD estimated from a short-term exposure may serve as the basis of a quantitative risk assessment of long-term exposure. This approach can also help prioritize chemicals for future testing and may aid in distinguishing between tumorigenic and non-tumorigenic compounds in the absence of traditional chronic rodent bioassays.

Figures and Tables

Figure 1.1. Range of transcriptional benchmark dose estimates

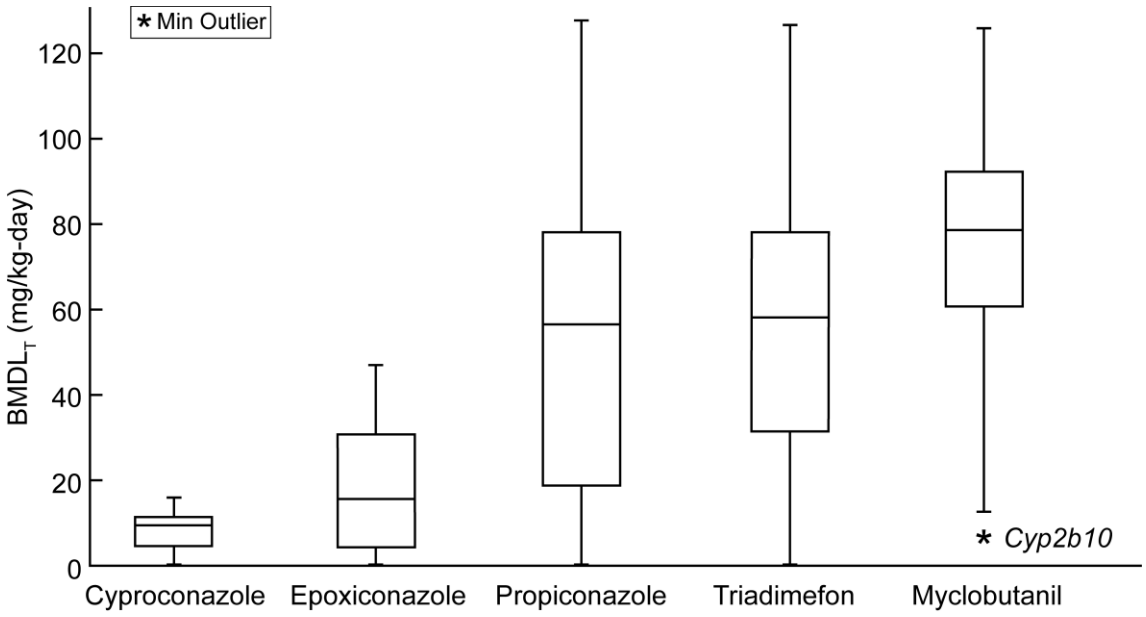

Figure 1.1 legend. The median and ranges of 30-day transcriptional benchmark dose estimates ($BMDL_T$) for the 5 conazoles based on refined 48-probe gene subset show concordance with the tumorigenic potency gradient. The transcriptional benchmark dose ($BMDL_T$ of 6.9 mg/kg-day) for *Cyp2b10* was identified as a statistical lower outlier for myclobutanil, the non-tumorigenic conazole.

Figure 1.2. Direct concordance of benchmark dose estimates for Cyp2b10 gene transcription and protein measurements at 30 days

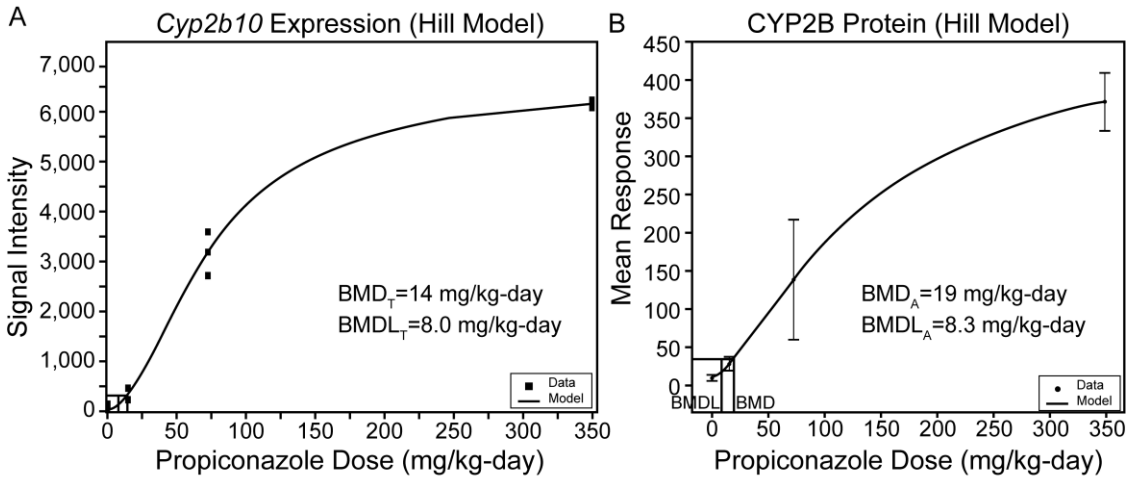

Figure 1.2 legend. The graphical output of (A) transcriptional and (B) apical (i.e. protein) benchmark dose (BMD_T and BMD_A, respectively) modeling and corresponding 95% lower confidence limit benchmark dose ($BMDL_T$ and $BMDL_A$, respectively) for pentoxyresorufin depentylase activity (PROD, pmol resorufin formed/min/mg microsomal protein) for propiconazole is shown. The estimates for triadimefon and myclobutanil were also concordant (see Table 2; graphs not shown). The models were based on the data reported by Allen *et al.* (2006) and Hester *et al.* (2012). No data were available for PROD measurements at 30 days for cyproconazole or epoxiconazole.

Figure 1.3. 30-d transcriptional benchmark dose estimates for some genes mirrored the tumorigenic potency gradient

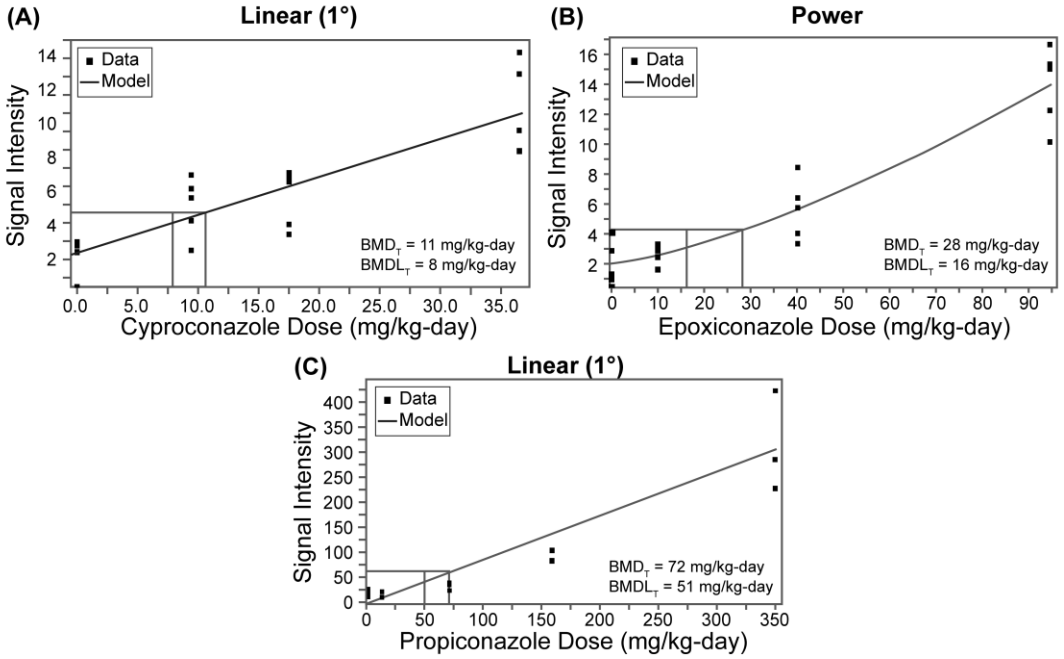

Figure 1.3 legend. The transcriptional benchmark doses (BMD_T) and corresponding 95% lower confidence limit benchmark doses ($BMDL_T$) for the *Akr1b7* gene for (A) cyproconazole, (B) epoxiconazole and (C) propiconazole are shown. Triadimefon and myclobutanil (weakly tumorigenic and non-tumorigenic, respectively) had a FC $\leq$ 5 for *Akr1b* at the highest dose, thus were excluded. The models were based on data of Hester *et al.* (2012) and Ward *et al.* (2006).

Table 1.1. Dose-responsive probe sets and their associated pathways at 30 days a

48 DOSE-RESPONSIVE PROBES AT 30 D			
Cyp2b10	*Por*	*Gadd45b*	*Chka*
Cyp2c55	*Tnfrsf19*	*Papss2*	*Ndst1*
Cyp2c54	*Nsl1*	*Abcc4*	*Ehno*
Cyp2c65	*Meig1*	*Nebl*	*Nfib*
Cyp2b9	*Lrrc67*	*Mt2*	*Ttc39c*
Gstm3	*S100a8*	*Slco1a4*	*Ddx46*
Gstt3	*Atg1612*	*Gm10419*	*Hectd2*
Smpd3	*Ikbke*	*Lonrf3*	*Serpina9*
Srxn1	*Ndrg1*	*Lcn13*	*Prlr*
Akr1b7	1443137_at	*Dnaic1*	1451681_at
Orm2	1438068_at	*Rbbp8*	*Ddx6*
Orm3	*Cd36*	*Tlr2*	*C2cd2*
FUNCTIONAL ANNOTATION [b]			
CAR/RXR Activation (2.36E-13) P450 Metabolism (2.22E-09) Glutathione Depletion - Hepatocellular Hypertrophy (5.84E-07) LPS/IL-1 Mediated Inhibition of RXR Function (2.69E-09) NRF2-Mediated Oxidative Stress Response (7.8E-08) [c]			

[a] Clear cells are induced and shaded cells are repressed by FC ≥ 5 in the 330-probe cluster for at least one conazole at the highest dose

[b] Top 5 pathways identified by IPA analysis with the corresponding p value in parentheses

[c] Not one of the top 5 pathways for triadimefon or propiconazole

See Supplement Table S1 for signal intensity fold-change values across dose levels

Table 1.2. Direct gene (transcriptional) and apical BMDL dose-response concordance at 30 days [a]

	Cypro-conazole	**Epoxi-conazole**	**Propi-conazole**	**Triad-imefon**	**Myclo-butanil**
30-day $BMDL_T$ for *Cyp2b10* gene	2.7 mg/kg-day	1.4 mg/kg-day	8.0 mg/kg-day	13 mg/kg-day	6.9 mg/kg-day
30-day $BMDL_A$ for PROD activity	Not available	Not available	8.3 mg/kg-day	11 mg/kg-day	8.1 mg/kg-day

[a] Modeled from data of Allen *et al.* (2006), Nesnow *et al.* (2009), and Hester *et al.* (2012)

Table 1.3. 30-day transcriptional and 30-day apical benchmark dose estimates

	Cypro-conazole BMDL (mg/kg-day)	Epoxi-conazole BMDL (mg/kg-day)	Propi-conazole BMDL (mg/kg-day)	Triad-imefon BMDL (mg/kg-day)	Myclo-butanil BMDL (mg/kg-day)
Mean transcriptional $BMDL_T$ [a]	8	18	52	55	75
Median transcriptional $BMDL_T$ [a]	9	16	56	58	78
Mean relative liver weight ($BMDL_A$)[b]	6	8	54	48	33
	Cypro-conazole	Epoxi-conazole	Propi-conazole	Triad-imefon	Myclo-butanil
Ratio of median $BMDL_T$ to $BMDL_A$ [c]	1.5	2.0	1.0	1.2	2.4

[a] Dose-responsive genes from the conazole subset

[b] Based on data of Allen *et al.* (2006) and Hester *et al.* (2012)

[c] $BMDL_A$ refers to increased mean relative liver weight with the benchmark response set to one control group SD according to U.S. EPA (2012) guidelines

Table 1.4. Liver tumor incidence used for benchmark dose modeling

Chemical	Strain (exposure duration)	Estimated mean consumed dose (target concentrations)	Adenoma [a]	Carcinoma [a]	Adenoma or Carcinoma [a]	Study Reference
Cyproconazole [b]	CD-1 (81 weeks)	0, 0.69, 1.84, 13.2, or 27.9 mg/kg-day (0, 5, 15, 100, 200 ppm)	6/92, 4/49, 5/48, 12/47, 12/48 [b]	*0/92, 0/49, 3/48, 3/47, 1/47*	6/92, 4/49, 8/48, 15/47, 13/48 [b]	Warren *et al.*, 1989- based on Peffer, 2011 and U.S. EPA, 1990
Epoxiconazole	C57Bl/6 NCrlBr (78 weeks)	0, 0.17, 0.81, 35.3, 72.2 mg/kg-day (0, 1, 5, 200 or 500 ppm)	*0/61, 0/30, 0/34, 0/44, 3/42* [2]	1/86, 0/40, 0/46, 3/48, 33/50	1/86, 0/40, 0/46, 3/48, 34/50	Mellert, 1992- based on U.S. EPA, 2001
Propiconazole [c]	CD-1 (79 weeks)	0, 11, 59, 108 mg/kg-day (0, 100, 500, 850 ppm)	1/60, 0/60, 3/60, 10/60	*1/60, 3/60, 2/60, 2/60* [2]	2/60, 3/60, 5/60, 12/60	Gerspach, 1997- based on Dewhurst and Dellarco, 2004
Triadimefon	NMRI (84 weeks)	0, 13.5, 76, 550 mg/kg-day (0, 50, 300, 1800 ppm)	3/50, 3/50, 4/50, 11/50	Not observed	3/50, 3/50, 4/50, 11/50	Bomhard and Hahnemann, 1986- based on Dewhurst and Dellarco, 2004
Myclobutanil	CD-1 (78 weeks)	0, 13.7, 70.2, or 393 mg/kg-day (0, 100, 500, or 2000 ppm) [d]	Not observed	Not observed	Not observed	Anderson *et al.*, 1993- based on California Department of Food and Agriculture, 2000; Goldman and Harris, 1986- INCHEM, 1992 and California Dept. Food and Agriculture, 2000 [d]

[a] Control rate up to rate in highest modeled dose group, respectively; Italicized rates were not modeled since a <10% increase above controls was seen in highest treated group

[b] Top dose (200 ppm) for cyproconazole was omitted due to a non-monotonic dose-response

[c] Individual animal data were not available to adjust for increased mortality in all groups, including controls

[d] Original study tested 100 and 500 ppm and second study tested 2000 ppm; the results were not modeled since no tumors were observed

Table 1.5. Comparison of 30-day and chronic benchmark dose estimates

Chronic $BMDL_A$ [a]	Cypro-conazole BMDL (mg/kg-day)	Epoxi-conazole BMDL (mg/kg-day)	Propiconazole [b] BMDL (mg/kg-day)	Triadimefon BMDL (mg/kg-day)	Myclo-butanil BMDL (mg/kg-day)
Adenoma	3.0 [c]	>72 [d]	68	270	Not observed [e]
Carcinoma	>28 [d]	33	>108 [d]	Not observed	
Adenoma or Carcinoma	2.1 [c]	33	65	270	
30-day BMDL	Cypro-conazole BMDL (mg/kg-day)	Epoxi-conazole BMDL (mg/kg-day)	Propiconazole BMDL (mg/kg-day)	Triadimefon BMDL (mg/kg-day)	Myclo-butanil BMDL (mg/kg-day)
Increased mean relative liver weight ($BMDL_A$) [f]	6	8	54	48	33
Transcriptional $BMDL_T$ [f]	9	16	56	58	78

[a] Liver tumors in male mice estimated from 18-month studies
[b] Individual animal data were not available to adjust for increased mortality in all groups, including controls
[c] High dose (200 ppm) was omitted due to non-monotonic dose response
[d] Incidence at the highest dose was <10%
[e] Highest consumed dose was 393 mg/kg-day
[f] From Table 3

CHAPTER 2

DOSE-RESPONSE MODELING OF EARLY MOLECULAR AND CELLULAR KEY EVENTS IN THE CAR-MEDIATED HEPATOCARCINOGENESIS PATHWAY

Abstract

Phenobarbital (PB), a widely-used sedative, is a prototypical nongenotoxic hepatocarcinogen in rodents but not humans. The mode of action (MOA), which is attributed to activation of the constitutive androstane receptor (CAR), is considered qualitatively not plausible for the assessment of human cancer risk. While it has been reported that the hepatic effects of PB are dose-dependent and exhibit a threshold, very few studies have examined dose and temporal thresholds for key events in the MOA. In the present study, male and female CD-1 mice were administered dietary PB at 0, 0.15, 1.5, 15, 75, or 150 mg/kg-day for 2 or 7 days to characterize multiple apical and molecular endpoints below, at (~75 mg/kg-day), and above the carcinogenic dose level of PB and examine these responses using transcriptional and apical benchmark dose (BMD_T and BMD_A) modeling. While the no-observable transcriptional effect level for global gene expression was 15 mg/kg-day in both sexes on both days, pathway level BMD_T estimates suggested sex- and time-specific differences. At 2 days, several xenobiotic metabolism and cell protective pathways were activated at lower doses and to a greater degree in females. These pathways were attenuated at 7 days based on higher median pathway BMD_T estimates and showed little sex-specific differences. Hepatocellular proliferation was the

most sensitive indicator of PB exposure with female mice more than an order of magnitude more sensitive than males based on BMD_A estimates for bromodeoxyurine (BrdU) immunohistochemistry, contrary to sex-specific differences in sensitivity to hepatocarcinogenesis. Taken together, the present study illustrates that dose-response assessment of transcriptional and apical key events after short-term exposures can inform potency for early key events in the CAR-mediated hepatotumorigenic MOA and thus inform the quantitative risk assessment of other CAR activating xenobiotics.

Introduction

Phenobarbital (PB), a widely-used sedative and anti-epileptic drug, is a nongenotoxic and prototypical CAR agonist that induces liver tumors in rodents but not humans (Elcombe *et al.*, 2014; Holsapple *et al.*, 2006). Prolonged therapy with PB or similar sedatives, while not associated with liver tumors, is associated with increased liver size, hepatocyte swelling, and ultrastructural signs of smooth endoplasmic reticulum proliferation in humans (Aiges *et al.*, 1980; Holsapple *et al.*, 2006; IARC, 2001; Pirttiaho *et al.*, 1978, Whysner *et al.*, 1996).

The MOA for rodent liver tumors arising from PB-like hepatic microsomal cytochrome P450 inducers was determined to be unlikely in humans after consideration of kinetic and dynamic factors (Elcombe *et al.*, 2014; Holsapple *et al.*, 2006; Meek *et al.*, 2003; Whysner *et al.*, 1996). Thus, tumors that arise secondary to an adaptive response to metabolizing repeated xenobiotic exposures are considered less relevant to cancer risk assessment relative to other modes of nongenotoxic (i.e. epigenetic) rodent hepatocarcinogenicity, such as cytotoxicity/oxidative stress, activation of the peroxisome proliferator-activated receptor alpha (PPARα), hormonal perturbation, immunosuppression, or porphyria (Boobis *et al.*, 2009; Holsapple *et al.*, 2006, Klaunig *et al.*, 2003; Meek *et al.*, 2003).

Liver hypertrophy accompanies Cyp450 induction, with Cyp2b10 being the predominant and prototypical gene response indicative of a PB-like metabolic response in mice (Honkakoski and Negishi, 1997; Ueda *et al.*, 2002). Transient early waves of replicative DNA synthesis occur in hepatocytes, followed by inhibition of apoptosis, liver hypertrophy, the development of altered hepatic foci and ultimately, tumors. In mice lacking functional CAR, PB does not increase liver weight, induce Cyp2b, increase cell proliferation, or cause liver tumors (Huang *et al.*, 2005; Yamamoto *et al.*, 2004).

A threshold dose-response approach can be employed in quantitative cancer risk assessment when supported by MOA information (Boobis *et al.*, 2006) based on the assumption that the adverse outcome (i.e., cancer) will not occur if exposure concentrations are below levels that do not alter tumorigenic key events. While it has been reported that the hepatic effects of PB are dose-dependent and exhibit a threshold (Elcombe *et al.*, 2014), very few studies have been conducted in multiple-dose protocols to that allow for dose-response assessment. In male CD-1 mice, the no-observable-effect level (NOEL) and tumorigenic dose was 10 and 75 mg/kg-day, respectively, after chronic dietary PB exposure (Whysner *et al.*, 1996). In male C57BL/10J mice, the NOEL and tumorigenic dose was 200 ppm (22 mg/kg-day) and 1000 ppm (113 mg/kg-day), respectively, after chronic dietary PB exposure (Jones *et al.*, 2009). Thus, these studies suggest the "threshold" for PB tumorigenesis in male mice may be between 22 and 75 mg/kg-day. Corresponding NOEL and tumorigenic doses in female mice have not been reported.

There are also very few published studies to include dose-response assessment for concurrently altered transcriptional and apical toxicity endpoints in parallel, particularly in the suspected threshold region considered more relevant to human and environmental exposures. Also lacking has been a concordance analysis of these early transcriptional and apical alterations across dose and time to contribute to the weight-of-evidence for the heptatotumorigenic MOA. Concordance analyses of dose and temporal relationships between key events and the ultimate apical effect contribute greatly to the weight-of-evidence for a particular MOA (Boobis *et al.*, 2006; Julien *et al.*, 2009), particularly the ability to link key molecular events to an adverse outcome at the biological level (Ankley *et al.*, 2010). The time-sensitive nature of toxicogenomic-based predictive profiles (Boverhof and Zacharewski, 2006; Paules, 2003), requires quantitative estimates of how the measurable intermediate key events relate to each other and progress over time leading to tumors. Being a potent and prototypical CAR agonist, low-dose potency estimates for transcriptional and apical key events after short-term PB exposures also facilitates the quantitative risk assessment of other CAR activating xenobiotics.

Materials and Methods

Six-week old male and female CD-1 mice were administered dietary PB at 0, 0.15, 1.5, 15, 75, or 150 mg/kg-day for 2 or 7 days. The 75 mg/kg-day dose was tumorigenic in male CD-1 mice after chronic feeding (Whysner *et al.*, 1996). At 2 and 7 days, traditional

clinical or "apical" endpoints assessed in 4 mice per sex and dose included plasma PB levels, cholesterol, alanine aminotransferase, aspartate aminotransferase, and triglycerides; Cyp1a1, Cyp1a2, Cyp2b10, Cyp3a11, and Cyp4a10 gene expression (measured by or via quantitative Polymerase Chain Reaction); enzyme activities representative of Cyp1a (via O-dealkylation of ethoxyresorufin), Cyp2b (via pentoxyresorufin), and Cyp3a (via benzyloxyresorufin) expression; hepatocyte cell proliferation (via continuous osmotic mini-pumps with bromodeoxyuridine) and associated liver weight and histopathology lesions.

Also at 2 and 7 days, mouse liver gene expression was assessed in 4 mice per dose and dose with Affymetrix Mouse Genome 430 2.0 GeneChip arrays (Affymetrix, Santa Clara, CA). This whole mouse genome array interrogates 34,000 variants and 39,000 transcripts from well-characterized mouse genes using 45,000 probe sets.

Dose-response modeling of apical and transcriptional data.

BMD-response analysis was conducted to estimate the dose at which specific genes, cellular pathways, and apical effects were altered above or below background (i.e., controls). BMD estimates for apical endpoints (BMDA), which included liver weight, hepatocellular proliferation, and liver qPCR and enzyme activity, were conducted using BMD software version 2.4 with the benchmark response set to one control standard deviation from the control mean (BMD_{1SD}) and included the lower 95% confidence limit

($BMDL_{1SD}$; Davis *et al.*, 2011; EPA, 2012). Best-fit model selection included consideration of the global goodness-of-fit *p* value (≥ 0.1), local scaled residual values of less than /2/, visual fit, and Akaike's Information Criterion (AIC is $-2L + 2p$, where L is the log-likelihood at the maximum likelihood estimates for p estimated parameters; Akaike, 1973) (U.S. EPA, 2012), and the margin between the BMD_{10} and $BMDL_{10,}$ with a preferences for ratios < 2 (Muri *et al.*, 2009).

Transcriptional benchmark dose (BMD_T) analysis of the liver microarray data was conducted using BMDExpress version 1.4.1 (Thomas *et al.*, 2007; Yang *et al.*, 2007) with some modifications. Briefly, the estimated consumed dietary intake (mg/kg-day) served as the dose metric and normalized linear signal intensities for all probe sets were fit as continuous data to the following 5 dose response models—Hill, linear, 2◦ polynomial, 3◦ polynomial, and power models. Each model was run assuming constant variance and the benchmark response factor was set to 1.349 the standard deviation in the control animals to estimate a BMD_T with a 10% increase in tail area (Thomas *et al.*, 2007). For the best-fit model selection, a nested likelihood ratio test was performed on the linear and polynomial models. If the more complex model provided a significantly improved fit ($p < 0.05$), the more complex model was selected. The simpler model was selected if the more complex model did not provide a significantly improved fit (Posada and Buckley, 2004). Similar to BMD_A guidelines (EPA, 2012), models with a global goodness-of-fit *p* value < 0.1 were excluded; *p* values of 1 indicate a perfect fit (i.e., the model's predicted response is identical

to the observed response). To select the best globally fitting model with the least complexity, the AIC for the selected polynomial model was then compared with the AIC for the Hill and power models. The model with the lowest AIC was selected as the final model. In cases where the "k" slope parameter for the Hill model was out of bounds, the Hill model was excluded from the final selection. Probe sets with a BMD_T value greater than the highest dose or a global goodness-of-fit *p* value<0.1 were considered unacceptable fits and thus were excluded. Affymetrix probe sets were converted into unique genes based on their NCBI Entrez Gene ID and promiscuous probe sets that measured more than one gene were removed. In addition to the BMDT analysis, IPA (Ingenuity Pathway Analysis, Ingenuity Systems, www.ingenuity.com) was used to map the differentially expressed genes (DEGs) to canonical pathways to reveal biologic processes inherent in the significantly filtered gene lists. Then, the median BMD_T and lower 95% confidence limit ($BMDL_T$) values from the genes represented in each pathway with an adequate statistical fit were used to summarize each pathway. $BMDL_T$ for key genes and pathways were also compared to apical benchmark dose levels ($BMDL_A$) to examine sex-specific differences, concordance, and progression.

Results

Differentially expressed genes (DEG) and most significant canonical pathways

There were less than 100 DEGs for the 0.15, 1.5, and 15 mg/kg-day groups in both sexes on both days (data not shown). The 75 mg/kg-day dose marked a transition point

from the 15 mg/kg-day dose where there was a 10-fold increase in the number of significant sequences for 2-day males and a corresponding 20-fold increase for the 7-day males compared with the 0.15 mg/kg-day dose. This trend was reciprocated in females at 2 and 7 days. The maximum number of significant sequences was observed in both sexes at the 150 mg/kg-day dose. Thus, the no-observable transcriptional effect level (NOTEL) and lowest observable transcriptional effect level (LOTEL) is considered 15 mg/kg-day and 75 mg/kg-day, respectively, for global gene expression in both sexes on both days. These NOTEL and LOTEL values are also consistent with the principal component analysis from this study (PCA results not shown).

The most significant canonical pathways identified from a classical *de novo* analysis of the genomic data included many redundant xenobiotic metabolism (CAR/PXR) and to a lesser extent cell-cycle and cellular stress response pathways (results not shown). When the redundant *de novo* metabolic pathways were condensed, the most prominent canonical pathways identified by IPA analysis at 2 days in both sexes included phase I and II metabolism, cell-cycle and cellular stress pathways, such as protein ubiquitination (**Figure 2.1**). In addition, the Eif2 signaling pathway and the role of Brca1 in the DNA damage response were also identified as prominent pathways in females at 2 days. As mentioned previously and consistent with lower plasma PB at 7 days compared with 2 days suggesting metabolic adaptation, global gene expression and gene-gene interactions were attenuated at 7 days compared with 2 days.

Transcriptional and apical benchmark dose-response analysis

Transcriptional (BMD_T) and apical (BMD_A) benchmark dose levels were estimated to describe potency in the low-dose region. The multiple low-dose levels, particularly when assessing global gene expression, facilitated low-dose extrapolation to approximate the doses below which changes in specific genes, cellular pathways, or apical effects could not be discerned from controls. Transcriptional benchmark dose levels for *Cyp2b10* expression, considered a biomarker of CAR activation, were comparable between both sexes and time points based on the highest intensity probe (1451787_at). The *Cyb2b10* BMD_T were 16 and 11 mg/kg-day in males and females at 2 days, respectively, and 8 and 8 mg/kg-day in males and females at 7 days, respectively. Factoring in the fit of the dose-response curve, the lower 95% confidence interval $BMDL_T$ estimate was 6 mg/kg-day at 2 and 7 days in both sexes. These BMD_T/$BMDL_T$ estimates for *Cyp2b10* are consistent with the NOTEL and LOTEL for *Cyp2b10* of 1.5 and 15 mg/kg-day, respectively, based on the DEG lists for both sexes on both days.

While the NOTEL was 15 mg/kg-day for global gene expression in both sexes on both days, pathway-level transcriptional benchmark dose (BMD_T) estimates (excluding redundant metabolic pathways as previously mentioned) suggested sex- and time-specific differences. Based on median BMD_T estimates at 2 days, the doses required to activate 2 significant cell-cycle pathways, Cell Cycle Control of Chromosomal Replication, and Cell Cycle: G2/M DNA Damage Checkpoint Regulation, were comparable between each other

and between the sexes (median BMD_T of ~50 mg/kg-day). However, median BMD_T estimates for xenobiotic metabolism, PXR/RXR activation, protein ubiquitination, Eif2 signaling, role of Brca1 in DNA damage, and glutathione-mediated detoxification pathways were approximately 2 to 4-fold lower in females (**Table 2.1**). These pathways were attenuated at 7 days based on higher median BMD_T estimates and showed little sex-specific differences. Overall, the range of pathway BMD_T estimates provides a more refined dose-response assessment compared to the global NOTEL of 15 mg/kg-day and the lowest observed transcriptional effect level (LOTEL) of 75 mg/kg-day for global gene expression in the liver (**Figure 2.2**).

BMD_A estimates of the apical endpoints are summarized in **Table 2.2**. In the low-dose region, BMD_{1SD} estimates suggest that PROD induction occurred at lower doses than BROD in both sexes and at lower doses in male compared to female mice. Of the dose-related apical liver effects, hepatocellular proliferation resulted in the lowest BMD_{1SD} estimates, which were more than an order of magnitude lower in females and progressed with time compared to males. The hepatocellular proliferation BMD_{1SD} values were 0.9 and 0.1 mg/kg-day in female mice fed PB for 2 and 7 days, respectively, compared to 13 and 14 mg/kg-day in male mice fed PB for 2 and 7 days, respectively. BMD_A levels were not estimated for hepatic histopathology (hepatocellular hypertrophy, mitotic figures, or necrosis) due to the small sample size per dose group (n=4). Unlike continuous data such as liver weight and cell proliferation for which the benchmark response is set to one control

group SD, the minimum sample size to estimate a 10% effect level for incidence data that is within the power of detection is 10 (1 out of 10 animals affected).

Comparisons of BMD_T and BMD_A Estimates

Benchmark dose estimates inform low-dose potency and enable a concordance analysis of key events at multiple levels of biological organization. BMD_{1SD} estimates for Cyp2B enzyme activity as measured via PROD, which ranged from 0.2-5 mg/kg-day, were lower than the BMD_T for *Cyp2b10* transcript levels, which ranged from 8-16 mg/kg-day. The variability of BMD_{1SD} estimates for *Cyp2b10* quantified by qPCR (5 to 28 mg/kg-day) was attributed to standard deviation estimates approximated based on the range rule (maximum value - minimum value/4), since standard deviation for qPCR data are not calculated analogously to those used by the benchmark dose models. Median BMD_T estimates for differentially expressed gene transcripts that mapped to the Mitotic Roles in Polo-like Kinases pathway was lower in males (44 mg/kg-day) compared to females (74 mg/kg-day). Median BMD_T estimates for other significant cell cycle pathways were comparable between sexes (46-56 mg/kg-day; **Table 2.1**) and higher than BMD_A estimates for hepatocellular proliferation, particularly in females (~0.1 to 0.9 mg/kg-day). Thus, BrdU labeling was a more sensitive measure of hepatocellular proliferation compared to transcriptional analysis of cell-cycle pathways, most likely due to the additive nature of the proliferation endpoint versus the single point-in-time measure for gene expression.

Discussion

The current dose-response and time-course study establishes NOTEL, NOAEL, and corresponding transcriptional (BMD_T) and apical (BMD_A) benchmark dose levels for several key and associated events that have been proposed for a PB-induced liver tumor MOA. These POD estimates, particularly when anchored together, can be used to inform the potency of PB relative to other CAR-activating xenobiotics with potential concern for human health risks.

Our study is the first to calculate a low-dose threshold for hepatocyte cell proliferation in male and female mice as well as to couple these estimates to other transcriptional and apical response measures. "Cell cycle" pathways are active after up to 3 days of PB exposure but less so after 7 to 14 exposure days (Currie, 2012) and these coincide with apical markers of DNA-synthesis or cell proliferation. Hepatocyte cell proliferation is considered a defining key event in the mode of rodent hepatotumorigenicity, not only since it is a sensitive measurable key event, but also since it may inform the human relevance of rodent liver tumors. Liver cell proliferation is not observed in CAR-humanized mice exposed to PB (Ross *et al.*, 2010) or upon long-term therapy with PB in humans.

Beyond the mapping of differentially expressed genes to cellular pathways, the current study is the first to use benchmark dose modeling to discern sex-specific differences

in early key events involved in PB-induced liver effects. An advantage of the present study design for dose-response modeling and low-dose extrapolation was the inclusion of multiple doses below (0.15, 1.5, and 15 mg/kg-day), at (75 mg/kg-day), and above (150 mg/kg-day) the NOEL and tumorigenic dose of 10 and 75 mg/kg-day, respectively, in CD-1 mice fed PB for 2 years (Whysner *et al.*, 1996). Notably, the NOTEL and LOTEL for global gene expression (15 and 75 mg/kg-day, respectively) in both sexes at both 2 and 7 days are consistent with these previously reported chronic effect levels.

One of the extrapolation assumptions inherent in the use of chronic rodent bioassay data to predict carcinogenic potential in humans is that high-dose responses in rodents are relevant at exposure doses which are orders of magnitude lower (Cohen and Ellwein, 1992). PB is a prototypical nongenotoxic carcinogen in which a threshold dose-response approach can be employed in quantitative cancer risk assessment when supported by MOA information (Boobis *et al.*, 2006) based on the assumption that the adverse outcome (i.e. cancer) will not occur if exposure concentrations are below levels that do not alter tumorgenic key events. When consistent with apical effects, transcriptional changes in genes and pathways can also serve as quantitative 'bioindicators' of treatment-related adverse responses (Preston, 2002). Given the 5-fold dose-spacing between the NOTEL and LOTEL, our pathway-level transcriptional benchmark dose (BMD_T) estimates may provide more informative dose estimates of pathway activation. Based on median BMD_T estimates, Phase I and II metabolism and cellular stress pathways were activated at 2- to 4-

fold lower doses in females compared to males at 2 days (**Table 2.1**). The enhanced ability to remove damaged proteins though Eif2 signaling or ubiquitination and to respond to DNA damage through Brca1 signaling combined with a greater CAR/PXR-mediated metabolism and glutathione-mediated detoxification capacity in females, could ultimately contribute to a lower susceptibility to tumor formation. Given the clear sex-specific differences in cell proliferation measured via BrdU, it is interesting that only one of the 3 prominent cell cycle pathways, the Mitotic Roles of Polo-like Kinases pathway, showed sex-specific differences in BMD_T estimates at 2 days (**Table 2.1**) with median BMD_T estimates suggesting activation at lower doses in males (44 mg/kg-day) compared to females (74 mg/kg-day). Since male mice are ultimately more susceptible to PB-induced tumor formation, the cell-cycle pathways reported here may be more reflective of PB's ability to exert CAR/PXR-mediated effects on the cell cycle compared to more general, albeit more sensitive BrdU measurements. While sex-specific potency differences in the Mitotic Roles of Polo-like Kinases pathway were identified at 2 days, it is difficult to propose which cell-cycle pathway(s) may ultimately contribute to liver tumor development given that the prominent cell-cycle pathways at 2 days were attenuated at 7 days in the present assessment. Further, liver cancer is known to be promoted by testosterone (Kemp and Drinkwater, 1989) and inhibited by ovarian hormones (Poole and Drinkwater, 1996). Recognizing the potency differences in BrdU response as counterintuitive to females ultimately having a lower liver tumor occurrence, the study duration of only 7 days may be a factor along with the interplay of modulating factors such as epigenetic changes (Phillips and Goodman, 2009), altered

gap junction intercellular communications (Chipman *et al.*, 2003), or altered regulation of apoptosis (Bursch *et al.*, 2005).

The pathway significance scores for "PXR/RXR Activation" were higher than for "Xenobiotic Metabolism" (Supplementary Spreadsheets S1-S4) in males, recognizing that both pathways overlap with respect to nuclear receptor activation (CAR, PXR, AhR, and PPARα). *Cyp2b10* was clearly the most potent Cyp isoform induced in both sexes on both days in terms of transcript abundance (fold change 35-100; Fig. 6), BMD_T (8-16 mg/kg-day), and qPCR gene expression (results not shown). *Cyp3a5*, a target gene of PXR activation, contributed to the PXR/RXR significance score only in males (fold change of 3-5 and BMD_T = 77-105 mg/kg-day) consistent with qPCR data (results not shown). AhR (fold change of 1.4 and BMD_T = 81 mg/kg-day in females) or *Cyp1a2* (fold change < 2 and BMD_T = 15 - 19 mg/kg-day in both sexes) contributed to the pathway significance scores only at 2 days. PPARα and/or *Cyp4a* transcription was repressed in both sexes in the present assessment, which is consistent with the low qPCR expression values for *Cyp4a10* (data not shown). These results suggest that CAR is the primary nuclear receptor mediating early liver effects in CD-1 mice exposed to phenobarbital.

In conclusion, these results identified low-dose transitions for apical and molecular endpoints which are consistent with the tumorigenic response to PB in rodents. To our knowledge, this is the first study to comprehensively characterize multiple key apical and

molecular endpoints below, at, and above the PB carcinogenic dose and to estimate potency in the low-dose region with benchmark dose (BMD) modeling. Being consistent with the known tumorigenic response of PB, our results also have utility when conducting quantitative risk assessments of CAR-mediated hepatocarcinogenesis.

Figures and Tables

Figure 2.1. Most significant cellular pathways at 2 days according to sex

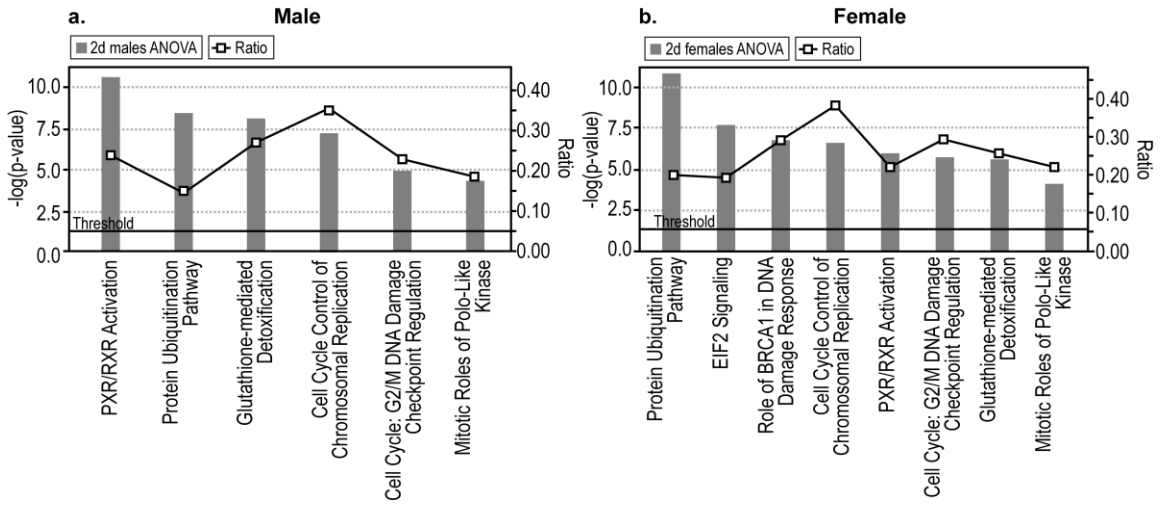

Figure 2.1 Legend. Selected significant cellular pathways altered according to sex after the redundant de novo metabolic pathways were condensed. This figure highlights a more prominent cellular stress response in females compared to males in which metabolic pathways predominate. This figure was generated by mapping DEGs in Ingenuity Pathway Knowledgebase®.

Figure 2.2. Range of transcriptional BMD levels (mg/kg-day) for selected pathways significantly altered in both sexes at 2 days

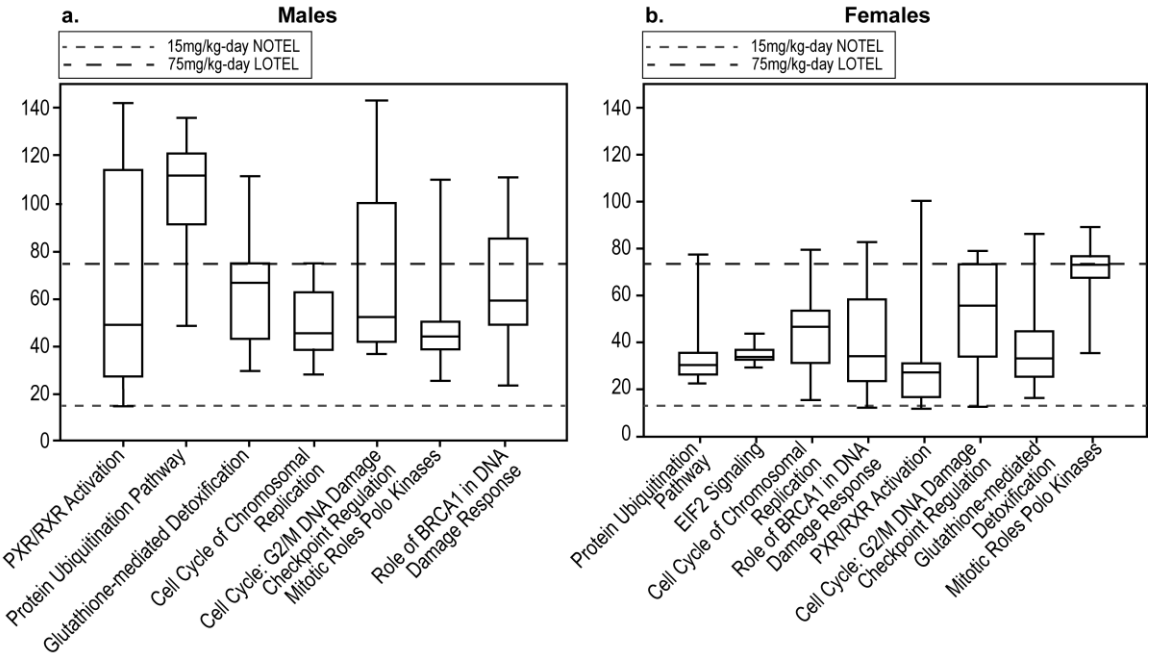

Figure 2.2 Legend. The range of transcriptional BMD levels (mg/kg-day) for selected pathways significantly altered in both sexes at 2 days. Corresponding values at 7 days were attenuated and thus not shown. Horizontal hatched-lines define the 15 mg/kg-day NOTEL and 75 mg/kg-day LOTEL.

Table 2.1. Pathway-level transcriptional benchmark dose estimates in male and female CD-1 mice exposed to phenobarbital in the diet for 2 or 7 days[1]

	2 days						7 days					
	Male			Female			Male			Female		
	% of path-way [2]	Median BMD (mg/kg-day)	Median BMDL (mg/kg-day)	% of path-way	Median BMD (mg/kg-day)	Median BMDL (mg/kg-day)	% of Path-way	Median BMD (mg/kg-day)	Median BMDL (mg/kg-day)	% of pathway	Median BMD (mg/kg-day)	Median BMDL (mg/kg-day)
Xenobiotic Metabolism	39% (29/75)	66	48	40% (30/75)	26	16	24% (18/75)	44	30	41% (31/75)	60	44
PXR/RXR Activation	15% (13/87)	49	37	15% (13/87)	27	16	10% (9/87)	46	35	15% (13/87)	46	35
Protein Ubiquitination Pathway	10% (27/268)	117	71	13% (36/268)	30	18	1% (2/268)	127 [3]	77 [3]	6% (16/268)	124	77
Eif2 Signaling Pathway [4]	3% (6/200)	123	76	8% (15/200)	34	19	0% (0/200)	Not Applicable		1% (2/200)	108 [3]	69 [3]
Cell Cycle Control of Chromosomal Replication	35% (11/31)	46	34	39% (12/31)	47	35	10% (3/31)	106	67	19% (6/31)	90	51
Role of Brca1 in DNA Damage Response [5]	18% (12/65)	60	43	26% (17/65)	34	19	8% (5/65)	85	57	11% (7/65)	70	40
Cell Cycle: G2/M DNA Damage Checkpoint Regulation	19% (9/48)	52	39	27% (13/48)	56	41	8% (4/48)	85	57	13% (6/48)	95	63
Mitotic Roles of Polo-like Kinases [5]	13% (9/70)	44	34	17% (12/70)	74	51	4% (3/70)	112	70	3% (2/70)	112 [3]	70 [3]
Glutathione-mediated Detoxification	20% (9/44)	67	48	20% (9/44)	33	19	16% (7/44)	42	25	23% (10/44)	54	41

[1] Median BMD (and 95% lower confidence limit BMDL) values from DEGs (see methods) that mapped to significant IPA pathways at 2 days and their corresponding values at 7 days.

[2] Percentage of pathway represented (number of DEGs with acceptable dose-response fits/total number in pathway).

[3] Average of 2 DEGs remaining in analysis at 7 days.

[4] Eif2 Signaling was a prominent pathway only in females at 2 days. Although 22/37 probes mapping to this pathway were unacceptable fits, the 15 probes with acceptable fits had very similar BMD_T values (see Fig. 8b; the corresponding benchmark dose estimates in males are shown for comparison).

[5] Role of Brca1 in DNA Damage Response and Mitotic Roles of Polo-like Kinases were more prominent (% represented) in females at 2 days compared to males (the corresponding benchmark dose estimates in males are shown for comparison).

Table 2.2. Benchmark dose estimates for apical and biomarker endpoints in male and female CD-1 mice exposed to phenobarbital in the diet for 2 or 7 days.

	Male		Female	
2 days	BMD [1] (mg/kg-day)	BMDL [1] (mg/kg-day)	BMD [1] (mg/kg-day)	BMDL [1] (mg/kg-day)
Absolute liver weight	110	97	73	49
Relative liver weight	79	68	69	47
Hepatic Cyp2b (PROD)	0.2	0.1	4.7	2.6
Hepatic Cyp3a (BROD)	2.3	1.3	8.7	5.1
Cyp2b10 qPCR [2]	28	18	13	10
Hepatocyte cell proliferation	13	10	0.9	0.6
	Male		Female	
7 days	BMD [1] (mg/kg-day)	BMDL [1] (mg/kg-day)	BMD [1] (mg/kg-day)	BMDL[1] (mg/kg-day)
Absolute liver weight	30	24	20	5.8
Relative liver weight	20	16	12	7.0
Hepatic Cyp2b (PROD)	2.4	1.7	-	-
Hepatic Cyp3a (BROD)	7.8	4.8	2.9	0.3
Cyp2b10 qPCR [2]	18	13	5.2	4.1
Hepatocyte cell proliferation	14	11	0.1	0.1

CHAPTER 3

DOSE- AND TIME-COURSE INDICATORS OF EARLY KEY EVENTS IN A CYTOTOXICITY-MEDIATED MODE OF ACTION FOR RODENT URINARY BLADDER TUMORIGENESIS

Abstract

Diuron is a substituted urea compound used worldwide as a broad-spectrum herbicide. In carcinogenicity studies, diuron induces urinary bladder tumors in rats after chronic high-dose dietary exposures most likely through a cytotoxicity-mediated mode of action (MOA). The present assessment estimates potency for activation of key functional pathways in this MOA identified from global gene expression profiling at 7 days and 20 weeks and examines their concordance with apical key events over time, including urothelial cell cytotoxicity, proliferation, hyperplasia and ultimately tumors. The most sensitive pathways in the urothelium at 20 weeks involved immune cell responses based on lower quartile (Q1) pathway transcriptional benchmark dose levels (BMD_T) of 4-5 mg/kg-day, consistent with the apical benchmark dose (BMD_A) of 4 mg/kg-day for urothelial cytotoxicity observed using scanning electron microscopy. Xenobiotic metabolism/detoxification and oxidative stress pathways were active at Q1 BMD_T of 25-31 mg/kg-day, consistent with the BMD_A for urothelial simple hyperplasia of 22 mg/kg-day at 20 weeks and the suspected tumor threshold of 23-32 mg/kg-day at 2 years. A similar metabolic and oxidative stress response with comparable potency was seen at 7 days (Q1

BMD_T of 18-25 mg/kg-day) without ultrastructural or histopathological evidence of urothelial alterations. Using a case study approach, this assessment demonstrates that dose responses corresponding to key MOA events and tumorigenic potency can be established based on transcriptional effects following short-term exposure.

Keywords: transcriptional benchmark dose, diuron, dose-response, mode of action, phenotypic anchoring, urinary bladder

Introduction

Dose- and time-course indicators for early key events in a xenobiotic mode of action (MOA) contribute to the weight of evidence for a proposed MOA and foster efficiency in quantitative risk assessment (Ankley *et al.*, 2010; Boobis *et al.*, 2006; Julien *et al.*, 2009; Meek *et al.*, 2014). Diuron (3-(3,4-dichlorophenyl)-1,1-dimethylurea) is a substituted urea compound used worldwide as both a pre- and a post-emergent broad-spectrum herbicide to control a wide variety of annual and perennial broadleaf and grassy weeds in crop and non-crop areas (Da Rocha *et al.*, 2014; U.S. EPA, 2003). In guideline carcinogenicity bioassays, this compound resulted in urinary bladder tumors in Wistar rats after chronic high-dose dietary exposures, with male rats showing greater sensitivity than female rats (Bayer AG, 1985- as reported by APVMA, 2011 and U.S. EPA, 1997). Previous research has demonstrated a cytotoxicity-mediated mode of action (MOA) for urothelial tumors and proposed that the key events involve metabolism to putative toxic moieties, mainly N-(3,4-dichlorophenyl) urea (DCPU). This metabolite is excreted and concentrated in the urine, leading to direct cytotoxicity characterized by urothelial cell degeneration, necrosis, and cellular exfoliation, followed by sustained regenerative cell proliferation, urothelial hyperplasia, and eventually tumors (Cardosa *et al.*, 2013; Da Rocha *et al.*, 2014; Ihlaseh-Catalano *et al.*, in preparation; Ihlaseh *et al.*, 2011).

Prior studies indicate a low concern for the genotoxicity and mutagenicity of diuron as an alternative MOA for urinary bladder tumorigenesis (de Camargo, 2013; Health

Canada, 2011; U.S. EPA, 2003). This evidence includes lack of mutagenicity in 11 assays encompassing six strains of *S. typhimurium* (TA97, TA98, TA100, TA1535, TA1537, TA1538) as well as *Escherichia coli* pKM101 exposed to a range of diuron concentrations up to 5000 μg/plate with and without metabolic activation with rodent liver S9 fractions (reviewed by APVMA, 2011). Diuron was also not mutagenic in eukaryotic test systems at the hypoxanthine–guanine phosphoribosyltransferase locus in Chinese hamster ovary (CHO) cells. Several other assays support low concern for diuron genotoxicity (reviewed by APVMA, 2011 and U.S. EPA, 2003) including analyses of the target urothelial cells in vivo (Nascimento *et al.*, 2006). Interpretation of positive or equivocal responses (reviewed by APVMA, 2011 and Gee, 2010), such as for clastogenicity in cultured human lymphocytes (Herbold, 1989) or altered DNA synthesis/repair in rat primary hepatocytes (Arce, 1985), is confounded by concurrent cytotoxicity, visible test substance precipitation, and/or lack of reproducibility/confirmation.

For nongenotoxic carcinogens, a threshold dose-response approach can be employed in quantitative cancer risk assessment when supported by MOA information (Boobis *et al.*, 2006; U.S. EPA, 2005) based on the assumption that the adverse outcome (i.e., cancer) will not occur if exposure concentrations are below levels that do not induce key events preceding tumorigenesis. When consistent with apical effects, transcriptional changes in genes and pathways can also serve as quantitative bioindicators of treatment-related adverse responses (Preston, 2002). Benchmark dose levels are useful in quantitative

risk assessment not only as preferred points of departure relative to NOAEL and LOAEL (no- and lowest-observable adverse effect levels, respectively) values but also as standardized means of comparing low-dose potency for chemicals associated with the same effects or MOA (U.S EPA, 2012). Further, the ability to couple transcriptional and apical dose-responses after short-term exposures is consistent with the 21st century vision for more efficient risk assessment with reduced animal testing (Bhat *et al.*, 2013).

Diuron was selected as the present case study due to the availability of dose- and time-course data for key events associated with the threshold MOA for urinary bladder tumorigenesis. Recognizing this, the large dose spacing and steep dose-response for bladder tumor formation, as observed in the diuron 2-year rat feeding study (Bayer AG, 1985- as reported by APVMA, 2011 and U.S. EPA, 1997), makes discerning a putative threshold for urothelial cytotoxicity challenging. At 0, 25, 250 or 2500 ppm dietary diuron, the incidence of bladder tumors was 2%, 0%, 2% and 73%, respectively, in male rats. Further, recent 20-week dietary exposure studies that included additional and more closely spaced dose levels, and notably a 1250 ppm dose group, suggested that the peak response may be achieved at dietary concentrations lower than 2500 ppm (at which 70% of rats had urothelial hyperplasia), possibly at 1250 ppm (at which 80% of rats had urothelial hyperplasia) (Cardoso *et al.*, 2013; Ihlaseh *et al.*, 2011). This evidence, in combination with the lack of mutagenicity and the non-linear dose-response for tumor formation,

supports the importance for identifying a threshold dose for diuron-induced urothelial cytotoxicity.

The purpose of the present assessment was to extend previous research on diuron's cytotoxicity-mediated MOA by conducting quantitative benchmark dose-response modeling in order to estimate low-dose potency for activation of key genes and functional pathways identified from global expression profiling at 7 days and 20 weeks. These transcriptional benchmark dose (BMD_T) levels were compared to apical benchmark dose (BMD_A) levels for key events, including urothelial cell injury, proliferation, hyperplasia and tumors, in order to determine whether the cytotoxicity-mediated MOA for rodent urinary bladder tumorigenesis and its corresponding dose threshold could be discerned at these earlier time points. We anticipate that these types of potency estimates generated from short-term evaluation methods can be used for chemicals lacking chronic/carcinogenicity data and thus help prioritize future research needs and assessment strategies.

Materials and Methods

Test diet preparation and animal exposure protocols have been described previously (Cardosa *et al.*, 2013; Ihlaseh-Catalano *et al.*, in preparation; Ihlaseh *et al.*, 2011). Briefly, these multiple-dose level studies were designed to assess urinary bladder histomorphology using light and/or scanning electron microscopy (SEM) and global gene expression with

Affymetrix rat 230 2.0 whole genome arrays after 7 days or 20 weeks of dietary diuron (97% purity) exposure in male Wistar rats, the more sensitive sex. Urinary bladder cell proliferation via bromodeoxyuridine (BrdU) immunohistochemistry was also assessed after 20 weeks of exposure (Cardosa *et al.*, 2013). The 7-day and 20-week studies were conducted in the same facility (Department of Pathology, Botucatu Medical School, UNESP—Univ Estadual Paulista, Botucatu, Brazil). Urinary bladder RNA was processed at the U.S. EPA National Health and Environmental Effects Research Laboratory (Research Triangle Park, NC). In the 7-day study, urinary bladder gene expression was assessed in four rats per dose at dietary diuron concentrations of 0, 125, 500, or 2500 ppm for 7 days; 2 outliers (one control and low-dose rat) were omitted from further analysis based on clearly divergent Principal Component Analysis (PCA) profiles (Ihlaseh-Catalano *et al.*, in preparation). In the 20-week studies, gene expression was assessed in 3 rats per dose at 0, 60, 125, 500, 1250, or 2500 ppm in the 20-week studies (Cardosa *et al.*, 2013; Ihlaseh *et al.*, 2011). The highest dose of 2500 ppm was considered tumorigenic based on the 24-month rat feeding study (Bayer AG, 1985; based on APVMA, 2011 and U.S. EPA, 1997). Urothelial cytotoxicity was evaluated by histopathology and SEM in ten rats per dose, as reported previously (Cardosa *et al.*, 2013; Ihlaseh *et al.*, 2011); these data are summarized in **Table 3.1**.

Transcriptional benchmark dose (BMD_T) estimation

BMD_T are intended to reflect the dose at which transcription is altered above or below controls in an approach analogous to BMD_A for traditional toxicity data (Bhat *et al*., 2013; Geter *et al*., 2014). In the present assessment and comparable to analyses described previously (Cardosa *et al*., 2013; Ihlaseh-Catalano *et al*., in preparation; Ihlaseh *et al*., 2011), statistically differentially expressed genes (DEGs) were identified from global expression profiling at 7 days and 20 weeks by importing the raw signal intensities from each scan (.cel files) into profiles using Rosetta Resolver software (Rosetta Inpharmatics, Kirkland, WA) and Rosetta error model for normalization (Weng *et al*., 2006) and a one-way ANOVA by dose with a Benjamini-Hochberg false discovery rate test ($p \leq 0.05$) for significance. Fold change (FC) for each sequence was computed for each calculated ratio, representative of a given sequence abundance. IPA software (Ingenuity Pathway Analysis, Ingenuity® Systems, www.ingenuity.com) was used for functional annotation of the DEGs to canonical pathways. Given that only a fraction of DEGs altered by chemical exposure will be annotated to biological pathways, a FC cut-off for inclusion was not applied in the present assessment based on previous studies determining that, of the fraction of DEGs that map to pathways, only a portion of these will be dose-responsive and result in acceptable BMD_T statistical fits (Bhat *et al.*, 2013; Geter *et al.*, 2014). In the present assessment, the most significant pathways with less than 5 BMD_T values were omitted from further analyses due to the low confidence associated with proposing a potency for pathway activation (see Results).

While previous expression profiling assessing urinary bladder dose-response relationships at 20 weeks did not include quantitative dose-response modeling, qualitative patterns were seen such that the four treatment groups could be combined into 2 larger groups, a "low-dose group" (60 and 125 ppm) predominantly reflecting a metabolic response and a "high-dose group" (1250 and 2500 ppm) represented by genes and pathways involved in amino acid metabolism, energy metabolism, lipid metabolism, oxidative stress response, signaling, immune system adhesion, and cofactor/vitamin metabolism (Ihlaseh *et al.*, 2011). This separation was supported by distinct intragroup similarities and intergroup differences in several aspects of the data, including the principal component, Venn diagram, and pathway-level analyses, as well as the statistically significant increase in incidence of urothelial simple hyperplasia at 1250 and 2500 ppm but not at 60 or 125 ppm (Ihlaseh *et al.*, 2011). Similarly, the incidence of urothelial simple hyperplasia and cell proliferation was statistically increased at 1250 and 2500 ppm but not $\leq$ 500 ppm dietary diuron in another 20-week study (Cardoso *et al*., 2013) and the incidence of bladder tumors was increased at 2500 ppm but not at the intermediate dose of 250 ppm at 2 years (Bayer AG, 1985).

The main purpose of the present transcriptional dose-response assessment was to estimate BMD_T for functional pathways altered at diuron doses associated with key events in the MOA, specifically urothelial cell proliferation, hyperplasia and tumors. To do this, BMD_T and 95% lower confidence limit ($BMDL_T$) for each DEG comprising the most

significant pathways in the "high-dose group" (1250 and 2500 ppm) at 20 weeks were estimated (i.e. one BMD_T/$BMDL_T$ for each DEG assessed across the range of experimental doses) with BMDExpress software (version 1.4.1, 2012). In the 7-day study (Ihlaseh-Catalano *et al.*, in preparation), given the lack of urothelial lesions observable via light or SEM evaluations and the short-term duration, BMD_T and $BMDL_T$ were estimated for the most significant pathways across all dose levels (125 to 2500 ppm). The estimated mean consumed dietary diuron dose (mg/kg-day) over the course of treatment was the dose metric for BMD_T modeling. For the 7-day study (Ihlaseh-Catalano *et al.*, in preparation), the mean diuron intakes were estimated to be 0, 11.9, 47.2, or 204.2 mg/kg-day at dietary diuron concentrations of 0, 125, 500 or 2500 ppm, respectively. For the 20-week study (Ihlaseh *et al.*, 2011), the mean diuron intakes were estimated to be 0, 3.6, 7.7, 77.4, or 149.5 mg/kg-day at dietary diuron concentrations of 0, 60, 125, 1250, or 2500 ppm, respectively.

Normalized linear signal intensities for each probe set were fit to Hill, power (restricted), linear (1°), and polynomial (2°) dose-response models. Each model was run assuming constant variance, and the benchmark response factor was set to 1.349 of the control group standard deviation (SD). This represents 11% change in signal intensity tail area due to allowance for a 1% change (0.5% in each tail) to occur in the absence of exposure (Thomas *et al.*, 2007b; Yang *et al.*, 2007). This 10% change in transcriptional response, either up- or down-regulated compared to controls, is intended to be analogous

to apical benchmark dose modeling. For best-fit model selection, a nested likelihood ratio test was performed on the linear and polynomial 2° models. If the more complex model provided a significantly improved fit ($p < 0.05$), the more complex model was selected. The simpler model was selected if the more complex model did not provide a significantly improved fit. Similar to apical benchmark dose guidelines (U.S. EPA, 2012), models with a global goodness-of-fit p value < 0.1 were excluded; p values of 1 indicate a perfect fit (i.e., the predicted response of model is identical to the observed response). To select the best globally-fitting model with the least complexity, the Akaike Information Criterion (AIC is $-2L + 2p$, where L is the log-likelihood at the maximum likelihood estimates [MLEs] for p estimated parameters) (Aikaike, 1973) for the selected polynomial model was then compared with the AIC for the Hill and power models. The model with the lowest AIC was selected as the final model. In cases where the ‘‘k’’ slope parameter for the Hill model was out of bounds, the Hill model was excluded from the final selection. Unacceptable fits that were excluded from further analyses were probe sets with a BMD_T value greater than the highest dose or a global goodness-of-fit p value < 0.1. For remaining models with an adequate statistical fit, the best-fitting BMD_T for each DEG comprising the most significant canonical pathways were selected. Potency for pathway activation was summarized using the lower quartile (Q1) and median (Q2) BMD_T values for pathways with at least 5 BMD_T values.

Apical benchmark dose (BMD_A) estimation for urinary bladder tumors and urothelial precursor key events

Apical effects are clinical, functional, or morphologic effects such as increased cell proliferation or histopathologic target organ lesions. Currently, these effects are used to inform more traditional types of quantitative risk assessment. Mean consumed dietary diuron dose (mg/kg-day) over the course of treatment served as the dose metric for BMD_A modeling using Benchmark Dose software (version 2.4, U.S. EPA, 2013). As reported above for the first 20-week study (Ihlaseh *et al.,* 2011), the mean diuron intakes ranged from 3.6 to 149.5 mg/kg-day for dietary diuron concentrations from 60 to 2500 ppm. For the second 20-week study (Cardoso *et al.,* 2013), mean diuron intakes were estimated in the present assessment to be 0, 3.5, 7.5, 30.3, 76.3, or 146.5 mg/kg-day at dietary diuron concentrations of 0, 60, 125, 500, 1250, or 2500 ppm, respectively, These mg/kg-day doses were slightly higher than reported by Cardoso *et al.* (2013) since the original estimates (2.73 to 101.6 mg/kg-day) were based on mean terminal body weight values, which were lower than controls at study termination at the high dose levels. In contrast, the present assessment used the 20-week body weight and food intake averages. The study designs and results between both 20-week studies were comparable but used slightly different dose spacing (Cardoso *et al.,* 2013; Ihlaseh *et al.,* 2011); thus, BMD_A values of urothelial hyperplasia were estimated for each study as well as for the merged study results to determine whether a statistically improved BMD_A fit could be obtained with the additional dose levels, as recommended by U.S. EPA (2012) guidance. For urinary bladder tumors

after lifetime exposure (Bayer AG, 1985), diuron intake and incidence data were as reported by APVMA (2011) and U.S. EPA (1997). Mean diuron intakes were reported to be 0, 1.02, 10.46, or 111.17 mg/kg-day at dietary diuron concentrations of 0, 25, 250, or 2500 ppm, respectively.

Consistent with U.S. EPA (2012) guidelines for quantal data, the 10% response rate above the control incidence (BMD_{10}) and its lower 95% confidence limit ($BMDL_{10}$) were estimated for the incidence of simple hyperplasia observed via light microscopy and for urothelial alterations observed via SEM after 20 weeks (Cardosa *et al.*, 2013; Ihlaseh *et al.*, 2011), as well as for the combined incidence of urinary bladder papillomas and carcinomas after chronic dietary exposure for 24 months (Bayer AG, 1985; based on APVMA, 2011 and U.S. EPA, 1997) in male rats. Based on urothelial BrdU labeling data reported in Cardosa *et al.*, (2013), the central estimate (BMD_{1SD}) and its lower 95% confidence interval for the response at one control standard deviation was used to define the benchmark response ($BMDL_{1SD}$) for increased urothelial cell proliferation at 20 weeks, consistent with U.S. EPA (2012) guidelines for continuous response data. The urothelial data used for BMD_A modeling are presented in **Table 3.1**.

The 5 factors collectively taken into consideration for selecting the best-fit model included the global goodness-of-fit *p* value (must be ≥ 0.1 but highest value preferred); lowest AIC value, Chi^2 residual values of less than 2 at each dose level, visual fit (U.S.

EPA, 2012), and the margin between the BMD_{10} and $BMDL_{10,}$ with a preference for ratios < 2 (Muri *et al*., 2009). The best-fit BMD_A levels for urothelial cell proliferation, simple hyperplasia, and altered morphology on SEM at 20 weeks and bladder tumors at 2 years were compared to the 7-day and 20-week lower quartile (Q1) and median (Q2) $BMDL_T$ estimates as a measure of potency for activation of the most significant functional pathways. Urothelial lesions were not observed in the 7-day study (Ihlaseh-Catalano *et al.*, in preparation) and thus BMD_A values were not estimated at 7 days.

Results

Apical responses in the urinary bladder after diuron exposure

No morphological lesions of the urothelium were evident via light microscopy or SEM in the 7-day study at any dose, including the highest tested (and tumorigenic) dietary concentration of 2500 ppm (Ihlaseh-Catalano *et al.*, in preparation). Of note, another 7-day dietary study found a low incidence of simple hyperplasia (1 of 10 rats) at the only tested concentration of 2500 ppm (Da Rocha *et al.*, 2012); these rats also had a slightly higher rate of urothelial alterations visible via SEM (4 of 10 rats had Grade 3 on a 5-point scale) compared to controls (1 of 10 rats had Grade 3). While the single dose level design precludes estimation of a BMD_{10} for simple hyperplasia, the empirical 10% response level for simple hyperplasia is 2500 ppm (mg/kg-day intake not reported) in the Da Rocha *et al.* (2012) 7-day study.

A dose-related increase in urothelial simple hyperplasia was evident after 20 weeks of dietary diuron exposure in 2 separate and comparably designed studies that tested up to 2500 ppm (Cardosa *et al.*, 2013; Ihlaseh *et al.*, 2011). It should be noted that the peak hyperplasia response (80%) was attained at 1250 ppm relative to 2500 ppm (70%). The same pattern was observed with increased urothelial cell proliferation (7x and 4x compared to controls at 1250 and 2500 ppm, respectively). U.S. EPA (2012) guidance assumes benchmark dose modeling in the monotonic response range (i.e., that a higher dose will have an equal or greater effect than a lower dose) and recognizes that non-monotonic relationships are common with high-dose data. Thus, benchmark dose modeling of urothelial hyperplasia and cell proliferation in the present assessment was conducted without including the high dose data (2500 ppm). Urothelial hyperplasia data were modeled for each individual study (Cardosa *et al.*, 2013; Ihlaseh *et al.*, 2011) and with the merged data from both studies to determine whether a statistically improved fit and thus higher confidence in BMD levels could be obtained with the higher number of dose levels. The results of benchmark dose modeling of urothelial lesions are summarized in **Table 3.2**. Overall, the best fitting model (Probit, global goodness-of-fit p value of 0.642) identified a BMD_A and its 95th percentile lower limit ($BMDL_A$) for urothelial simple hyperplasia at 20 weeks of 22 mg/kg-day and 16 mg/kg-day, respectively, obtained from the merged study data (**Fig. 3.1**). When modeled independently, the best-fitting model for each study (Probit) identified the same BMD_A and $BMDL_A$ (22 mg/kg-day and 14 mg/kg-day, respectively; model results not shown) which were also similar to the merged data. However, both

studies independently had slightly lower global goodness-of-fit *p* values (0.5469 or 0.3411) compared to the merged data.

Urothelial cytotoxicity was investigated with SEM at 20 weeks in only the Cardoso *et al.* (2013) study and the BMD_A and its 95th percentile lower limit ($BMDL_A$) for urothelial lesions observable with SEM was 4 mg/kg-day and 2 mg/kg-day, respectively (**Fig. 3.1**). While there was a dose-related increase in urothelial cell proliferation measured via BrdU immunohistochemistry in the same study (Cardoso *et al.*, 2013), the BMD_{1SD} and $BMDL_{1SD}$ for this response was 52 and 45 mg/kg-day, respectively (**Fig. 3.1**), suggesting that BrdU labeling is a less sensitive indicator of diuron toxicity to the urothelium at 20 weeks relative to light or SEM evaluations of the urothelium.

With respect to the BMD for urothelial tumors in male rats in the 2-year study (Bayer AG, 1985), the BMD_{10} and $BMDL_{10}$ for the combined incidence of urinary bladder papilloma and carcinoma was 32 mg/kg-day and 17 mg/kg-day, respectively (model results not shown) based on tumor rates of 2%, 0%, 2%, and 73% at 0, 25 (1 mg/kg-day), 250 (11 mg/kg-day), and 2500 ppm (111 mg/kg-day), respectively. However, as mentioned, the 20-week studies that included more closely spaced dose levels and a 1250 ppm concentration identified a peak hyperplasia response (80% at 1250 ppm) compared to the highest concentration of 2500 ppm (70%) (Cardosa *et al.*, 2013; Ihlaseh *et al.*, 2011) (**Table 3.1**). Thus, the steep dose response for tumors suggests a threshold dose for diuron-induced

urothelial cytototoxicity but the 10-fold dose spacing introduces uncertainty in the threshold region between the mid (2% tumors at 250 ppm) and high-dose (73% tumors at 2500 ppm) in the chronic study. Since the urothelial simple hyperplasia rate at 20 and 52 weeks (70%) is the same as the tumor rate at 2 years (73%) at 2500 ppm, a hypothetical 1250 ppm concentration with a tumor rate of 80% (mirroring the hyperplasia rate at 1250 ppm at 20 weeks) would result in a projected BMD_{10} and $BMDL_{10}$ of 23 mg/kg-day and 14 mg/kg-day, respectively (model results not shown). Overall, the BMD_{10} and $BMDL_{10}$ for urothelial tumors (combined incidence of papilloma or carcinoma) is 32 mg/kg-day and 17 mg/kg-day, respectively, based on the empirical data, but could be slightly lower if the peak response is attained at 1250 ppm, a dose which was not tested chronically.

A BMD_{10} for urothelial hyperplasia in male rats from the 2-year study (Bayer AG, 1985) was not estimated since the incidence was not dose-related, being observed at 13/50 (26%), 5/50 (10%), 16/50 (32%) and 14/49 (29%) male rats at 0, 25, 250, or 2500 ppm, respectively (all severity grades combined or Grades 1, 2, and 3). Based on the incidence of Grade 2 or 3 hyperplasia, which was increased in high-dose rats compared to controls (2/50, 0/50, 1/50 and 13/49 male rats at 0, 25, 250, or 2500 ppm, respectively), the BMD_{10} and $BMDL_{10}$ is 74 mg/kg-day and 60 mg/kg-day, respectively. However, the hyperplasia rate at 2 years and thus the corresponding BMD_{10} estimates were not considered plausible since the rate of Grade 2 or 3 hyperplasia at 2500 ppm at 2 years (27%) was lower than the hyperplasia rate at 2500 ppm at 20 weeks (70%; Cardosa *et al.*, 2013; Ihlaseh *et al.*, 2011)

and 52 weeks (70%; Bayer AG, 1985) as well as the bladder tumor rate at 2500 ppm at 2 years (73%; Bayer AG, 1985). Further, the 20- and 52-week hyperplasia rates at 2500 ppm were the same as the 2-year tumor rate, which is consistent with the temporal progression of proposed key events in the cytotoxicity-mediated MOA.

Similar to the lack of a reliable BMD for urothelial hyperplasia in male rats in the 2-year study (Bayer AG, 1985), a BMD for could not be estimated for the rate of urothelial hyperplasia at 52 weeks since mean diuron intake (mg/kg-day) at 52 weeks (or food intake and body weight data to estimate the intake) were not available. Similar to the 2-year rates, the incidence of urothelial hyperplasia (all severity grades combined or Grades 1, 2, or 3) at 52 weeks was not clearly dose-related in treated rats compared to controls (3/10, 5/10, 5/10 and 7/10 male rats at 0, 25, 250, or 2500 ppm, respectively). However, as mentioned, the incidence of Grade 2 or 3 urothelial hyperplasia at 52 weeks was consistent with the 20 week studies in that 0/10, 0/10, 1/10 and 7/10 male rats at 0, 25, 250, or 2500 ppm, respectively, were affected (Bayer AG, 1985).

20-week global expression profiling studies

Global expression profiling of male rat urinary bladder tissue was assessed after multiple-dose exposures for 7 days or 20-weeks. Relative to the 7-day study, the 20-week exposure is more reflective of a long-term exposure scenario. Similar to the previous IPA analysis (Ihlaseh *et al.*, 2011), the overall most significant canonical pathways at diuron

exposures inducing a significant increase in urothelial hyperplasia (1250 and 2500 ppm) included aryl hydrocarbon receptor (AhR) signaling, xenobiotic metabolism/detoxification, and oxidative stress pathways such as glutathione-mediated detoxification and Nrf2-mediated oxidative stress, followed by immune response (T-cell) and intracellular signaling pathways **(Table 3.3)**. The most significant pathways tended to have more genes comprising the pathway and contributing to the significance score. For example, the most significant dose-related pathway (-log *p* value of 8.2), AhR signaling, had 24 genes that comprised the significance score and 17 of these genes had acceptable BMD_T statistical fits (17 of 171 or 10% of the total genes in this pathway). However, the pathway significance scores did not necessarily correlate to potency for pathway activation (i.e., the most sensitive pathway) based on median or Q1 BMD_T values for genes comprising each significant pathway (**Table 3.4)**. Whereas the AhR signaling pathway was the most significant pathway, the most sensitive pathways at 20 weeks were immune (T-cell) response pathways since they had the lowest Q1 BMD_T values (4-5 mg/kg-day) (**Fig. 3.2**). The 3 related T-cell response pathways included CD28 signaling in T-helper cells (9 of 136 pathway genes, Q1 BMD_T of 5 mg/kg-day), calcium-induced T-lymphocyte apoptosis (8 of 71 pathway genes, Q1 BMD_T of 5 mg/kg-day), and Nur77 signaling in T lymphocytes (7 of 208 pathway genes, Q1 BMD_T of 4 mg/kg-day). Three common DEGs in these pathways that were also the most sensitive (i.e., had the lowest BMD_T of 4-5 mg/kg-day) represented 3 isoforms of major histocompatibility complex class II proteins (HLA-DMB, HLA-DRA, and HLA-DRB1). As a comparative measure of potency, the Q1

BMD_T for the 17 genes comprising the most significant pathway, AhR signaling, was 28 mg/kg-day (**Appendix C Table C1**). Three related ethanol degradation pathways, 2 related RhoGDI/RhoA signaling pathways, and the lipid antigen presentation by CD1 pathway were omitted since they had less than 5 BMD_T values available to propose potency for pathway activation at 20 weeks (**Table 3.3).**

Notably, the Q1 BMD_T values of 4 mg/kg-day for the most sensitive pathways (i.e., T-cell or immune responses, **Table 3.4**) were consistent with the apical BMD_A of 4 mg/kg-day for ultrastructural urothelial lesions observable with SEM at 20 weeks. The incidence of exposed rats with SEM lesions judged as severe (Grade 4 and 5) was increased compared to controls and characterized by areas of necrosis and cell hyperplasia (Cardoso *et al.*, 2013). Thus, ultrastructural lesions were evident at 5-fold lower doses than observable via light microscopy based on the BMD_A of 22 mg/kg-day for urothelial simple hyperplasia. Xenobiotic metabolism/detoxification and oxidative stress pathways were active at Q1 BMD_T of 25-31 mg/kg-day, consistent with the apical BMD_{10} for urothelial simple hyperplasia of 22 mg/kg-day and the suspected tumor threshold of 23 mg/kg-day (based on hypothetical peak at 1250 ppm) to 32 mg/kg-day (based on empirical study data) at 2 years. Median (Q2) BMD_T of 33-53 mg/kg-day for the same xenobiotic metabolism/detoxification and oxidative stress pathways corresponded well to the apical BMD_{10} for urothelial cell proliferation of 52 mg/kg-day (lower 95% confidence limit $BMDL_{10}$ of 45 mg/kg-day).

7-day global expression profiling study

Despite the lack of urothelial alterations visible via scanning or light microscopic evaluation at 7 days, several of the same canonical pathways operative at 20 weeks were also the most statistically enriched pathways at 7 days (**Table 3.5**). Overall, the most significant pathways had Q1 BMD_T of 15-36 mg/kg-day corresponding to similar median BMD_T estimates of 24-42 mg/kg-day **(Table 3.6** and **Fig. 3.3**). For 5 xenobiotic metabolism/detoxification and oxidative stress pathways also prominent at 20 weeks, Q1 BMD_T at 7 days were 21-25 mg/kg-day corresponding to median BMD_T of 25-34 mg/kg-day. The 5 common pathways at 7 days and 20 weeks, recognizing some redundancy in annotation and function (**Appendix C**), included AhR signaling, xenobiotic metabolism signaling, glutathione-mediated detoxification, Nrf2-mediated oxidative stress, and LPS/IL-1-mediated inhibition of RXR function, consistent with a cytotoxicity-mediated MOA.

There were also some distinctions between the 7-day and the 20-week transcriptional profiles. For example, the most significant pathway was "inhibition of matrix metalloproteases" (MMP), in which 6 of 40 pathway genes were represented with a Q1 BMD_T of 36 mg/kg-day; **Tables 3.5 and 3.6**). These genes have important roles in several bladder cancer-enhancing cellular processes, such as extracellular matrix remodeling, angiogenesis, apoptosis, epithelial-to-mesenchymal transition and cell proliferation (Szarvas *et al*., 2011). In an 8-week dietary study in rats assessing the

tumorigenic dose (2500 ppm or 200 mg/kg-day) of diuron, the expression of several MMP genes was among the most highly altered based on FC values, and these results were confirmed with real time PCR (da Rocha *et al.*, 2013). Further, human urothelial (1T1) cells individually exposed to proposed diuron metabolites (N-(3,4-dichlorophenyl)urea, N-(3,4-dichlorophenyl)-3-methylurea, or 3,4-dichloroaniline) also showed altered expression of MMP isoforms confirmed with rt-PCR in the same study (da Rocha *et al.*, 2013). The relevance or potency of other top pathways at 7 days but not 20 weeks, such as the hepatic fibrosis / hepatic stellate cell activation (12 of 181 pathway genes with Q1 BMD_T of 25 mg/kg-day) and vitamin D receptor (VDR)/RXR (7 of 88 pathway genes with Q1 BMD_T of 17 mg/kg-day) pathways, to the cytotoxicity MOA is unclear given the low percentage of the pathway represented with DEGs and the lower number of BMD_T values comprising the pathway potency estimates (**Table 3.5**). Nonetheless, the BMD_T values for the overall most significant pathways at 7 days had a narrow range based on both Q1 (15-36 mg/kg-day) and median (24-42 mg/kg-day) estimates (**Table 3.6**) and were consistent with many of the most significant pathways at 20 weeks and with the proposed key events in the MOA, such as metabolism to one or more toxic moieties, oxidative stress, cytotoxicity, regenerative hyperplasia, and ultimately tumors. Further, the concordant BMD_T and BMD_A potency estimates at 7 days and 20 weeks with the tumor BMD_A at 2 years suggests that threshold doses that correspond to tumorigenic potency can be established for key events in the cytotoxicity-mediated mode of urothelial tumorigenicity as early as 7 days.

Discussion

The present research was a case study of diuron to estimate BMD_T for the most significant functional pathways altered at doses associated with key events in the MOA, and to examine the concordance of BMD_T with BMD_A for urothelial hyperplasia, cell proliferation and tumors. Moreover, we sought to determine whether the cytotoxicity-mediated MOA for rodent urinary bladder tumorigenesis and its corresponding threshold could be discerned with BMD_T and BMD_A modeling at shorter-term study durations. BMD_T estimates can serve as a measure of low-dose potency for key operative genes and pathways and when comparable to apical BMD_A estimates can serve as phenotypic anchors that contribute to the weight of evidence for proposed key events in a chemical MOA (Bhat *et al*., 2013). If consistent with the ultimate adverse outcome that might traditionally serve as the basis of quantitative risk assessment and potential chemical regulation, short-term BMD_T estimates have the potential to improve the efficiency of toxicity testing and risk assessment while reducing animal usage.

Diuron has been reported to be an agonist of the AhR (Takeuchi *et al.*, 2011; Zhao *et al.* 2006), and the initial key event in the MOA is proposed to be metabolism of diuron to one or more toxic moieties (Da Rocha *et al*., 2013, 2014). Xenobiotic metabolism and AhR signaling pathways were among the most significant pathways identified at 20 weeks and 7 days (**Tables 3.3 and 3.5**). While the "xenobiotic metabolism pathway" includes several families of nuclear receptors commonly activated by xenobiotic exposures such as

the constitutive androstane receptor (CAR), pregnane X receptor (PXR), AhR, and peroxisome proliferator-activated receptor (PPAR), only Cyp1a1, Cyp1b1, and the AhR repressor (AHRR) contributed to the "xenobiotic metabolism pathway" significance score for diuron exposures of 20 weeks (Appendix C Table C4) or 7 days (Appendix C Table C15). These results suggest that AhR may be important mediator of diuron metabolism. These 2 overlapping metabolic pathways had 17 DEGs in common that comprised their pathway significance scores at 20 weeks (Cyp1a1, Cyp1b1, AHRR, 3 aldehyde dehydrogenase isoforms, eight glutathione-S-transferase isoforms, 2 heat shock proteins, and NAD(P)H dehydrogenase, quinone 1 or NQO1). The Q1 BMD_T values of 25 and 28 mg/kg-day for the urothelial xenobiotic and AhR signaling pathways at 20 weeks (**Table 3.4**), respectively, were similar to the BMD_A of 22 mg/kg-day for simple hyperplasia at 20 weeks, suggesting that cytotoxic metabolites may arise via Cyp1a1 and/or Cyp1b1-mediated metabolism. As noted above, human and rat urothelial cells exposed individually to the proposed major or minor diuron metabolites (N-(3,4-dichlorophenyl)urea, N-(3,4-dichlorophenyl)-3-methylurea, and/or 3,4-dichloroaniline) showed highly altered expression of various MMP isoforms confirmed with rt-PCR (Da Rocha *et al*., 2013). Due to their diverse roles in bladder cancer signaling, several MMP isoforms have been investigated as diagnostic or prognostic biomarkers and as therapeutic targets (Szarvas *et al*., 2011).

While not differentially expressed compared to controls at the lowest dose of 60 ppm diuron (3.6 mg/kg-day), Cyp1b1 was differentially induced at ≥ 125 ppm diuron for 20 weeks with a FC of 6, 10 and 9 at 125 ppm (7.7 mg/kg-day), 1250 ppm (77 mg/kg-day), and 2500 ppm (150 mg/kg-day), respectively. Further, the BMD_T for Cyp1b1 of 4.5 mg/kg-day at 20 weeks (model results not shown) was comparable to the apical BMD_{10} of 4 mg/kg-day estimated in the present assessment for urothelial lesions observable via SEM based on data reported by Cardoso *et al.* (2013). Cyp1a1 had a non-monotonic and non-dose-related expression pattern at 20 weeks since it had FC values of 3 at 60 and 1250 ppm and 2 at 2500 ppm but was not differentially expressed at 125 ppm. Thus, the BMD_T for Cyp1a1 at 20 weeks was an unacceptable fit. While the AhR signaling pathway was also a prominent pathway at 7 days, expression of both Cyp1a1 and Cyp1b1 were repressed consistent with low-potency BMD_T values (85 and 94 mg/kg-day, respectively; model results not shown).

Non-DNA reactive substances induce bladder cancer in rodents by increasing urothelial cell proliferation (i.e., increasing cell formation) through cytotoxicity and regenerative proliferation and hyperplasia (Cohen *et al.*, 2007; Cohen, 1998). Of the MOA investigated here, production of reactive metabolites is best supported by available evidence and considered most plausible for diuron (Da Rocha *et al.*, 2014) compared to production of urinary solids such as precipitate, crystals, and/or calculi or extreme alterations in urine composition, such as extremes of volume, pH, or dilution. These latter

2 MOAs were investigated and determined not to be prominent after diuron exposures (Da Rocha *et al.*, 2010; Nascimento *et al.*, 2006). Recognizing that AhR may be important mediator of diuron metabolism and that sustained AhR receptor activation is mitogenic in the rodent liver eventually leading to liver tumors (Budinsky et al., 2014), suggests that this mechanism may also play a role in bladder cancer. However, whether this MOA is operational in the bladder or also contributes to urothelial tumorigenicity associated with diuron exposure is unclear. Liver tumors were not observed in the 2 year bioassay of diuron (Bayer AG, 1985- as reported by APVMA, 2011 and U.S. EPA, 1997).

The most sensitive pathways in the present assessment based on the lowest pathway Q1 BMD_T of 4-5 mg/kg-day involved 3 related immune response pathways at 20 weeks (**Table 3.4**), consistent with the BMD_A of 4 mg/kg-day for SEM lesions judged as severe (Grade 4 and 5) that were characterized as necrosis and hyperplasia (Cardoso *et al.*, 2013). Necrotic cell death can release proinflammatory signals and stimulate inflammatory cells to enter the surrounding tissue microenvironment to survey the extent of tissue damage and remove associated necrotic debris (Hanahan and Weinburg, 2011). The Q1 BMD_T of 4-5 mg/kg-day estimated for immune pathways were below the 20-week NOAEL of 8 mg/kg-day for simple hyperplasia and the 2-year NOAEL of 11 mg/kg-day for bladders tumors, supporting the notion of this be more of an adaptive and not necessarily an adverse response. Transcriptional alterations in immune cell pathways were also seen in human and rat urothelial cells exposed to the bioactive metabolite of arsenic, dimethylarsinous acid,

for which a cytotoxicity-mediated MOA for rodent bladder tumors has also been attributed (Sen *et al.*, 2007).

Overall, BMD_T values in the present assessment for the overall most significant pathways at 7 days, many of which involved metabolic, detoxification, and oxidative stress responses, were consistent with BMD_T values for the same highly significant pathways at 20 weeks and with the proposed potency for apical key events in the MOA, including urothelial cell proliferation and hyperplasia at 20 weeks and tumors at 2 years. As a function of dose and time, phenotypically-anchored short-term (i.e., 2 days to 4 weeks) BMD_T and/or BMD_A estimates for early key events in a nongenotoxic MOA for mouse hepatocarcinogenesis were also highly consistent (i.e., within 2- to 5-fold) with potency estimates for the ultimate adverse outcome (Bhat *et al.*, 2013; Geter *et al.*, 2014; Wood *et al.*, 2014). Along with the present assessment, these types of case studies collectively encompassed multiple species (i.e., rat and mouse), target tissues (i.e., urinary bladder or liver), MOAs and/or molecular initiating events (cytotoxicity or receptor activation), and exposure durations ranging from 2 days to 20 weeks. Thus, short-term BMD_T and BMD_A modeling approaches demonstrate broad utility in quantitative cancer risk assessment, particularly for nongenotoxic carcinogens with a threshold dose-response.

In conclusion, the present study results suggest that threshold doses corresponding to tumorigenic potency can be established for key events in a rodent model of cytotoxicity-

mediated urothelial tumorigenicity based on a study as short as 7 days. The identification of low-dose thresholds for early key events in a carcinogenic MOA enables more efficient quantitative risk estimates of chronic exposure. If studies of additional chemicals confirm these results, future risk assessments may derive potency estimates generated from these short-term evaluation methods and use them for untested chemicals suspected of sharing the same MOA. This approach would help prioritize future research needs and improve assessment strategies.

Figures and Tables

Figure 3.1. Apical benchmark dose levels in urinary bladder of male rats fed diuron for 20 weeks

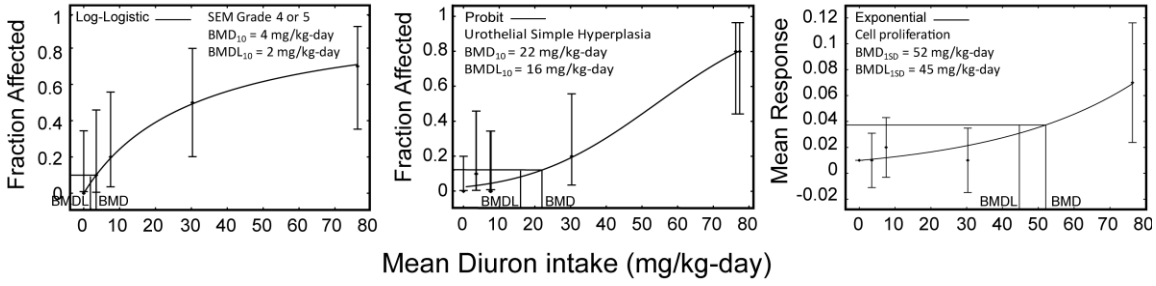

Figure 3.1. Legend. Based on the best-fitting $BMD_{10}/BMDL_{10}$ model estimates, urothelial lesions visible via SEM were the most sensitive apical response followed by urothelial simple hyperplasia. Based on $BMD_{1SD}/BMDL_{1SD}$ estimates, urothelial cell proliferation measured via BrdU was the least sensitive of the examined apical parameters at 20 weeks.

Figure 3.2. Range of pathway transcriptional benchmark dose levels (BMD_T) in the urinary bladder of male rats fed diuron for 20 weeks

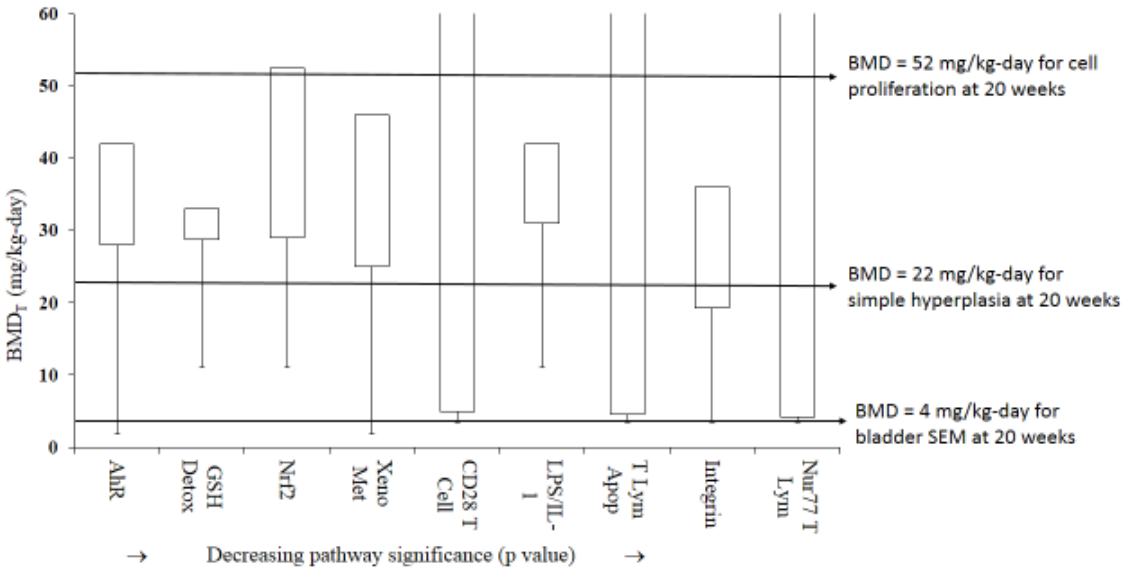

Figure 3.2 Legend. The lower quartile (Q1, bottom of bar) and median (Q2, top of bar) BMD_T for DEGs comprising the most significant pathways (increasing p value from left to right, see Table 3.3) operative at diuron doses (≥ 1250 ppm or ≥ 77 mg/kg-day) associated with significant increases in urothelial cell proliferation and hyperplasia at 20 weeks. Pathways involved metabolism/ detoxification, oxidative stress, immune function, and intracellular signaling, and these potency estimates were consistent with the BMD_A for apical key events at 20 weeks.

Figure 3.3. Range of pathway transcriptional benchmark dose levels (BMD_T) in the urinary bladder of male rats fed diuron for 7 days

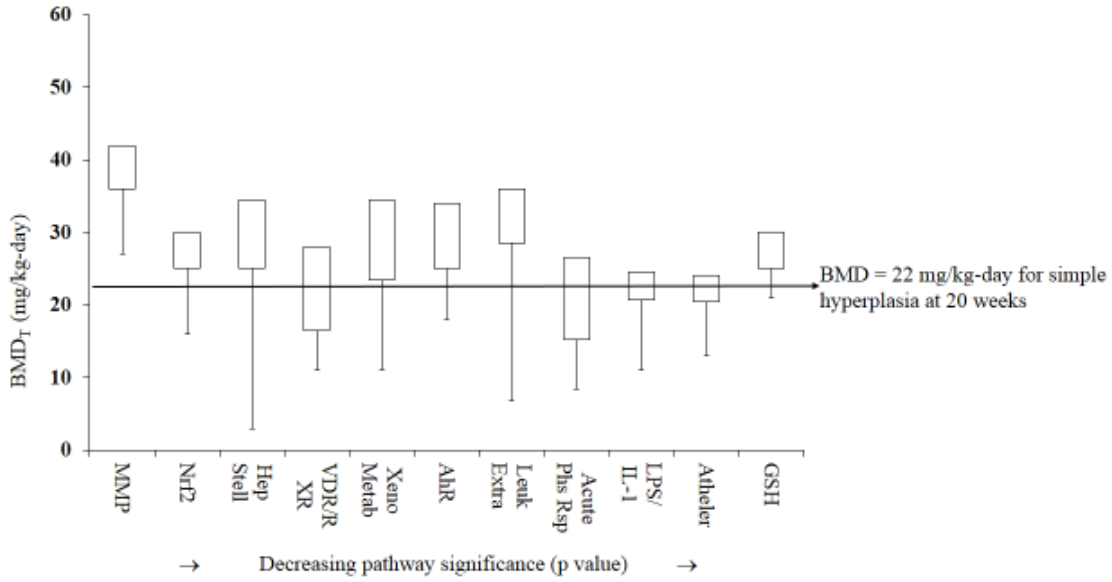

Figure 3.3 Legend. The lower quartile (Q1, bottom of bar) and median (Q2, top of bar) BMDT for DEGs comprising the most significant pathways (increasing p value from left to right, see Table 3.4) operative across all diuron doses (≥ 125 ppm or ≥ 12 mg/kg-day) at 7 days without associated urothelial lesions. Like 20 weeks, pathways were involved with metabolism/ detoxification, oxidative stress, immune function, and intracellular signaling, and these potency estimates were consistent with apical BMDA for urothelial hyperplasia at 20 weeks.

Table 3.1. Urothelial lesion incidence in male rats considered for benchmark dose modeling [1]

Dietary Diuron (ppm)	20 Weeks (Cardosa *et al.*2013; Ihlaseh *et al.*, 2011) [2,3]				Chronic Study (Bayer AG, 1985) [4]								
						Urothelial Hyperplasia				Tumors			
	Mean diuron intake (mg/kg-day)	Simple Hyperplasia	Scanning Electron Micro-scopy (SEM) Grade 4 or 5 [5]	BrdU Labeling Index (mean ±SD)	Mean diuron intake (mg/kg-day) [4]	Week 52, All grades (1, 2, or 3)	Week 52, Grades 2 or 3	Terminal, All grades (1, 2, or 3)	Terminal, Grades 2 or 3	Papill-oma	Carcinoma	Papilloma or carcinoma
0	0	0/10	0/10	0.01 ± 0 .00	0	3/10	0/10	13/50 (26%)	2/50 (4%)	0/49 (0%)	1/49 (2%)	1/49 (2%)
25	Not evaluated				1.0	5/10	0/10	5/50 (10%)	0/50 (0%)	0/50 (0%)	0/50 (0%)	0/50 (0%)
60	3.5	1/10	1/10	0.01 ± 0.02	Not evaluated							
	3.6	1/10	Not evaluated									
125	7.5	0/10	2/10	0.02 ± 0.03								
	7.7	0/10	Not evaluated									
250	Not evaluated				10.47	5/10	1/10	16/50 (32%)	1/50 (2%)	0/49 (0%)	1/49 (2%)	1/49 (2%)
500	30.3	2/10	5/10	0.01 ± 0.02	Not evaluated							
1250	76.3	8/10	7/10	0.07 ± 0.05								
	77.4	8/10	Not evaluated									
2500 [6]	146.5	7/10	4/10	0.04 ± 0.02	111	7/10	7/10	14/49 (29%)	13/49 (27%)	1/48 (2%)	35/48 (73%)	35/48 (73%)
	149.5	7/10	Not evaluated									

[1] No urothelial lesions were observed at 7 days at up to 2500 ppm (Ihlaseh *et al.*, in preparation).
[2] 20-week studies were modeled separately and merged to determine whether a statistically improved BMD fit could be obtained with more dose levels.
[3] The same rates of hyperplasia were also observed at 125, 500 and 2500 ppm in a 20-week study by Nascimento *et al.* (2006)
[4] Diuron intake and incidence data at 2 years as reported by APVMA (2011) and U.S. EPA (1997) based on Bayer AG (1985); mean diuron intake (mg/kg-day) at 52 weeks not reported
[5] The severity of urothelial SEM alterations judged as Grades 1, 2, or 3 in treated rats were comparable to controls.
[6] The highest dose (2500 ppm) was omitted in BMD modeling due to the non-montonic dose response consistent with U.S. EPA (2012) guidance.

Table 3.2. Apical benchmark dose (BMD_A) results in the urinary bladder at 20 weeks and 2 years

Exposure Duration	Study	Endpoint	Model	P value[1]	BMD[2] (mg/kg-day)	BMDL[2] (mg/kg-day)
20 weeks	Cardosa *et al.* (2013)	Ultrastructural alterations via scanning electron microscopy (SEM)	Log-logistic	1	4	2
	Cardosa *et al.* (2013)	Simple hyperplasia	Probit	0.5469	22	14
	Ihlaseh *et al.* (2011)	Simple hyperplasia	Probit	0.3411	22	14
	Cardosa *et al.* (2013) and Ihlaseh *et al.* (2011); Merged	Simple hyperplasia	Probit	0.6412	22	16
	Cardosa *et al.* (2013)	Cell proliferation via BrdU	Expon-ential 2	0.6392	52	45
2 years	Bayer AG (1985)	Hyperplasia (not further specified)	See Results		Not modeled	
	Bayer AG (1985)	Papilloma or carcinoma	Multistage	0.5989	32	17

[1] Global goodness-of-fit P value must be >0.1 for an acceptable fit according to U.S. EPA (2012); P = 1 indicates model's predicted response is identical to the observed response

[2] Benchmark response set at 10% increase above controls for incidence data and 1control group SD for cell proliferation according to U.S EPA (2012) guidelines

Table 3.3. Most significant canonical pathways at 20 weeks

Functional Annotation	-log P value	# DEGs/ total in pathway [1]	# BMD_T (% of pathway) [2]
Aryl Hydrocarbon Receptor Signaling	8.20	24/171	17 (10%)
Glutathione-mediated Detoxification	8.03	11/44	10 (23%)
Nrf2-mediated Oxidative Stress Response	7.24	26/195	14 (7%)
Xenobiotic Metabolism Signaling	6.15	31/304	21 (7%)
Ethanol Degradation II [3]	4.22	8/43	4 (9%)
Ethanol Degradation IV [3]	4.13	6/29	3 (10%)
CD28 Signaling in T Helper Cells	3.88	15/136	9 (7%)
Clathrin-mediated Endocytosis Signaling	3.85	20/198	9 (5%)
RhoGDI Signaling [3]	3.74	19/201	4 (2%)
LPS/IL-1 Mediated Inhibition of RXR Function	3.65	22/245	15 (6%)
Calcium-induced T Lymphocyte Apoptosis	3.54	10/71	8 (11%)
Integrin Signaling	3.48	20/208	8 (4%)
Ethanol Degradation III [3]	3.37	5/40	4 (10%)
Nur77 Signaling in T Lymphocytes	3.29	9/208	7 (3%)
RhoA Signaling [3]	3.27	14/122	4 (3%)
Lipid Antigen Presentation by CD1 [3]	3.17	6/30	2 (7%)
Noradrenaline and Adrenaline Degradation [3]	3.13	7/53	4 (8%)
Mitochondrial Dysfunction [3]	3.09	17/201	4 (2%)

[1] Number of DEGs contributing to the pathway significance score calculated by IPA analysis

[2] Due to exclusion of DEGs with an unacceptable BMD_T fit as described in the Methods

[3] Omitted from Figure 3.2 due to <5 genes with BMD_T values comprising pathway as described in the Methods

Table 3.4 Pathway transcriptional benchmark dose summary at 20 weeks

	BMD_T (mg/kg-day)			$BMDL_T$ (mg/kg-day)		
Functional Annotation	Q1	Mean	Median	Q1	Mean	Median
Aryl Hydrocarbon Receptor Signaling	28	47	42	19	31	31
Glutathione-mediated Detoxification	29	38	33	20	26	24
Nrf2-mediated Oxidative Stress Response	29	56	53	20	36	37
Xenobiotic Metabolism Signaling	25	48	46	17	32	33
CD28 Signaling in T Helper Cells	5	54	65	0.4	32	37
Clathrin-mediated Endocytosis Signaling	61	77	87	42	48	49
LPS/IL-1 Mediated Inhibition of RXR Function	31	45	42	22	31	31
Calcium-induced T Lymphocyte Apoptosis	5	53	69	1	32	43
Integrin Signaling	19	51	36	11	32	25
Nur77 Signaling in T Lymphocytes	4	51	73	1	31	49

Table 3.5. Most significant canonical pathways at 7 days

Functional Annotation	-log P value	# DEGs/ total in pathway[1]	# BMD_T/ (% of pathway[2]
Inhibition of Matrix Metalloproteases	4.72	13/40	6 (15%)
NRF2-mediated Oxidative Stress Response	4.68	34/195	15 (8%)
Hepatic Fibrosis / Hepatic Stellate Cell Activation	4.48	28/155	12 (8%)
VDR/RXR Activation	3.86	18/88	7 (8%)
Xenobiotic Metabolism Signaling	3.57	44/304	23 (8%)
Complement System [3]	3.37	10/35	1 (3%)
Intrinsic Prothrombin Activation Pathway [3]	3.3	9/37	4 (11%)
Aryl Hydrocarbon Receptor Signaling	3.22	25/171	17 (10%)
Leukocyte Extravasation Signaling	3.15	32/210	14 (7%)
Ceramide Biosynthesis [3]	3.09	4/16	1 (6%)
Glycogen Degradation II [3]	3.02	5/16	1 (6%)
Acute Phase Response Signaling	3.00	28/181	12 (7%)
LPS/IL-1 Mediated Inhibition of RXR Function	2.93	34/245	16 (7%)
Extrinsic Prothrombin Activation Pathway [3]	2.74	6/22	4 (18%)
Atherosclerosis Signaling	2.64	21/138	11 (8%)
Glutathione-mediated Detoxification	2.62	8/44	5 (11%)
Glycogen Degradation III [3]	2.58	5/18	1 (13%)
Glutathione Redox Reactions I [3]	2.58	6/24	3 (24%)

[1] Number of DEGs contributing to the pathway significance score calculated by IPA analysis

[2] Due to some of the DEGs having an unacceptable BMD_T fit as described in the Methods

[3] Omitted from Figure 3.3 due to <5 genes with BMD_T values comprising pathway as described in the Methods

Table 3.6. Pathway transcriptional benchmark dose summary at 7 days

	BMD_T (mg/kg-day)			$BMDL_T$ (mg/kg-day)		
Functional Annotation	Q1	Mean	Median	Q1	Mean	Median
Inhibition of Matrix Metalloproteases	36	55	42	18	35	27
NRF2-mediated Oxidative Stress Response	25	66	30	15	40	16
Hepatic Fibrosis / Hepatic Stellate Cell Activation	25	67	35	15	39	18
VDR/RXR Activation	17	52	28	11	32	16
Xenobiotic Metabolism Signaling	24	65	35	14	39	18
Aryl Hydrocarbon Receptor Signaling	25	66	34	15	40	18
Leukocyte Extravasation Signaling	29	62	36	16	38	18
Acute Phase Response Signaling	15	47	27	10	27	15
LPS/IL-1 Mediated Inhibition of RXR Function	21	50	25	13	27	14
Atherosclerosis Signaling	21	30	24	13	19	14
Glutathione-mediated Detoxification	25	28	30	15	16	16

GENERAL CONCLUSIONS

The overall objective of this research was to determine if results of short-term global gene expression profiling can be used to inform potency and early key events in a carcinogenic MOA and thus collectively serve as a strategy to prioritize future or data-poor existing chemicals for further testing. Toxicological characterization of the approximately 80,000 chemicals in commerce using the traditional battery of toxicology studies is not economically or technologically feasible in the foreseeable future (NRC, 2007a). In addition to fostering efficiency in quantitative risk assessment, dose- and time-course indicators for key events also contribute to the weight of evidence for a proposed MOA (Ankley *et al*., 2010; Boobis *et al.*, 2006; Julien *et al*., 2009; Meek *et al.*, 2014).

The present studies used quantitative dose-response modeling to estimate low-dose potency for activation or repression of key genes and pathways, and these transcriptional benchmark dose (BMD_T) estimates were comparable and thus phenotypically anchored to benchmark dose estimates for apical responses (BMD_A) at the cellular and tissue level which were observed after the same exposure duration. These BMD_T and BMD_A were also consistent with the MOA and potency (i.e., BMD_A) for ultimate adverse outcomes or final key events that might traditionally serve as the basis of quantitative risk assessment and potential chemical regulation.

Another objective of this research was to characterize the magnitude of transcriptomic-to-phenotypic uncertainty. A critical element to toxicogenomic-driven quantitative risk assessment is understanding the magnitude of transcriptomic-to-phenotypic extrapolation uncertainty. When this extrapolation, which includes dose- and time considerations, can be more fully characterized, a low-dose transcriptional POD estimated from a short-term exposure may serve as the basis of a quantitative risk assessment of long-term exposure. With the conazole research, our 30-day median $BMDL_T$ estimates were within one-half order of magnitude of the chronic $BMDL_A$ for hepatocellular tumors (Bhat *et al.*, 2013). With the phenobarbital research, our 2-day median pathway $BMDL_T$ estimates were consistent with the No-observable Effect Level (NOEL) and the hepatotumorigenic dose (Geter *et al.*, 2014). Finally, our median pathway $BMDL_T$ estimates were also the same as the suspected urinary bladder tumor threshold for diuron. Thus, our short-term BMD_T values were within 5-fold of the suspected tumor threshold for all 3 case studies. The current quantitative risk assessment paradigm for nongenotoxic carcinogens involves a composite uncertainty factor that encompasses up to 5 individual areas of uncertainty (interspecies, intraspecies, LOAEL to NOAEL, study duration, and database deficiencies) each with an assigned factor value of either 1x, 3x, or 10x in order to derive the acceptable lifetime exposure level, such as a Reference Dose (RfD) (U.S. EPA, 2002; WHO/IPCS, 2005). By definition, the uncertainty associated with a chronic oral RfD spans perhaps an order of magnitude (U.S. EPA, 2011b). Thus, our

results to date indicate that short-term BMD_T values can serve as screening level PODs for quantitative risk assessment of chronic exposure.

The case studies were selected to encompass multiple rodent species, target tissues, modes of action, and exposure durations ranging from 2 days to 20 weeks and thus demonstrate the potential for broad utility. Further, the chemical agents are considered nongenotoxic carcinogens, with PB being a classic prototype. For nongenotoxic carcinogens, a threshold dose-response approach can be employed in quantitative cancer risk assessment when supported by MOA information (Boobis *et al.*, 2006) based on the assumption that the adverse outcome (i.e., cancer) will not occur if exposure concentrations are below levels that do not alter tumorigenic key events. When consistent with apical effects, transcriptional changes in genes and pathways can also serve as quantitative bioindicators of treatment-related adverse responses (Preston, 2002). Thus, our BMD_T and BMD_A estimates inform threshold dose-response approaches for nongenotoxic carcinogens.

The present research illustrates the utility in MOA research for integrated BMD_A and BMD_T modeling approaches based on short-term exposure data. The evaluated study designs had at least 3 treatment doses and a control. Cases where more dose levels were available, such as the 5 treatment levels in the PB studies and 4 treatment levels in the 20-week diuron studies, tended to result in improved BMD model fits and thus increased

confidence in low-dose extrapolation. Similarly, sample sizes as low as 3 were amenable to deriving BMD_T estimates, recognizing that sample sizes less than 10 are outside the power of detecting and thus estimating a BMD_A at the 10% response rate for histopathology lesions.

In conclusion, this research demonstrated the utility of short-term global expression profiling for informing potency with respect to MOA and quantitative risk assessment of long-term exposures. Further, the case studies encompassed multiple rodent species, target tissues, MOA, and exposure durations ranging from 2 days to 20 weeks, and thus demonstrate the potential of this approach for serving as a chemical testing and prioritization strategy.

REFERENCES

Aiges, H. W., Daum, F., Olson, M., Kahn, E., and Teichberg, S. (1980). The effects of phenobarbital and diphenylhydantoin on liver function and morphology. *J. Pediatr*. **97**, 22-26.

Akaike, H. (1973). Information theory and an extension of the maximum likelihood principle. In *Proceedings of the 2nd International Symposium on Information Theory*, (B. N. Petrov and F. Csaki Eds.), pp. 267–281, Akademiai Kiado, Budapest, Hungary.

Allen, J. W., Wolf, D. C., George, M. H., Hester, S. D., Sun, G., Thai, S. F., Delker, D. A., Moore, T., Jones, C., Nelson, G., Roop, B. C., Leavitt, S., Winkfield, E., Ward, W. O. and Nesnow, S. (2006). Toxicity profiles in mice treated with hepatotumorigenic and non-hepatotumorigenic triazole conazole fungicides: Propiconazole, triadimefon, and myclobutanil. *Toxicol. Pathol*. **34**, 853-62.

Anderson, D. M., O'Hara, G. P., and Brown, W. R. (1993). RH-3866: Dietary Oncogenicity Study in Female, Rohm and Haas Company, Spring House, PA; Protocol #: 89P-261; Unpublished Report #: 89R-261; 3/17/93. As cited by California Department of Food and Agriculture, 2000.

Ankley, G. T., Bennett, R. S., Erickson, R. J. Hoff, D. J., Hornung, M. W., Johnson, R. D., Mount, D. R., Nichols, J. W., Russom, C. L., Schmieder, P. K., Serrrano, J. A., Tietge, J. E., and Villeneuve, D. L. (2010). Adverse outcome pathways: A conceptual framework to support ecotoxicology research and risk assessment. *Environ. Toxicol. Chem*. **29**, 730–41.

Arce, G. T. (1985). Assessment of diuron in the in vitro unscheduled DNA synthesis assay in primary rat hepatocytes. Lab: EI du Pont de Nemours and Company, Inc., Haskell Laboratory for Toxicology and Industrial Medicine, Newark, Delaware 19714. Report No: 51553. As reported by APVMA (2011).

Australian Pesticides and Veterinary Medicine Authority (APVMA). (2011). Review of the Mammalian Toxicology and Metabolism/Toxicokinetics of Diuron . Diuron Human Health Assessment. Available at: www.apvma.gov.au/products/review/docs/diuron_human_health.doc. Accessed on March 3, 2014.

Auerbach, S. S., Shah, R. R., Mav, D., Smith, C. S., Walker, N. J., Vallant, M. K., Boorman, G. A. and Irwin, R .D. (2010). Predicting the hepatocarcinogenic potential of alkenylbenzene flavoring agents using toxicogenomics and machine learning. *Toxicol. Appl. Pharmacol*. **243**, 300-14.

Bayer AG. (1985). Diuron: Study for chronic toxicity and carcinogenicity with Wistar rats (Administration in diet for up to two years). Lab: Bayer AG Institute of Toxicology, Wuppertal, Friedrich-Ebert-Strasse 217-333, West Germany. Report No: 51470. Du Pont Report No: D/Tox 17. As reviewed by APVMA (2011) and U.S. EPA (1997).

Bhat, V. S., Hester, S. D., Nesnow, S. and Eastmond, D. A. (2013). Concordance of transcriptional and apical benchmark dose levels for conazole-induced liver effects in CD-1 mice. *Toxicol. Sci.* **136**, 205-215.

Bomhard, E. and Hahnemann, S. (1986). MEB 6447 (common name: triadimefon, the active ingredient of Bayleton). Carcinogenicity study on NMRI mice (21-month administration in the feed). Unpublished report No. 16719 from Bayer AG, Wuppertal, Germany. Submitted to WHO by Bayer CropScience AG, Monheim, Germany. Based on Dewhurst and Dellarco, 2004.

Boobis, A. R., Cohen, S. M., Dellarco, V., McGregor, D., Meek, M. E., Vickers, C., Willcocks, D., and Farland, W. (2006). IPCS framework for analyzing the relevance of a cancer mode of action for humans. *Crit. Rev. Toxicol*. **36**, 781–792.

Bourdon, J. A., Williams, A., Kuo, B., Moffat, I., White, P. A., Halappanavar, S. *et al.* (2013). Gene expression profiling to identify potentially relevant disease outcomes and support human health risk assessment for carbon black nanoparticle exposure. *Toxicol.* **303**:83-93.

Boverhof, D. R. and T. R. Zacharewski. (2006). Toxicogenomics in Risk Assessment: Applications and Needs *Toxicol. Sci*. **89**, 352-360.

Budinsky, R. A., Schrenk, D., Simon, T., Van den Berg, M., Reichard, J. F., Silkworth, J. B. and Rowlands, J. C. (2013). Mode of action and dose-response framework analysis for receptor-mediated toxicity: the aryl hydrocarbon receptor as a case study. *Crit. Rev. Toxicol.* **44,** 83-119.

Bruno, M., Moore, T., Nesnow, S., and Ge, Y. (2009). Protein carbonyl formation in response to propiconazole-induced oxidative stress. *J. Proteome. Res*. **8**:2070–2078.

Burke, M. D., and Mayer, R. T. (1983). Differential effects of phenobarbitone and 3-methylcholanthrene induction on the hepatic microsomal metabolism and cytochrome P-450-binding of phenoxazone and a homologous series of its n-alkyl ethers (alkoxyresorufins). *Chem. Biol. Interact*. **45**, 243-58.

California Department of Food and Agriculture. (2000). Medical Toxicology Branch. Summary of Toxicology Data. Myclobutanil. SB 950-(not assigned), Tolerance # 51315 Chemical Code #: 2245. Original version 02/03/1987. Last updated 9/21/2000.

Cardoso, A. P. F., Ihlaseh Catalano, S. M., da Rocha, M. S., Nascimento e Pontes, M. G., de Camargo, J. L. V., and de Oliveira, M. L. C. S. (2013). Dose–response of diuron [3-(3, 4-dichlorophenyl)-1, 1-dimethylurea] in the urothelial mucosa of Wistar rats. *Toxicol*, **312,** 1-5.

Chen, P. -J., Moore, T., and Nesnow, S. (2008). Cytotoxic effects of propiconazole and its metabolites in mouse and human hepatoma cells and primary mouse hepatocytes. *Toxicol. In Vitro* **22**, 1476–1483.

Chen, P. J., Padgett, W. T., Moore, T., Winnik, W., Lambert, G. R., Thai, S. F., Hester, S. D., and Nesnow, S. (2009). Three conazoles increase hepatic microsomal retinoic acid metabolism and decrease mouse hepatic retinoic acid levels *in vivo*. *Toxicol. Appl. Pharmacol*. **234**, 143–155.

Chiu, W. A., Euling, S. Y., Scott, C. S., and Subramaniam, R. P. (2013). Approaches to advancing quantitative human health risk assessment of environmental chemicals in the post-genomic era. *Toxicol. Appl. Pharmacol.* ***271,*** 309-323.

Choe, S. E., Boutros, M., Michelson, A. M., Church, G. M., and Halfon, M. S. (2005). Preferred analysis methods for Affymetrix GeneChips revealed by a wholly defined control dataset. *Genome Biol*. **6,** R16.

Cohen, S. M. (1998). Urinary bladder carcinogenesis. *Toxicol. Pathol.* **26**, 121–127.

Cohen, S. M., Ohnishi, T., Clark, N., M., He, J., and Arnold, L. L. (2007). Investigations of rodent urinary bladder carcinogens: collection, processing, and evaluation of urine and bladders. *Toxicol. Pathol.* **35**, 337-47.

Currie, R. A. (2012). Toxicogenomics: the challenges and opportunities to identify biomarkers, signatures and thresholds to support mode-of-action. *Mutat. Res*. **746**, 97-103.

Da Rocha, M. S., Nascimento, M. G., Cardoso, A. P. F., de Lima, P. L., Zelandi, E. A., de Camargo, J. L. V., & de Oliveira, M. L. C. (2010). Cytotoxicity and regenerative proliferation as the mode of action for diuron-induced urothelial carcinogenesis in the rat. *Toxicol. Sci.* **113**, 37-44.

Da Rocha, M. S., Arnold, L. L., Pennington, K. L., Muirhead, D., Dodmane, P. R., Anwar, M. M., *et al.* and Cohen, S. M. (2012). Diuron-induced rat bladder epithelial cytotoxicity. *Toxicol. Sci.* **130**, 281-288.

Da Rocha, M. S., Arnold, L. L., Dodmane, P. R., Pennington, K. L., Qiu, F., De Camargo, J. L. V., and Cohen, S.M. (2013). Diuron metabolites and urothelial cytotoxicity: *In vivo*, *in vitro* and molecular approaches. *Toxicol.* **314**, 238– 246.

Da Rocha, M. S., Arnold, L. L., De Oliveira, M. L. C. S., Catalano, S. M. I., Cardoso, A. P. F., Pontes, M. G., Ferrucio, B., Dodmane, P.R., Cohen, S. M., and De Camargo, J. L. V. (2014). Diuron-induced rat urinary bladder carcinogenesis: Mode of action and human relevance evaluations using the International Programme on Chemical Safety framework. *Crit. Rev. Toxicol.* **44**, 393-406.

De Camargo, J. L. V. (2013). Chemical carcinogenesis – mode of action to inform quantitative human risk. In *BMC Proceedings* (Vol. 7, No. Suppl 2, p. K10). BioMed Central Ltd.

Davis, J. A., Gift, J. S., and Zhao, Q. J. (2011). Introduction to benchmark dose methods and U.S. EPA's benchmark dose software (BMDS) version 2.1.1. *Toxicol. Appl. Pharmacol*. **254,** 81-91.

Dellarco, V., Henry, T., Sayre, P., Seed, J. and Bradbury, S. (2010). Meeting the common needs of a more effective and efficient testing and assessment paradigm for chemical risk management. *J. Toxicol. Environ. Health, Part B.* **13**, 347-60.

Dewhurst, I., and Dellarco, V. (2004). In International Programme on Chemical Safety Joint FAO/WHO Meeting on Pesticide Residues in Food. Available at: http://whqlibdoc.who.int/publications/2006/9241665203_eng.pdf

Edwards, S. W. and Preston, R. J. (2008). Systems Biology and Mode of Action Based Risk Assessment. *Toxicol. Sci*. **106**, 312-18.

Elcombe, C. R., Peffer, R. C.,Wolf, D. C., Bailey, J., Bars, R., Bell, D., Cattley, R. C., Ferguson, S. S., Geter, D., Goetz, A., *et al.* (2014).Mode of action and human relevance analysis for nuclear receptor-mediated liver toxicity: A case study with phenobarbital as a model constitutive androstane receptor (CAR) activator. *Crit. Rev. Toxicol.* **44**, 64–82

Ellinger-Ziegelbauer, H., Gmuender, H., Bandenburg, A. and Ahr, H. J. (2008). Prediction of a carcinogenic potential of rat hepatocarcinogens using toxicogenomics analysis of short-term in vivo studies. *Mutat. Res*. **637**, 23-39.

Fielden, M. R., Adai, A., Dunn II, R. T., Olaharski, A., Searfoss, G. Sina J., Aubrecht, J., Boitier, E., Nioi, P., Auerbach, S., Jacobson-Kram, D., Raghavan, N., Yang, Y., Kincaid, A., Sherlock, J., Chen, S.-J., and Car, B. (2011). Development and evaluation of a genomic signature for the prediction and mechanistic assessment of nongenotoxic hepatocarcinogens in the rat. *Toxicol. Sci*. **124**, 54-74.

Gee, J. (2010). Summary on toxicologic data. Diuron. Medical Toxicology Branch. Department of Pesticide Regulation. California Environmental Protection Agency. 7p. Available at: cdpr.ca.gov/docs/risk/toxsums/pdfs/231.pdf. Accessed on April 16, 2014.

Gerspach, R. (1997). Propiconazole (CGA 64250) Tech.: 18-month oncogenicity study in mice. Novartis Crop Protection AG, Stein, Switzerland. Unpublished report No. 943126 (Syngenta No. CGA64250/3142). Submitted to WHO by Syngenta Ltd, Basle, Switzerland. Based on Dewhurst and Dellarco, 2004.

Geter, D. R., Bhat, V. S., Gollapudi, B. B., Sura, R., and Hester, S. D. (2014). Dose-response modeling of early molecular and cellular key events in the CAR-mediated hepatocarcinogenesis pathway. *Toxicol. Sci*. **138**, 425-445.

Goetz, A. K., Bao,W., Ren, H., Schmid, J. E., Tully, D. B., Wood, C., Rockett, J. C., Narotsky, M. G., Sun, G., Lambert, G. R., Thai, S. F., Wolf, D. C., Nesnow, S., Dix, D. J., 2006. Gene expression profiling in the liver of CD-1 mice to characterize the hepatotoxicity of triazole fungicides. *Toxicol. Appl. Pharmacol*. **215**, 274-84.

Goldman, P. R. and Harris, J. C. (1986). RH-3866: Dietary chronic and oncogenicity study in mice. Report No. 84R-023. Unpublished report dated October 17, 1986 from Rohm and Haas Company, Spring House, PA, USA. Based on California Department of Food and Agriculture, 2000 and INCHEM, 1992.

Hamadeh, H. K., Bushel, P. R., Jayadev, S., DiSorbo, O., Bennett, L., Li, L., Tennant, R., Stoll, R., Barrett, J. C., Paules, R. S., *et al.* (2002a). Prediction of Compound Signature Using High Density Gene Expression Profiling. *Toxicol. Sci*. **67**, 232–40.

Hamadeh, H. K., Bushel, P. R., Jayadev, S., Martin, K., DiSorbo, O., Sieber, S., Bennett, L., Tennant, R., Stoll, R., Barrett, J. C., *et al.* (2002b). Gene expression analysis reveals chemical-specific profiles. *Toxicol. Sci.* **67**, 219–231.

Hanahan, D., and Weinberg, R. A. (2011). Hallmarks of cancer: the next generation. *Cell.* **144,** 646-674.

Hannas, B. R., Lambright, C. S., Furr, J., Evans, N., Foster, P. M., Gray, E. L., and Wilson, V. S. (2012). Genomic biomarkers of phthalate-induced male reproductive developmental toxicity: a targeted RT-PCR array approach for defining relative potency. *Toxicol. Sci*. **125**, 544-57.

Health Canada. (2010). Proposed Re-evaluation Decision PRVD2010-14 Myclobutanil. Available at: http://www.hc-sc.gc.ca/cps-spc/pest/part/consultations/_prvd2010-14/prvd2010-14-eng.php.

Health Canada. (2011). Screening Assessment for the Challenge. Urea, N'-(3,4-dichlorophenyl)-N,N-dimethyl- (Diuron), Chemical Abstracts Service Registry Number 330-54-1. Environment Canada, Health Canada, Ontario Canada. Available at: http://www.ec.gc.ca/ese-ees/6BC4E5D3-6E96-4EB2-938F-1BF7F2CC5701/batch10_330-54-1_en.pdf. Accessed on April 16, 2014.

Herbold, B. A. (1989). In vitro cytogenetic study with human lymphocytes for the detection of induced clastogenic effects. Lab: Bayer AG. Study No: T0029478. Unpublished study. Based on APVMA, 2011.

Hester, S. D., Wolf, D. C., Nesnow, S, and Thai, S. F. (2006). Transcriptional profiles in liver from rats treated with tumorigenic and non-tumorigenic triazole conazole fungicides: Propiconazole, triadimefon, and myclobutanil. *Toxicol. Pathol.* **34**, 879-94.

Hester, S., Moore, T., Padgett, W. T., Murphy, L., Wood, C. E., and Nesnow, S. (2012). The hepatocarcinogenic conazoles: cyproconazole, epoxiconazole, and propiconazole induce a common set of toxicological and transcriptional responses. *Toxicol. Sci*. **127**, 54-65.

Hester, S. D. and Nesnow, S. (2008). Transcriptional responses in thyroid tissues from rats treated with a tumorigenic and a non-tumorigenic triazole conazole fungicide. *Toxicol. Appl. Pharmacol*. **227**, 357-69.

Holsapple, M. P., Pitot, H. C., Cohen, S. M., Boobis, A. R., Klaunig, J. E., Pastoor, T., Dellarco, V. L. and Dragan, Y. P. (2006). Mode of action in relevance of rodent liver tumors to human cancer risk. *Toxicol. Sci*. **89**, 51–56.

Honkakoski, P. and Negishi, M. (1997). Characterization of a Phenobarbital-responsive Enhancer Module in Mouse P450 Cyp2b10 Gene. *J. Biol. Chem*. **272**, 14943-14949.

Huang, W., Zhang, J., Wahington, M., Liu, J., Parant, J. M., Lozano, G., Moore, D. D. (2005). Xenobiotic stress induces hepatomegaly and liver tumors via the nuclear receptor constitutive androstane receptor. *Mol. Endocrinol.* **19**, 1646-1653.

Hunter, B., Scholey, D. and Heywood, R. (1982). CGA 64250 long-term feeding study in mice (final report). Unpublished report No. CBG/196/81827, October 20, Huntingdon Research Centre, Huntingdon, England.

IARC (International Agency for Research on Cancer). (2001). IARC Monographs on the Evaluation of Carcinogenic Risks to Humans. Volume 79. Some Thyrotropic Agents. IARC Press, Lyon.

INCHEM (1992). Monograph 847. Myclobutanil (Pesticide residues in food: 1992 evaluations Part II Toxicology). Available at: http://www.inchem.org/documents/jmpr/jmpmono/v92pr13.htm.

Ihlaseh, S. M., Bailey, K. A., Hester, S. D. Jones, C., Ren, H., Cardoso, A. P. F., De Oliveira, M. L. C. S., Wolf, D. C., and de Camargo, J. L. V. (2011). Transcriptional profile of diuron-induced toxicity on the urinary bladder of male Wistar rats to inform mode of action. *Toxicol. Sci.* **122**, 330-338.

Ihlaseh-Catalano, S. M., Bailey, K. A., Cardoso, A. P., F., Ren, H., Fry, R. C., Camargo, J. L., V. and Wolf, D. C. Dose- and time- effects of gene expression profiles in urothelial cells from rats exposed to diuron for seven days. In preparation.

Jackson, A. F., Williams, A., Recio, L., Waters, M. D., Lambert, I. B., and Yauk, C. L. (2014). Case study on the utility of hepatic global gene expression profiling in the risk assessment of the carcinogen furan. *Toxicol. Appl. Pharmacol.* **274**, 63-77.

Jia, G., Takahashi, R., Zhang, Z., Tsuji, Y., and Sone, H. (2006). Aldo-keto reductase 1 family B7 is the gene induced in response to oxidative stress in the livers of Long-Evans Cinnamon rats. *Int. J. Oncol.* **29**, 829-38.

Jones, H. B., Orton, T. C., and Lake, B. G. (2009). Effect of chronic phenobarbitone administration on liver tumour formation in the C57BL/10J mouse. *Food Chem. Toxicol.* **47**, 1333–1340.

Julien, E., Boobis, A. R., Olin. S. S. ILSI Research Foundation Threshold Working Group. (2009). The Key Events Dose-Response Framework: a cross-disciplinary mode-of-action based approach to examining dose-response and thresholds. *Crit. Rev. Food Sci. Nutr.* **49**, 682-9.

Keller, D. A., Juberg, D. R., Catlin, N., Farland, W. H., Hess, F. G., Wolf, D. C., and Doerrer, N. G. (2012). Identification and characterization of adverse effects in 21st century toxicology. *Toxicol. Sci.* **126**, 291-7.

Klaunig, J. E., Babich, M. A., Baetcke, K. P., Cook, J. C., Corton, J. C., David, R. M., DeLuca, J. G., Lai, D. Y., McKee, R. H., Peters, J. M., Roberts, R. A. and Fenner-Crisp, P. A. (2003). PPARα Agonist-Induced Rodent Tumors: Modes of Action and Human Relevance. *Crit. Rev. Toxicol.* **33**, 655-780.

Kopec, A. K., Burgoon, L. D., Ibrahim-Aibo, D., Burg, A. R., Lee, A. W., Tashiro, C., Potter, D., Sharratt, B., Harkema, J. R., Rowlands, J. C., Budinsky, R. A., and Zacharewski, T. R. (2010). Automated dose-response analysis and comparative toxicogenomic evaluation of the hepatic effects elicited by TCDD, TCDF, and PCB126 in C57BL/6 mice. *Toxicol. Sci.* **118**, 286-97.

Liu, M. J., Takahashi, Y., Wada, T., He, J., Gao, J., Tian, Y., Li, S., and Xie, W. 2009. The Aldo-Keto Reductase Akr1b7 Gene Is a Common Transcriptional Target of Xenobiotic Receptors Pregnane X Receptor and Constitutive Androstane Receptor. *Mol. Pharmacol.* **76**, 604-11.

Lubet, R. A., Mayer, R. T., Cameron, J. W., Nims, R. W., Burke, M. D., Wolff, T., and Guengerich, F. P. (1985). Dealkylation of pentoxyresorufin: a rapid and sensitive assay for measuring induction of cytochrome(s) P-450 by phenobarbital and other xenobiotics in the rat. *Arch. Biochem. Biophys*. **238**, 43-8.

Manning, G. E., Mundy, L. J., Crump, D., Jones, S. P., Chiu, S., Klein, J., Konstantinov, A., Potter, D., and Kennedy, S. W. (2013). Cytochrome P4501A induction in avian hepatocyte cultures exposed to polychlorinated biphenyls: Comparisons with AHR1-mediated reporter gene activity and in ovo toxicity. *Toxicol. Appl. Pharmacol*. **266**, 38-47.

Manuppello, J. and Willett, C. (2008). Longer Rodent Bioassay Fails to Address 2-Year Bioassay's Flaws. *Environ. Health Perspec*. **116**, A516–7.

Mathijs, K., Brauers, K. J., Jennen, D. G., Lizarraga, D., Kleinjans, J. C., and van Delft, J. H. (2010). Gene expression profiling in primary mouse hepatocytes discriminates true from false-positive genotoxic compounds. *Mutagenesis*. **25**, 561-8.

Meek, M. E., Bucher, J. R., Cohen, S. M., Dellarco, V., Hill, R. N., Lehman-McKeeman, L. D., Longfellow, D. G., Pastoor, T., Seed, J., and Patton, D. E. (2003). A framework for human relevance analysis of information on carcinogenic modes of action. *Crit. Rev. Toxicol*. **33**, 591-653.

Meek, M. E., Boobis, A., Cote, I., Dellarco, V., Fotakis, G., Munn, S. and Vickers, C. (2014). New developments in the evolution and application of the WHO/IPCS framework on mode of action/species concordance analysis. *J. Appl. Toxicol.* **34,** 1-18.

Mellert, W. (1992). Study on the potential carcinogenicity of epoxiconazole feeding study in C57BL/6NCrlBr mice administered via the diet for 78 weeks. Department of Toxicology, BASF Aktiengesellschaft, Ludwigshafen/Rein, Germany, for BASF Corporation, Agricultural Products, Research Triangle Park, North Carolina, and completed July 1992 (Registration Document No. 92/10699; MRID No. 44335018). Unpublished. Based on U.S. EPA, 2001.

Muri, S. D., Schlatter, J. R., and Brüschweiler, B. J. (2009). The benchmark dose approach in food risk assessment: Is it applicable and worthwhile? *Food Chem. Toxicol.* **47**, 2906-2925.

Nascimento, M. G., De Oliveira, M. L. C. S., Lima, A. S., and De Camargo, J. L. V. (2006). Effects of Diuron [3-(3, 4-dichlorophenyl)-1, 1-dimethylurea] on the urinary bladder of male Wistar rats. *Toxicol.* **224**, 66-73.

National Research Council (NRC). (2007a). Toxicity Testing in the 21st Century: A Vision and a Strategy. National Academy Press, Washington, DC.

National Research Council (NRC). (2007b). Applications of Toxicogenomic Technologies to Predictive Toxicology and Risk Assessment. National Academy Press, Washington, DC.

National Research Council (NRC). (2008). Phthalates and Cumulative Risk Assessment: The Task Ahead. Committee on the Health Risks of Phthalates, National Academy Press, Washington, DC.

National Research Council (NRC). (2009). Science and Decisions: Advancing Risk Assessment. National Academy Press, Washington, DC.

National Toxicology Program (NTP). (2013). Long-term study reports and abstracts. Available at: http://ntp-server.niehs.nih.gov/?objectid=D16D6C59-F1F6-975E-7D23D1519B8CD7A5. Last updated on January 17, 2013.

Nesnow, S., Ward, W., Moore, T., Ren, H., and Hester, S. D. (2009) Discrimination of tumorigenic triazole conazoles from phenobarbital by transcriptional analyses of mouse liver gene expression. *Toxicol. Sci*. **110**, 68-83.

Nesnow, S. (2013). Integration of toxicological approaches with "omic" and related technologies to elucidate mechanisms of carcinogenic action: Propiconazole, an example. *Cancer Lett.* **334**, 20-7.

Nesnow, S., Grindstaff, R. D., Lambert, G., Padgett, W. T., Bruno, M., Ge, Y., Chen, P. J. Wood, C. E., and Murphy, L. (2001). Propiconazole increases reactive oxygen species levels in mouse hepatic cells in culture and in mouse liver by a cytochrome P450 717 enzyme mediated process. *Chem. Biol. Interact*. **194**, 79-89.

Nesnow, S., Padgett, W. T., and Moore, T. (2011a). Propiconazole induces alterations in the heepatic metabolome of mice. relevance to propiconazole-induced hepatocarcinogenesis. *Toxicol. Sci*. **120**, 297-309.

OECD. (2007). OECD Environment Health and Safety Publications Series on Testing and Assessment No. 80. Guidance on grouping of chemicals. Environment Directorate, Paris 2007.
http://www.oecd.org/officialdocuments/displaydocumentpdf/?cote=env/jm/mono(2007)28&doclanguage=en.

Ortiz, P.A., Bruno, M.E., Moore, T., Nesnow, S., Winnik, W., and Ge, Y. (2010). Proteomic analysis of propiconazole responses in mouse liver: comparison of genomic and proteomic profiles. *J. Proteome. Res*. **9**, 1268–1278.

Paules, R. (2003). Phenotypic anchoring: Linking cause and effect. *Environ. Health Perspect*. **111**, A338–9.

Peffer, R. C. (2011). Cyproconazole Syngenta Response to the Proposed Inclusion of Cyproconazole on the List of Chemicals Submitted to the Carcinogen Identification Committee (July 2011). Available at: http://www.oehha.org/prop65/public_meetings/CIC101211/comments/prior/SyngentaCyproconazoleStubs.pdf

Pirttiaho, H. I., Sotaniemi, E. A., Ahokas, J. T., and Pitkänen U. (1978). Liver size and indices of drug metabolism in epileptics. *Brit. J. Clin. Pharmacol*. **6**, 273-278.

Pirttiaho, H. I., Sotaniemi, E. A., Pelkonen, R. O., and Pitkänen U. (1982). Hepatic blood flow and drug metabolism in patients on enzyme-inducing anticonvulsants. *Eur. J. Clin. Pharmacol*. **22**, 441-445.

Preston, R. J. (2002). Quantitation of molecular endpoints for the dose-response component of cancer risk assessment. *Toxicol. Pathol.* **30**, 112–116.

Ross, J., Plummer, S. M., Rode, A., Scheer, N., Bower, C. C., Vogel, O., Henderson, C. J., Wolf, C. R., and Elcombe, C. R. (2010). Human Constitutive Androstane Receptor (CAR) and Pregnane X Receptor (PXR) Support the Hypertrophic but not the Hyperplastic Response to the Murine Nongenotoxic Hepatocarcinogens Phenobarbital and Chlordane *In Vivo*. *Toxicol. Sci*. **116**, 452-66.

Ross, J. A., and Leavitt, S. A. (2010). Analysis of the mutations induced by conazole fungicides *in vivo*. *Mutagenesis*. **25**, 231–234.

Ross, J. A., Blackman, C. F., Thai, S. F., Li, Z., Kohan, M., Jones, C. P., and Chen, T. (2010). A potential microRNA signature for tumorigenic conazoles in mouse liver. *Mol. Carcinog*. **49**:320–323.

Ross, J. A., Moore, T., and Leavitt, S. A. (2009). *In vivo* mutagenicity of conazole fungicides correlates with tumorigenicity. *Mutagenesis.* **24**:149–152.

Rowlands, J. C., Budinsky, R., Gollapudi, B., Black, M. B., Wolfinger, R. D., Cukovic, D., Dombkowski, A., Thompson, C. M., Urban, J. D. and Thomas, R. S. (2013). A Genomics-Based Analysis of Relative Potencies of Dioxin-Like Compounds in Primary Rat Hepatocytes. *Toxicol. Sci.* **136**, 595-604.

Schmidt, D. R., Schmidt, S., Holmstrom, S. R. Makishima, M., Yu, R. T., Cummins C. L., Mangelsdorf, D. J., and Kliewer, S. A. (2011). AKR1B7 is induced by the farnesoid X receptor and metabolizes bile acids. *J. Biol. Chem*. **286**, 2425-32.

Schulpen, S. H., Pennings, J. L., Tonk, E., and Piersma, A. H. (2014). A statistical approach towards the derivation of predictive gene sets for potency ranking of chemicals in the mouse embryonic stem cell test. *Toxicol. Lett*.**225**:342-9.

Sen, B., Wolf, D. C., Turpaz, Y., Bugrim, A., Retief, J., and Hester, S. D. (2007). Identification of interspecies concordance of mechanisms of arsenic-induced bladder cancer. *Toxicol. In Vitro*, **21**, 1513-1529.

Slikker, W., Jr., Andersen, M. E., Bogdanffy, M. S., Bus, J. S., Cohen, S.D., Conolly, R. B., David, R. M., Doerrer, N. G., Dorman, D. G., Gaylor, D. W., Hattis, D., Rogers, J. M., Setzer, R. W., Swenberg, J. A. and Wallace, K. (2004). Dose-dependent transitions in mechanisms of toxicity: Case studies. *Toxicol. Appl. Pharmacol*. **20**, 226–94.

Sun, G., Thai, S. F., Tully, D. B., Lambert, G. R., Goetz, A. K., Wolf, D. C., Dix, D. J. and Nesnow, S. (2005). Propiconazole-induced cytochrome P450 gene expression and enzymatic activities in rat and mouse liver. *Toxicol. Lett.* **155**, 277-287.

Szarvas, T., Dorp, F.V., Ergun, S., and Rubben, H. (2011). Matrix metalloproteinases and their clinical relevance in urinary bladder cancer. *Nat. Rev. Urol*. **8**, 241–254.

Takeuchi, S., Iida, M., Yabushita, H., Matsuda, T., and Kojima, H. (2008). In vitro screening for aryl hydrocarbon receptor agonistic activity in 200 pesticides using a highly sensitive reporter cell line, DR-EcoScreen cells, and in vivo mouse liver cytochrome P450-1A induction by propanil, diuron and linuron. *Chemosphere*. **74**, 155-165.

Thomas, R. S., Pluta, L., Yang, L. and Halsey, T. A. (2007). Application of genomic biomarkers to predict increased lung tumor incidence in 2-year rodent cancer bioassays. *Toxicol. Sci*. **97**, 55–64.

Thomas, R.S., Bao, W., Chu, T.M., Bessarabova, M., Nikolskaya, T., Nikolsky, Y., Andersen, M.E. and Wolfinger, R.D. (2009). Use of short-term transcriptional profiles to assess the long-term cancer-related safety of environmental and industrial chemicals. *Toxicol. Sci*. **112**, 311–321.

Thomas, R. S., Clewell 3rd, H. J., Allen, B. C., Wesselkamper, S. C., Wang, N. C., Lambert, J. C., Hess-Wilson, J. K., Zhao, Q. J. and Andersen, M. E. (2011). Application of transcriptional benchmark dose values in quantitative cancer and noncancer risk assessment. *Toxicol. Sci.* **120**, 194-205.

Thomas, R. S., Himmelstein, M. W., Clewell 3rd, H. J., Yang, Y., Healy, E., Black, M. B. and Andersen, M. E. (2013). Cross-species transcriptomic analysis of mouse and rat lung exposed to chloroprene. *Toxicol. Sci.* **131**, 629-640.

U.S. Environmental Protection Agency (EPA). (1990). Memorandum: Cyproconazole - mouse carcinogenicity study. OPTS-128993-018. June 1990. MRID: 411472-01.

U.S. Environmental Protection Agency (EPA). (2000). Myclobutanil Pesticide Tolerance. OPP-300994; FRL-6555-5, May 2000. Available at: http://www.epa.gov/fedrgstr/EPA-PEST/2000/May/Day-10/p11571.htm

U.S. Environmental Protection Agency (EPA). (1997). Carcinogenicity Peer Review of Diuron. Office of Prevention, Pesticides, and Toxic Substances, Washington DC, December 18, 1997. Available at: http://www.epa.gov/pesticides/chem_search/cleared_reviews/csr_PC-035505_8-May-97_042.pdf. Accessed on March 31, 2014.

U.S. Environmental Protection Agency (EPA). (2001). Epoxiconazole- Report of the Cancer Assessment Review Committee. Office of Prevention, Pesticides and Toxic Substances. PC Code 123909. January 2001.

U.S. Environmental Protection Agency (EPA). (2002). A Review of the Reference Dose and Reference Concentration Process. EPA/630/P-02/002F. 01 Dec 2002. U.S. EPA, Risk Assessment Forum, Washington, DC. Available at: http://www.epa.gov/ncea/iris/RFD_FINAL[1].pdf.

U.S. Environmental Protection Agency (EPA). (2003). Registration Eligibility Decision for Diuron. List A. Case 0046. Office of Prevention, Pesticides and Toxic Substances. Washington, DC. Available at: http://www.epa.gov/oppsrrd1/REDs/diuron_red.pdf

U.S. Environmental Protection Agency (EPA). (2005). Guidelines for carcinogen risk assessment. EPA/630/P-03/001B. March 2005. Available at: http://cfpub.epa.gov/ncea/raf/recordisplay.cfm?deid=116283.

U.S. Environmental Protection Agency (EPA). (2006a). Reregistration Eligibility Decision (RED) for Propiconazole. EPA 738R-06-27, July 2006. Available at: http://www.epa.gov/oppsrrd1/REDs/propiconazole_red.pdf

U.S. Environmental Protection Agency (EPA). (2006b). Reregistration Eligibility Decision (RED) for Triadimefon and Tolerance Reassessment for Triadimenol. EPA 738-R-06-003, August 2006. Available at: http://www.epa.gov/oppsrrd1/REDs/triadimefon_red.pdf

U.S. Environmental Protection Agency (EPA). (2006c). Epoxiconazole Pesticide Tolerance. EPA–HQ–OPP–2005–0071; FRL–8080–9], September 2006. Available at: http://www.regulations.gov

U.S. Environmental Protection Agency (EPA). (2006d). Approaches for the Application of Physiologically Based Pharmacokinetic (PBPK) Models and Supporting Data in Risk Assessment. U.S. Environmental Protection Agency, National Center for Environmental Assessment, Washington, DC. EPA/600/R-05/043F, August 2006. Available at: http://cfpub.epa.gov/ncea/cfm/nceatools_human.cfm.

U.S. Environmental Protection Agency (EPA). (2008). Cyproconazole Pesticide Tolerance. EPA-HQ-OPP-2008-0149; [FRL-8362-9], May 2008. Available at: http://www.regulations.gov/#!documentDetail;D=EPA-HQ-OPP-2008-0149-0001

U.S. Environmental Protection Agency (EPA). (2011a). Framework for an EPA Chemical Safety for Sustainability Research Program. Office of Research and Development, Washington DC. June 1, 2011.

U.S. Environmental Protection Agency (EPA). (2011b). IRIS Glossary. Integrated Risk Information System (IRIS) Last updated on August 31, 2011. http://www.epa.gov/ncea/iris/help_gloss.htm.

U.S. Environmental Protection Agency (EPA). (2011c). APPENDIX A & B. Use of "Omic" Technology to Inform the Risk Assessment. Support Document for Case Study: Propiconazole. EPA-HQ-OPP-2011-0284-0003.

U.S. Environmental Protection Agency (EPA). (2012). Benchmark Dose Technical Guidance. Risk Assessment Forum. EPA/100/R-12/001. June 2012. Available at: http://www.epa.gov/raf/publications/benchmarkdose.htm.

U.S. Environmental Protection Agency (EPA). (2013). Benchmark Dose Software Version 2.4 released April 19, 2013. National Center for Environmental Assessment, Office of Research and Development. http://www.epa.gov/ncea/bmds/about.html.

U.S. Environmental Protection Agency (EPA). (2014). Integrated Risk Information System (IRIS). Frequent Questions. Last updated September 26, 2012. Available at: http://www.epa.gov/IRIS/. Accessed on March 10, 2014.

Ueda, A., Hamadeh, H. K., Webb, H. K., Yamamoto, Y., Sueyoshi, T., Afshari, C. A., Lehmann, J. M., and Negishi, M. (2002). Diverse roles of the nuclear orphan receptor CAR in regulating hepatic genes in response to phenobarbital. *Mol. Pharmacol*. **61**, 1-6.

Volat, F. E., Pointud, J. C., Pastel, E., Morio, B., Sion, B., Hamard, G., Guichardant, M., Colas, R., Lefrançois-Martinez, A. M., and Martinez, A. (2012). Depressed Levels of Prostaglandin F2α in Mice Lacking Akr1b7 Increase Basal Adiposity and Predispose to Diet-Induced Obesity. *Diabetes*. **61**, 2796-806.

Ward, W. O., Delker, D. A., Hester, S. D. Thai, S. F., Wolf, D. C., Allen, J. W. and Nesnow, S. (2006). Transcriptional profiles in liver from mice treated with hepatotumorigenic and nonhepatotumorigenic triazole conazole fungicides: Propiconazole, triadimefon, and myclobutanil. *Toxicol. Pathol*. **34**, 863-78.

Warren, S., Carpy, S., Müller, F. *et al.* (1988). SAN 619 F – Chronic Toxicity/Oncogenicity Feeding Study In Rats., Sandoz AG, Basel, Switzerland, unpublished report No. 357-R, CBK I.6858/87. (Syngenta File No. SAN619/6010) MRID 41164701. Based on U.S. EPA, 1990 and Peffer, 2011.

Waters, M.D., Jackson, M. and Lea, I. (2010). Characterizing and predicting carcinogenicity and mode of action using conventional and toxicogenomics methods. *Mut. Res.* **705**, 184–200.

Weng, L.,Dai, H., Zhan, Y., He, Y., Stepaniants, S. B., and Bassett, D. E. (2006). Rosetta error model for gene expression analysis. *Bioinformatics.* **22**, 1111–1121.

Whysner, J., Ross, P. M. and Williams G. M. (1996). Phenobarbital mechanistic data and risk assessment: enzyme induction, enhanced cell proliferation, and tumor promotion. *Pharmacol. Ther*. **71**, 153-91.

Wolf, D. C., Allen, J. W., George, M. H., Hester, S. D., Sun, G., Moore, T., Thai, S. F., Delker, D, Winkfield, E., Leavitt, S., Nelson, G., Roop, B. C., Jones, C., Thibodeaux, J., and Nesnow, S. (2006). Toxicity profiles in rats treated with tumorigenic and nontumorigenic triazole conazole fungicides: propiconazole, triadimefon, and myclobutanil. *Toxicol. Pathol*. **34**, 895-902.

Wood, C. E., Jokinen, M. P., Johnson, C. L., Olson, G. R., Hester, S., George, M., Chorley, B.N., Carswell, G., Carter, J. H., Wood, C. R., Bhat, V. S., Corton, J. C., and DeAngelo, A. B. (2014). Comparative Time Course Profiles of Phthalate Stereoisomers in Mice. *Toxicol. Sci.* **139**, 21-34.

World Health Organization/International Programme on Chemical Safety (WHO/IPCS). (2005). Chemical-specific adjustment factors for interspecies differences and human variability: Guidance document for use of data in dose/concentration-response assessment. World Health Organization/International Programme on Chemical Safety. World Health Organization, Geneva, 2005. http://whqlibdoc.who.int/publications/2005/9241546786_eng.pdf.

Yager, J. W., Gentry, P. R., Thomas, R. S., Pluta, L., Efremenko, A., Black, M., ... and Clewell, H. J. (2013). Evaluation of gene expression changes in human primary uroepithelial cells following 24-Hr exposures to inorganic arsenic and its methylated metabolites. *Environ. Mol. Mutagen.* **54**, 82-98.

Yamamoto, Y., Moore, R., Goldsworthy, T. L., Negishi, M., and Maronpot, R. R. (2004). The orphan nuclear receptor constitutive active/androstane receptor is essential for liver tumor promotion by phenobarbital in mice. *Cancer Res.* **64**, 7197-7200.

Yang, L., Allen, B. C. and Thomas, R. S. (2007). BMDExpress: A software tool for the benchmark dose analyses of genomic data. *BMC Genomics*. **8**, 387.

Yu, X., Griffith, W. C., Hanspers, K., Dillman III, J. F., Ong, H., Vredevoogd, M. A., and Faustman, E. M. (2006). A system-based approach to interpret dose- and time-dependent microarray data: Quantitative integration of gene ontology analysis for risk assessment. *Toxicol. Sci*. **92,** 560–577.

Zhao, B., Baston, D. S., Hammock, B., and Denison, M. S. (2006). Interaction of diuron and related substituted phenylureas with the Ah receptor pathway. *J. Biochem. Mol. Toxicol*, **20**, 103-13.

Appendix A: Chapter 1 Supplementary Data

Table A.1. Normalized fold change (FC) in signal intensity with increasing dose for the 48 dose-responsive probes. [a]

Mean consumed dose (mg/kg-day)[b]		9.4	17.5	36.5	9.9	40.2	94.5	15	72	350	13.3	78.1	257	13.8	71.7	269
Gene	Probe	Cypro 50 ppm	Cypro 100 ppm	Cypro 200 ppm	Epoxi 50 ppm	Epoxi 200 ppm	Epoxi 500 ppm	Propi 100 ppm	Propi 500 ppm	Propi 2500 ppm	Triad 100 ppm	Triad 500 ppm	Triad 1800 ppm	Myclo 100 ppm	Myclo 500 ppm	Myclo 2000 ppm
Cyp2c65	1429994_s_at	30.5	58.7	92.3	21.3	100	100	1.3	17.6	100	1.2	8.0	52.7	-1.4	3.5	72.4
Cyp2b10	1451787_at	32.1	57.6	69.1	100	100	100	41.1	100	100	6.3	100	100	14.2	100	100
Cyp2c55	1419582_at	10.1	24.1	45.2	11.4	56.9	100	1.8	22.5	67.8	1.5	16.2	49.4	2.0	12.7	45.0
1443137_at	1443137_at	13.1	24.6	28.8	27.0	69.2	100	1.7	13.6	33.1	1.3	12.6	23.6	1.7	7.6	19.6
S100a8	1419394_s_at	1.3	1.1	3.8	1.4	8.7	54.8	2.8	2.2	100	4.8	4.7	67.7	2.2	3.5	28.9
Gm10419	1436265_at	4.4	8.8	42.1	3.3	5.9	52.5	1.8	4.7	42.4	1.8	3.2	25.9	1.4	1.0	29.7
Nebl	1438452_at	1.2	3.6	18.1	1.3	8.8	48.9	-1.0	1.4	23.2	1.1	1.3	9.1	-1.3	1.3	8.8

Mean consumed dose (mg/kg-day)[b]		9.4	17.5	36.5	9.9	40.2	94.5	15	72	350	13.3	78.1	257	13.8	71.7	269
Gene	Probe	Cypro 50 ppm	Cypro 100 ppm	Cypro 200 ppm	Epoxi 50 ppm	Epoxi 200 ppm	Epoxi 500 ppm	Propi 100 ppm	Propi 500 ppm	Propi 2500 ppm	Triad 100 ppm	Triad 500 ppm	Triad 1800 ppm	Myclo 100 ppm	Myclo 500 ppm	Myclo 2000 ppm
Orm3	1450611_at	4.4	15	27.3	3.2	14.4	43.4	-1.1	-3.8	51.4	-4.1	1.8	49.8	-1.4	2.1	5.9
Gadd45b	1450971_at	2.3	3.8	23.1	2.2	5.3	20.5	-1.4	4.8	41.8	2.4	2.1	20.7	1.6	1.2	20.8
Gstm3	1427473_at	1.5	2.8	5.1	2.4	5.7	20.5	1.4	3.6	12.0	1.9	2.7	7.9	1.1	2.4	6.2
Lrrc67	1424977_at	3.9	4.0	3.9	3.4	5.9	20.2	1.6	3.8	15.3	1.3	1.4	7.4	-1.7	-1.7	4.6
Cyp2b9	1419590_at	2.3	3.6	3.8	5.9	12.7	18.7	-2.1	3.5	10.5	2.7	2.5	3.6	1.1	2.8	1.6
Meig1	1423410_at	1.7	2.5	4.8	2.3	6.4	12.8	1.3	-1.4	10.8	-2.0	1.8	5.4	1.2	-1.5	2.9
1438068_at	1438068_at	1.5	2.1	5.0	2.1	3.0	12.5	1.2	1.7	10.1	-1.8	1.3	8.1	1.3	1.0	8.0
Smpd3	1438665_at	1.3	2.8	3.4	2.0	6.1	11.4	-1.3	1.3	5.5	-1.9	-1.1	5.4	1.0	-1.1	2.1

Mean consumed dose (mg/kg-day)[b]		9.4	17.5	36.5	9.9	40.2	94.5	15	72	350	13.3	78.1	257	13.8	71.7	269
Gene	Probe	Cypro 50 ppm	Cypro 100 ppm	Cypro 200 ppm	Epoxi 50 ppm	Epoxi 200 ppm	Epoxi 500 ppm	Propi 100 ppm	Propi 500 ppm	Propi 2500 ppm	Triad 100 ppm	Triad 500 ppm	Triad 1800 ppm	Myclo 100 ppm	Myclo 500 ppm	Myclo 2000 ppm
Tnfrsf19	1448147_at	2.1	2.7	6.5	1.4	3.2	11.2	-1.7	-1.9	8.3		-1.2	4.3	-2.4	1.4	5.1
Abcc4	1443870_at	1.5	2.1	5.7	1.3	2.0	8.1	1.3	2.5	37.2	1.8	3.3	6.8	-1.5	2.5	5.1
Nsl1	1447705_at	3.2	4.0	5.2	4.1	7.5	7.9	-1.1	2.1	4.4	-1.0	1.6	3.6	1.2	1.2	3.6
Ndrg1	1450977_s_at	3.6	1.6	3.5	2.4	4.5	7.8	-1.1	1.3	7.4	1.3	-1.5	5.0	2.2	2.9	5.1
Akr1b7	1423556_at	2.5	3.6	7.0	1.0	2.8	7.4	1.0	1.5	16.1	1.5	1.5	3.2	1.1	1.7	2.8
Gstt3	1423891_at	2.3	3.1	3.6	1.7	2.6	6.4	-1.7	2.1	6.2	1.1	1.6	4.9	-1.2	-1.0	3.1
Cyp2c54	1455457_at	1.9	2.5	2.6	2.8	4.8	5.2	1.1	1.9	1.6	1.1	1.8	2.4	-1.1	1.6	2.4
Srxn1	1451680_at	1.1	1.1	1.4	1.7	3.0	5.2	1.2	-1.1	2.8	1.0	-1.1	1.7	1.1	-1.1	1.7

Mean consumed dose (mg/kg-day)[b]		9.4	17.5	36.5	9.9	40.2	94.5	15	72	350	13.3	78.1	257	13.8	71.7	269
Gene	Probe	Cypro 50 ppm	Cypro 100 ppm	Cypro 200 ppm	Epoxi 50 ppm	Epoxi 200 ppm	Epoxi 500 ppm	Propi 100 ppm	Propi 500 ppm	Propi 2500 ppm	Triad 100 ppm	Triad 500 ppm	Triad 1800 ppm	Myclo 100 ppm	Myclo 500 ppm	Myclo 2000 ppm
Papss2	1421989_s_at	2.0	2.2	2.6	3.1	2.9	5.2	1.2	1.4	5.9	1.2	-3.1	5.7	1.2	1.5	2.9
Slco1a4	1420405_at	3.5	6.2	7.0	1.7	2.6	4.4	-1.6	1.6	7.4	1.0	1.7	5.3	-2.2	2.0	7.1
Orm2	1420438_at	-1.0	1.6	3.0	1.2	3.1	4.2	1.3	-1.2	3.9	1.1	2.3	8.5	1.0	1.1	1.5
Mt2	1428942_at	1.6	3.5	7.4	1.0	3.8	3.4	-1.9	-1.5	2.7	-1.2	1.9	7.4	-3.2	1.4	2.1
Por	1416933_at	2.7	3.6	7.0	-1.2	2.0	2.8	-1.0	1.5	6.0	-1.0	1.7	4.7	1.0	1.6	2.3
Atg16l2	1429396_at	1.7	2.1	2.7	1.2	2.0	2.6	2.6	1.9	14.4	-1.3	1.6	11.0	1.0	6.6	7.7
Cd36	1450883_a_at	1.1	-1.2	1.7	1.5	1.4	2.5	1.3	1.5	5.6	-1.2	1.3	3.3	1.0	1.1	1.3
Ikbke	1417813_at	1.3	1.6	1.9	1.1	5.9	6.2	2.5	5.7	17.5	4.1	3.0	8.1	1.0	2.1	4.3

Mean consumed dose (mg/kg-day)[b]		9.4	17.5	36.5	9.9	40.2	94.5	15	72	350	13.3	78.1	257	13.8	71.7	269
Gene	Probe	Cypro 50 ppm	Cypro 100 ppm	Cypro 200 ppm	Epoxi 50 ppm	Epoxi 200 ppm	Epoxi 500 ppm	Propi 100 ppm	Propi 500 ppm	Propi 2500 ppm	Triad 100 ppm	Triad 500 ppm	Triad 1800 ppm	Myclo 100 ppm	Myclo 500 ppm	Myclo 2000 ppm
Ttc39c	1446769_at	-1.0	-1.1	-1.2	-1.1	-1.2	-1.5	-1.1	-1.5	-6.6	-1.1	-1.3	-3.8	1.1	1.0	-2.3
Enho	1428739_at	-1.2	-1.4	-1.5	-1.2	-1.2	-2.1	1.0	-1.7	-16.1	-1.2	-1.0	-7.2	1.2	-1.4	-3.2
Serpina9	1429285_at	-1.4	-2.7	-2.6	-1.1	-1.8	-3.0	-1.6	-2.2	-16.6	-2.2	-2.0	-14.5	-1.4	-2.4	-3.7
Hectd2	1438596_at	-1.7	-2.1	-3.5	1.4	-1.6	-3.8	2.7	1.4	-23.7	2.4	1.7	-3.1	1.4	1.6	-3.5
Prlr	1437397_at	-1.3	-1.4	-2.4	-1.1	-2.7	-5.2	-1.5	-1.0	-4.9	-1.1	-1.2	-2.9	-1.3	-1.4	-5.4
Ddx46	1457744_at	-1.7	-3.0	-2.8	-3.8	-6.0	-7.3	-5.1	-9.0	-8.5	-6.2	-5.2	-5.6	-4.8	-4.7	-6.7
Dnaic1	1437094_x_at	-2.0	-8.9	-11.9	-1.2	-1.3	-7.5	-3.2	-4.7	-5.8	-4.0	-3.6	-4.4	1.3	-4.2	-4.1
Lcn13	1428022_at	-1.6	-2.9	-8.3	-3.2	-1.4	-8.5	-1.4	-15.3	-31.9	-1.7	-12.2	-16.7	1.1	-3.6	-22.2

Mean consumed dose (mg/kg-day)[b]		9.4	17.5	36.5	9.9	40.2	94.5	15	72	350	13.3	78.1	257	13.8	71.7	269
Gene	Probe	Cypro 50 ppm	Cypro 100 ppm	Cypro 200 ppm	Epoxi 50 ppm	Epoxi 200 ppm	Epoxi 500 ppm	Propi 100 ppm	Propi 500 ppm	Propi 2500 ppm	Triad 100 ppm	Triad 500 ppm	Triad 1800 ppm	Myclo 100 ppm	Myclo 500 ppm	Myclo 2000 ppm
Chka	1442277_at	-1.4	-2.2	-2.9	-1.7	-2.4	-9.1	1.0	1.1	-2.2	1.7	1.3	-1.0	-1.0	-1.0	-1.2
C2Cd2	1425305_at	1.1	1.2	1.1	-4.5	-12.3	-12.7	-2.2	-2.8	-3.6	1.2	-1.7	-2.5	1.3	-1.8	-1.6
1451681_at	1451681_at	-1.3	-2.2	-4.6	-1.3	-5.3	-13.4	1.4	-1.6	-40.6	3.3	1.1	-3.0	1.1	-1.1	-4.2
Lonrf3	1436200_at	-1.4	-1.4	-2.1	-2.3	-3.6	-13.7	-2.0	1.1	-4.8	-2.0	-1.4	-2.4	-1.1	-1.7	-2.0
Ndst1	1422044_at	-1.4	-1.8	-2.2	-1.4	-1.5	-1.6	-1.2	-1.8	-5.9	-2.0	-3.7	-2.1	-1.4	-1.6	-4.6
Rbbp8	1427062_at	-3.7	-2.3	-1.7	-1.6	-2.0	-1.1	2.9	4.5	7.0	4.9	2.7	3.0	3.8	3.4	-1.7
Nfib	1438245_at	1.1	-1.1	1.0	1.1	1.1	-1.2	-1.4	-1.7	-5.4	-2.2	-2.1	-3.7	-2.4	-2.4	-2.3
Thr2	1419132_at	1.1	1.3	2.1	-1.2	2.8	4.9	1.5	2.1	6.5	2.1	2.1	2.9	-1.2	1.5	1.3

Mean consumed dose (mg/kg-day)[b]		9.4	17.5	36.5	9.9	40.2	94.5	15	72	350	13.3	78.1	257	13.8	71.7	269
Gene	Probe	Cypro 50 ppm	Cypro 100 ppm	Cypro 200 ppm	Epoxi 50 ppm	Epoxi 200 ppm	Epoxi 500 ppm	Propi 100 ppm	Propi 500 ppm	Propi 2500 ppm	Triad 100 ppm	Triad 500 ppm	Triad 1800 ppm	Myclo 100 ppm	Myclo 500 ppm	Myclo 2000 ppm
Ddx6	1439122_at	-2.7	-7.5	-5.0	-1.3	-1.7	-2.1	1.0	-1.4	-2.1	-1.5	-1.4	-1.4	-1.4	-1.4	-1.9

[a] Highlighted cells have a FC ≥ 5; the "cut-off" criterion for discernible dose-responsive behavior was a FC ≥ 5 at the high dose
[b] Mean consumed dose (mg/kg-day) for propiconazole, triadimefon and myclobutanil based on 13-week intake since intake at 30 d was not reported (Allen *et al.*, 2006)

Table A.2. Transcriptional benchmark dose estimates ($BMDL_T$) for the 48 dose-responsive probes[a]

Probe	Primary Sequence Name	Cyproconazole		Epoxiconazole		Propiconazole		Triadimefon		Myclobutanil	
		FC[b] at high dose	$BMDL_T$ (mg/kg-day)	FC at high dose	$BMDL_T$ (mg/kg-day)	FC at high dose	$BMDL_T$ (mg/kg-day)	FC at high dose	$BMDL_T$ (mg/kg-day)	FC at high dose	$BMDL_T$ (mg/kg-day)
1451787_at	Cyp2b10	69	2.7	100	1.4	100	8.0	100	13	100	6.9
1419582_at	Cyp2c55	45	5.2	100	4.2	68	12	49	15	45	33
1455457_at	CYP2c54	2.6		5.2	UF [c]	1.6		2.4		2.4	
1429994_s_at	Cyp2c65	92	1.2	100	8.0	58	60	53	26	72	54
1436265_at	Gm10419	42	12	53	31	42	67	26	53	30	80
1443137_at	1443137_at	29	3.1	100	4.0	33	9.0	24	12	20	30
1450611_at	Orm3	27	8.7	43	22	51	87	50	77	5.9	75
1450971_at	Gadd45b	23	13	21	36	42	77	21	39	21	83
1438452_at	Nebl	18	11	49	25	23	73	9.1	75	8.8	63
1428942_at	Mt2	7.4	15	3.4		2.7		7.4	70	2.1	
1423556_at	Akr1b7	7.0	7.9	7.4	16	16	51	3.2		2.8	
1420405_at	Slco1a4	7.0	4.6	4.4		7.4	66	5.3	90	7.1	63
1416933_at	Por	7.0	9.8	2.7		6.0	35	4.7		2.3	
1448147_at	Tnfrsf19	6.5	16	11	31	8.3	127	4.3		5.1	100
1443870_at	Abcc4	5.7	9.6	8.1	32	37	50	6.8	42	5.1	80
1447705_at	Nsl1	5.2	0.0	7.9	1.9	4.4		3.6		3.6	
1427473_at	Gstm3	5.1	9.8	21	19	12	11	7.9	33	6.2	77
1438068_at	1438068_at	5.0	10	13	30	10	35	8.1	62	8.0	82
1423410_at	Meig1	4.8		13	15	11	75	5.4	31	2.9	
1424977_at	Lrrc67	3.9		20	27	15	55	7.4	51	4.6	
1419590_at	CYP2b9	3.8		19	3.6	11	98	3.6		1.6	
1419394_s_at	S100a8	3.8		55	47	100	109	68	76	28.9	57
1423891_at	Gstt3	3.6		6.4	13	6.2	43	4.9		3.1	
1429396_at	Atg1612	2.7		2.6		14	42	11	78	8.0	114
1420438_at	Orm2	3.0		4.2		3.9		8.5	79	1.5	
1417813_at	Ikbke	1.9		6.2	10	18	61	8.1	93	4.3	

Probe	Primary Sequence Name	Cyproconazole		Epoxiconazole		Propiconazole		Triadimefon		Myclobutanil	
		FC[b] at high dose	$BMDL_T$ (mg/kg-day)	FC at high dose	$BMDL_T$ (mg/kg-day)	FC at high dose	$BMDL_T$ (mg/kg-day)	FC at high dose	$BMDL_T$ (mg/kg-day)	FC at high dose	$BMDL_T$ (mg/kg-day)
1450977_s_at	Ndrg1	3.5		7.8	0.1	7.4	92	5.0	UF	5.1	125
1427062_at	Rbbp8	-1.7		-1.1		7.0	3.3	3.0		-1.7	
1419132_at	Tlr2	2.1		4.9		6.5	59	2.9		1.3	
1438665_at	Smpd3	3.4		11.4	16	5.5	57	5.4	79	2.1	
1450883_a_at	Cd36	1.7		2.5		5.6	86	3.3		1.3	
1421989_s_at	Papss2	2.6		5.2	39	5.9	78	5.7	126	2.9	
1451680_at	Srxn1	1.4		5.2	UF	2.8		1.7		1.7	
1422044_at	Ndst1	-2.2		-1.6		-5.9	3	-2.1		-4.6	
1452893_s_at	Ehno	-1.5		-2.1		-16	87	-7.2	63	-3.2	
1438245_at	Nfib	1.0		-1.2		-5.4	97	-3.7		-2.3	
1446769_at	Ttc39c	-1.2		-1.5		-6.6	19	-3.8		-2.3	
1436200_at	Lonrf3	-2.1		-13.7	UF	-4.8		-2.4		-2.0	
1442277_at	Chka	-2.9		-9.1	0.1	-2.2		-1.0		-1.2	
1457744_at	Ddx46	-2.8		-7.3	UF	-8.5	17	-5.6	UF	-6.7	113
1438596_at	Hectd2	-3.5		-3.8		-23	UF	-3.1		-3.5	
1429285_at	Serpina9	-2.6		-3.0		-17	0.2	-15	0.0	-3.7	
1437397_at	Prlr	-2.4		-5.2	9.8	-4.9		-2.9		-5.4	78
1451681_at	1451681_at	-4.6		-13.4	6.8	-41	UF	-3.0		-4.2	
1428022_at	Lcn13	-8.3	16.0	-8.5	UF	-32	21	-17	31.0	-22.2	104
1439122_at	Ddx6	-5.0	3.8	-2.1		-2.1		-1.4		-1.9	
1425305_at	C2cd2	1.1		-12.7	0.04	-3.6		-2.5		-1.6	
1437094_x_at	Dnaic1	-12	5.1	-7.4	43	-5.8	7.6	-4.4		-4.1	

	Cypro-con-azole	Epoxi-con-azole	Propi-con-azole	Triad-imefon	Myclo-butanil
Mean	8	18	52	55	75
Median	9	16	56	58	78
SD	4.8	14.3	34.5	31.1	30.4
Count, including unacceptable fits (UF)	20	33	38	26	19
# of UF	0	5	2	2	0
Count excluding UF	20	28	36	24	19
Minimum	0.03	0.04	0.2	0.0	6.8

Probe	Primary Sequence Name	Cyproconazole		Epoxiconazole		Propiconazole		Triadimefon		Myclobutanil	
		FC[b] at high dose	$BMDL_T$ (mg/kg-day)	FC at high dose	$BMDL_T$ (mg/kg-day)	FC at high dose	$BMDL_T$ (mg/kg-day)	FC at high dose	$BMDL_T$ (mg/kg-day)	FC at high dose	$BMDL_T$ (mg/kg-day)
	Q1		4.4		4.2		19		31		60
	Q3		11		30		77		77		92
	Maximum		16		47		127		126		125
	Interquartile Ratio (IQR)		6.9		26		59		46		32
	Upper Outliers		0		0		0		0		0
	Lower Outliers		0		0		0		0		1 (Cyp2b10)

[a] Induced or repressed ≥5 FC at high dose within the 330-probe cluster for each conazole
[b] FC = fold change in signal intensity compared to controls
[c] UF = unacceptable fit (global goodness of fit p<0.1, BMD > high dose, and/or Hill k flag)

Table A.3. Best-fit models for increased mean relative liver weight at 30 days

Chemical	Model	p value [b]	BMD_{1SD} (mg/kg-day)	$BMDL_{1SD}$ (mg/kg-day)
Cyproconazole	Exponential #5	NA	10.7	6.1
Epoxiconazole	Hill	0.1044	12.1	7.9
Propiconazole	Exponential Model #2	0.7111	63.9	54.4
Triadimefon	Hill	NA	76.1	48.2
Myclobutanil	Exponential Model #2 and 3	0.9705	39.2	33.3

[a] Best fit model based on one control SD

[b] Acceptable global goodness-of-fit p value is >0.1

NA= not applicable (estimated mean equal to the observed mean)

Appendix B: Chapter 2 Supplementary Data

Table B.1. Xenobiotic metabolism pathway transcriptional benchmark dose summary in male mice at 2 and 7 days

					2d Male		7d Male	
Symbol	Entrez Gene Name	Affymetrix	Fold Change	Net-works	BMD (mg/kg-day)	BMDL (mg/kg-day)	BMD (mg/kg-day)	BMDL (mg/kg-day)
ABCC3	ATP-binding cassette, sub-family C (CFTR/MRP), member 3	1428988_at	2.640	15	25	8.8	26	9.3
AHR	aryl hydrocarbon receptor	1422631_at	1.585	15	81	56	8.2	5.1
ALDH1A1	aldehyde dehydrogenase 1 family, member A1	1416468_at	1.331	9	33	24	UF[1]	UF
CES1	carboxylesterase 1	1449486_at	2.400	10	66	48	UF	UF
Ces1d	carboxylesterase 1D	1435370_a_at	1.717	10	79	55	UF	UF
Ces2a	carboxylesterase 2A	1449375_at	2.287	10	49	37	62	45
Ces2b/Ces2c	carboxylesterase 2C	1424245_at	5.420	10	34	27	29	23
CYP1A2	cytochrome P450, family 1, subfamily A, polypeptide 2	1450715_at	1.764	14	15	3.1	124	75
CYP2B6	cytochrome P450, family 2, subfamily B, polypeptide 6	1451787_at	100	14	16	5.6	8.3	6.4
CYP2C8	cytochrome P450, family 2, subfamily C, polypeptide 8	1452501_at	-3.633	15	UF	UF	UF	UF
CYP2C9	cytochrome P450, family 2, subfamily C, polypeptide 9	1419582_at	69.690	19	45	34	15	9.8
CYP2C19	cytochrome P450, family 2, subfamily C, polypeptide 19	1429994_s_at	99.317	19	49	37	23	18
CYP3A5	cytochrome P450, family 3, subfamily A, polypeptide 5	1426064_at	5.215	19	105	68	77	53
FMO3	flavin containing monooxygenase 3	1449525_at	1.096	21	UF	UF	UF	UF
GSTA3	glutathione S-transferase alpha 3	1423437_at	1.416	15	111	71	UF	UF
GSTA5	glutathione S-transferase alpha 5	1421041_s_at	5.719	15	74	50	45	34
GSTK1	glutathione S-transferase kappa 1	1452823_at	-1.220	15	UF	UF	UF	UF
GSTM1	glutathione S-transferase mu 1	1416411_at	3.241	15	30	23	46	35
Gstm3	glutathione S-transferase, mu 3	1427473_at	13.825	15	49	30	42	25
GSTM3	glutathione S-transferase mu 3 (brain)	1416842_at	1.206	15	UF	UF	UF	UF

					2d Male		7d Male	
Symbol	Entrez Gene Name	Affymetrix	Fold Change	Net-works	BMD (mg/kg-day)	BMDL (mg/kg-day)	BMD (mg/kg-day)	BMDL (mg/kg-day)
GSTM4	glutathione S-transferase mu 4	1424835_at	2.852	15	37	29	UF	UF
GSTM5	glutathione S-transferase mu 5	1425626_at	2.132	15	67	48	3.5	0.1
GSTO1	glutathione S-transferase omega 1	1416531_at	-1.136	15	UF	UF	UF	UF
GSTT1	glutathione S-transferase theta 1	1418186_at	1.981	15	76	53	78	54
HSP90AA1	heat shock protein 90kDa alpha (cytosolic), class A member 1	1426645_at	1.258	13	110	68	UF	UF
KEAP1	kelch-like ECH-associated protein 1	1450746_at	1.217		124	77	UF	UF
KRAS	Kirsten rat sarcoma viral oncogene homolog	1459793_s_at	-1.287	12	UF	UF	UF	UF
LIPC	lipase, hepatic	1419560_at	-1.164	10	UF	UF	UF	UF
MAP2K5	mitogen-activated protein kinase kinase 5	1417854_at	-1.355	12	UF	UF	UF	UF
NQO1	NAD(P)H dehydrogenase, quinone 1	1423627_at	2.407	17	UF	UF	UF	UF
NQO2	NAD(P)H dehydrogenase, quinone 2	1449983_a_at	1.299	3	117	74	UF	UF
PIK3R1	phosphoinositide-3-kinase, regulatory subunit 1 (alpha)	1438682_at	-1.284	12	UF	UF	UF	UF
PPP2R5E	protein phosphatase 2, regulatory subunit B', epsilon isoform	1428461_at	-1.263		UF	UF	UF	UF
SULT1C2	sulfotransferase family, cytosolic, 1C, member 2	1449409_at	4.506	23	66	47	43	26
Sult1d1	sulfotransferase family 1D, member 1	1448973_at	2.462		82	57	51	38
UGT1A6	UDP glucuronosyltransferase 1 family, polypeptide A6	1426261_s_at	1.201	15	115	73	UF	UF
UGT1A9 (and others)	UDP glucuronosyltransferase 1 family, polypeptide A8	1424783_a_at	1.161	15	141	83	UF	UF
UGT2B7	UDP glucuronosyltransferase 2 family, polypeptide B7	1439624_at	1.592	15	63	46	128	76
UGT2B10	UDP glucuronosyltransferase 2 family, polypeptide B10	1427960_at	1.863	15	45	34	53	39
UGT2B17	UDP glucuronosyltransferase 2 family, polypeptide B17	1424934_at	1.144	15	122	76	UF	UF

					2d Male		7d Male	
Symbol	Entrez Gene Name	Affymetrix	Fold Change	Net-works	BMD (mg/kg-day)	BMDL (mg/kg-day)	BMD (mg/kg-day)	BMDL (mg/kg-day)
				Mean	70	46	48	32
				Median	66	48	44	30
				SD	36	22	36	23
				Count	29		18	
				UF	11		22	

[1]UF = unacceptable fit (global goodness of fit p<0.1, BMD > high dose, and/or Hill k flag)

Table B.2. Xenobiotic metabolism pathway transcriptional benchmark dose summary in female mice at 2 and 7 days

					2d Female		7d Female	
Symbol	Entrez Gene Name	Affymetrix	Fold Change	Net-works	BMD (mg/kg-day)	BMDL (mg/kg-day)	BMD (mg/kg-day)	BMDL (mg/kg-day)
ABCC2	ATP-binding cassette, sub-family C (CFTR/MRP), member 2	1450109_s_at	1.991		25	16	100	66
ABCC3	ATP-binding cassette, sub-family C (CFTR/MRP), member 3	1428988_at	3.293		14	10	17	10
AHR	aryl hydrocarbon receptor	1422631_at	1.432	6	19	13	46	35
ALDH1A1	aldehyde dehydrogenase 1 family, member A1	1416468_at	1.290	15	29	17	94	63
ALDH9A1	aldehyde dehydrogenase 9 family, member A1	1436689_a_at	-1.077	15	UF1	UF	UF	UF
CAMK1	calcium/calmodulin-dependent protein kinase I	1417605_s_at	-1.145	4	UF	UF	UF	UF
CES1	carboxylesterase 1	1449486_at	2.001		12	1.7	102	67
Ces1d	carboxylesterase 1D	1449081_at	1.670		30	18	58	43
Ces1e	carboxylesterase 1E	1419510_at	1.125		UF	UF	UF	UF
Ces2a	carboxylesterase 2A	1449375_at	3.097		16	12	34	26
Ces2b/Ces2c	carboxylesterase 2C	1424245_at	13.724		62	44	17	14
CES5A	carboxylesterase 5A	1459865_x_at	1.483		3.2	0.2	UF	UF
CHST15	carbohydrate (N-acetylgalactosamine 4-sulfate 6-O) sulfotransferase 15	1452092_at	-1.836		UF	UF	UF	UF
CREBBP	CREB binding protein	1435224_at	1.039	6	UF	UF	UF	UF
CYP1A2	cytochrome P450, family 1, subfamily A, polypeptide 2	1450715_at	1.698		18	13	66	47
CYP2B6	cytochrome P450, family 2, subfamily B, polypeptide 6	1451787_at	34.613	18	11	6.4	7.7	5.8
CYP2C8	cytochrome P450, family 2, subfamily C, polypeptide 8	1452501_at	-1.909		UF	UF	138	82
CYP2C9	cytochrome P450, family 2, subfamily C, polypeptide 9	1419582_at	100.000		25	13	23	12
CYP2C19	cytochrome P450, family 2, subfamily C, polypeptide 19	1429994_s_at	5.237		52	38	88	51
FMO3	flavin containing monooxygenase 3	1449525_at	-1.609		UF	UF	UF	UF
GSTA3	glutathione S-transferase alpha 3	1423437_at	1.443		UF	UF	120	75
GSTA5	glutathione S-transferase alpha 5	1421040_a_at	7.363		86	57	49	37

					2d Female		7d Female	
Symbol	Entrez Gene Name	Affymetrix	Fold Change	Net-works	BMD (mg/kg-day)	BMDL (mg/kg-day)	BMD (mg/kg-day)	BMDL (mg/kg-day)
GSTM1	glutathione S-transferase mu 1	1416411_at	2.932		30	18	25	10
Gstm3	glutathione S-transferase, mu 3	1427473_at	11.764		39	30	31	24
GSTM4	glutathione S-transferase mu 4	1424835_at	2.394		24	16	41	32
GSTM5	glutathione S-transferase mu 5	1425626_at	1.882		33	19	59	44
GSTT1	glutathione S-transferase theta 1	1418186_at	1.356		43	21	90	58
GSTT2/GSTT2B	glutathione S-transferase theta 2	1417883_at	1.288		27	17	137	82
HSP90AA1	heat shock protein 90kDa alpha (cytosolic), class A member 1	1437497_a_at	1.523	6	28	16	UF	UF
KEAP1	kelch-like ECH-associated protein 1	1450746_at	1.182	11	22	14	78	54
LIPC	lipase, hepatic	1419560_at	-1.237		UF	UF	UF	UF
MAOB	monoamine oxidase B	1434354_at	-1.176	9	UF	UF	UF	UF
MAP2K1	mitogen-activated protein kinase kinase 1	1416351_at	1.339	19	UF	UF	132	80
NDST1	N-deacetylase/N-sulfotransferase (heparan glucosaminyl) 1	1428367_at	-1.236		UF	UF	UF	UF
NQO1	NAD(P)H dehydrogenase, quinone 1	1423627_at	2.350		UF	UF	111	71
PPP2R5A	protein phosphatase 2, regulatory subunit B', alpha	1423911_at	-1.173		UF	UF	UF	UF
SULT1C2	sulfotransferase family, cytosolic, 1C, member 2	1449409_at	3.071		22	14	41	32
Sult1d1	sulfotransferase family 1D, member 1	1418138_at	1.493		26	16	38	30
SULT1E1	--	1420447_at	7.147		46	22	60	44
SUMO1	small ubiquitin-like modifier 1	1451005_at	1.118	6	UF	UF	112	71
UGT1A6	UDP glucuronosyltransferase 1 family, polypeptide A6	1426261_s_at	1.164		UF	UF	143	84
UGT1A9 (and others)	UDP glucuronosyltransferase 1 family, polypeptide A8	1424783_a_at	1.113		44	21	UF	UF
UGT2B7	UDP glucuronosyltransferase 2 family, polypeptide B7	1439624_at	1.876		24	15	82	57
UGT2B10	UDP glucuronosyltransferase 2 family, polypeptide B10	1427961_s_at	1.655		24	15	58	42

					2d Female		7d Female	
Symbol	Entrez Gene Name	Affymetrix	Fold Change	Net-works	BMD (mg/kg-day)	BMDL (mg/kg-day)	BMD (mg/kg-day)	BMDL (mg/kg-day)
UGT2B15	UDP glucuronosyltransferase 2 family, polypeptide B15	1419622_at	1.224		22	15	UF	UF
UGT2B17	UDP glucuronosyltransferase 2 family, polypeptide B17	1424934_at	1.129		35	19	UF	UF
				Mean	30	18	71	47
				Median	26	16	60	44
				SD	16	11	40	24
				Count	30		31	
				UF	16		15	

[1]UF = unacceptable fit (global goodness of fit p<0.1, BMD > high dose, and/or Hill k flag)

Table B.3. PXR/RXR pathway transcriptional benchmark dose summary in male mice at 2 and 7 days

					2d Male		7d Male	
Symbol	Entrez Gene Name	Affymetrix	Fold Change	Net-works	BMD (mg/kg-day)	BMDL (mg/kg-day)	BMD (mg/kg-day)	BMDL (mg/kg-day)
ABCC3	ATP-binding cassette, sub-family C (CFTR/MRP), member 3	1428988_at	2.640	15	25	8.8	26	9.3
ALDH1A1	aldehyde dehydrogenase 1 family, member A1	1416468_at	1.331	9	33	24	UF1	UF
Aldh1a7	aldehyde dehydrogenase family 1, subfamily A7	1418601_at	1.890	9	69	49	76	53
CPT1A	carnitine palmitoyltransferase 1A (liver)	1460409_at	-1.220	3	UF	UF	UF	UF
CYP1A2	cytochrome P450, family 1, subfamily A, polypeptide 2	1450715_at	1.764	14	15	3.1	124	75
CYP2B6	cytochrome P450, family 2, subfamily B, polypeptide 6	1451787_at	100.000	14	16	5.6	8.3	6.4
CYP2C8	cytochrome P450, family 2, subfamily C, polypeptide 8	1452501_at	-3.633	15	UF	UF	UF	UF
CYP2C9	cytochrome P450, family 2, subfamily C, polypeptide 9	1419582_at	69.690	19	45	34	15	10
CYP2C19	cytochrome P450, family 2, subfamily C, polypeptide 19	1429994_s_at	99.317	19	49	37	23	18
CYP3A5	cytochrome P450, family 3, subfamily A, polypeptide 5	1426064_at	5.215	19	105	68	77	53
FOXO1	forkhead box O1	1416981_at	-1.413		UF	UF	UF	UF
FOXO3	forkhead box O3	1434831_a_at	-1.226		UF	UF	UF	UF
GSTM1	glutathione S-transferase mu 1	1416411_at	3.241	15	30	23	46	35
HMGCS2	3-hydroxy-3-methylglutaryl-CoA synthase 2 (mitochondrial)	1423858_a_at	-1.344		UF	UF	UF	UF
NR3C1	nuclear receptor subfamily 3, group C, member 1 (glucocorticoid receptor)	1453860_s_at	1.850		UF	UF	UF	UF
PAPSS2	3'-phosphoadenosine 5'-phosphosulfate synthase 2	1421989_s_at	3.902	15	56	42	117	72
PRKACA	protein kinase, cAMP-dependent, catalytic, alpha	1447720_x_at	-1.157	11	UF	UF	UF	UF
PRKAR1A	protein kinase, cAMP-dependent, regulatory, type I, alpha	1452032_at	-1.235		UF	UF	UF	UF
PRKAR2A	protein kinase, cAMP-dependent, regulatory, type II, alpha	1428783_at	1.283		143	84	UF	UF

					2d Male		7d Male	
Symbol	Entrez Gene Name	Affymetrix	Fold Change	Net-works	BMD (mg/kg-day)	BMDL (mg/kg-day)	BMD (mg/kg-day)	BMDL (mg/kg-day)
SLCO1B3	solute carrier organic anion transporter family, member 1B3	1427826_a_at	2.350	19	123	76	UF	UF
UGT1A9 (and others)	UDP glucuronosyltransferase 1 family, polypeptide A9	1424783_a_at	1.161	15	141	83	UF	UF
				Mean	65	41	57	37
				Median	49	37	46	35
				SD	47	29	44	27
				Count	13		9	
				UF	8		12	

[1]UF = unacceptable fit (global goodness of fit p<0.1, BMD > high dose, and/or Hill k flag)

Table B.4. PXR/RXR pathway transcriptional benchmark dose summary in female mice at 2 and 7 days

					2d Female		7d Female	
Symbol	Entrez Gene Name	Affymetrix	Fold Change	Net-works	BMD (mg/kg-day)	BMDL (mg/kg-day)	BMD (mg/kg-day)	BMDL (mg/kg-day)
ABCC2	ATP-binding cassette, sub-family C (CFTR/MRP), member 2	1450109_s_at	1.991		25	16	100	66
ABCC3	ATP-binding cassette, sub-family C (CFTR/MRP), member 3	1428988_at	3.293		14	10	17	10
ALAS1	aminolevulinate, delta-, synthase 1	1424126_at	3.979	16	28	0.1	131	79
ALDH1A1	aldehyde dehydrogenase 1 family, member A1	1416468_at	1.290	15	29	17	UF[1]	UF
Aldh1a7	aldehyde dehydrogenase family 1, subfamily A7	1418601_at	2.379	15	16	12	41	32
CES3	carboxylesterase 3	1451600_s_at	-1.235	14	UF	UF	17	14
CYP1A2	cytochrome P450, family 1, subfamily A, polypeptide 2	1450715_at	1.698		18	13	66	47
CYP2B6	cytochrome P450, family 2, subfamily B, polypeptide 6	1451787_at	34.613	18	11	6.4	7.7	5.8
CYP2C8	cytochrome P450, family 2, subfamily C, polypeptide 8	1452501_at	-1.909		UF	UF	138	82
CYP2C9	cytochrome P450, family 2, subfamily C, polypeptide 9	1419582_at	100.000		25	13	23	12
CYP2C19	cytochrome P450, family 2, subfamily C, polypeptide 19	1429994_s_at	5.237		52	38	88	51
GSTM1	glutathione S-transferase mu 1	1416411_at	2.932		30	18	25	10
HMGCS2	3-hydroxy-3-methylglutaryl-CoA synthase 2 (mitochondrial)	1431833_a_at	-1.825		UF	UF	UF	UF
PAPSS2	3'-phosphoadenosine 5'-phosphosulfate synthase 2	1421989_s_at	1.703		32	18	46	35
PPARA	peroxisome proliferator-activated receptor alpha	1457721_at	-1.621	18	133	96	UF	UF
PRKACA	protein kinase, cAMP-dependent, catalytic, alpha	1447720_x_at	-1.306	16	UF	UF	UF	UF
PRKAR2A	protein kinase, cAMP-dependent, regulatory, type II, alpha	1452915_at	1.259		27	16	118	74
UGT1A9 (and others)	UDP glucuronosyltransferase 1 family, polypeptide A9	1424783_a_at	1.113		UF	UF	UF	UF

					2d Female		7d Female	
Symbol	Entrez Gene Name	Affymetrix	Fold Change	Net-works	BMD (mg/kg-day)	BMDL (mg/kg-day)	BMD (mg/kg-day)	BMDL (mg/kg-day)
				Mean	34	21	63	40
				Median	27	16	46	35
				SD	32	24	47	29
				Count	13		13	
				UF	6		7	

[1]UF = unacceptable fit (global goodness of fit $p<0.1$, BMD > high dose, and/or Hill k flag)

Table B.5. Protein ubiquitination pathway transcriptional benchmark dose summary in male mice at 2 and 7 days

					2d Male		7d Male	
Symbol	Entrez Gene Name	Affymetrix	Fold Change	Net-works	BMD (mg/kg-day)	BMDL (mg/kg-day)	BMD (mg/kg-day)	BMDL (mg/kg-day)
ANAPC5	anaphase promoting complex subunit 5	1435177_a_at	1.151	22	UF[1]	UF	UF	UF
CDC20	cell division cycle 20 homolog (S. cerevisiae)	1416664_at	40.290	7	48	36	136	80
CDC34	cell division cycle 34 homolog (S. cerevisiae)	1434879_at	1.533	22	74	52	UF	UF
DNAJC9	DnaJ (Hsp40) homolog, subfamily C, member 9	1426473_at	1.464		49	37	UF	UF
HSP90AA1	heat shock protein 90kDa alpha (cytosolic), class A member 1	1426645_at	1.258	13	110	68	UF	UF
HSPA8.	heat shock 70kDa protein 8	1420622_a_at	-1.071	12	UF	UF	UF	UF
HSPE1	heat shock 10kDa protein 1 (chaperonin 10)	1422579_at	1.212	12	112	71	UF	UF
NEDD4L	neural precursor cell expressed, developmentally down-regulated 4-like, E3 ubiquitin protein ligase	1423270_at	-1.377	6	UF	UF	118	73
PSMA1	proteasome (prosome, macropain) subunit, alpha type, 1	1415695_at	1.276	18	91	61	UF	UF
PSMA3	proteasome (prosome, macropain) subunit, alpha type, 3	1448442_a_at	1.145	5	UF	UF	UF	UF
PSMA4	proteasome (prosome, macropain) subunit, alpha type, 4	1460339_at	1.192	18	131	80	UF	UF
PSMA5	proteasome (prosome, macropain) subunit, alpha type, 5	1424681_a_at	1.172	18	123	76	UF	UF
PSMA7	proteasome (prosome, macropain) subunit, alpha type, 7	1423568_at	1.278	18	UF	UF	UF	UF
PSMB2	proteasome (prosome, macropain) subunit, beta type, 2	1448262_at	1.145	18	142	84	UF	UF
PSMB3	proteasome (prosome, macropain) subunit, beta type, 3	1460198_a_at	1.096	18	UF	UF	UF	UF
PSMB4	proteasome (prosome, macropain) subunit, beta type, 4	1451205_at	1.165	18	121	75	UF	UF
PSMB5	proteasome (prosome, macropain) subunit, beta type, 5	1415676_a_at	1.126	18	UF	UF	UF	UF
PSMB6	proteasome (prosome, macropain) subunit, beta type, 6	1448822_at	1.147	18	121	76	UF	UF
PSMC1	proteasome (prosome, macropain) 26S subunit, ATPase, 1	1416005_at	1.215	18	118	74	UF	UF

					2d Male		7d Male	
Symbol	Entrez Gene Name	Affymetrix	Fold Change	Net-works	BMD (mg/kg-day)	BMDL (mg/kg-day)	BMD (mg/kg-day)	BMDL (mg/kg-day)
PSMC3	proteasome (prosome, macropain) 26S subunit, ATPase, 3	1416282_at	1.168	18	103	67	UF	UF
PSMC4	proteasome (prosome, macropain) 26S subunit, ATPase, 4	1416290_a_at	1.264	18	117	74	UF	UF
PSMC6	proteasome (prosome, macropain) 26S subunit, ATPase, 6	1417771_a_at	1.144	18	UF	UF	UF	UF
PSMD1	proteasome (prosome, macropain) 26S subunit, non-ATPase, 1	1429291_at	1.323	18	103	67	UF	UF
PSMD3	proteasome (prosome, macropain) 26S subunit, non-ATPase, 3	1448479_at	1.340	5	108	70	UF	UF
PSMD4	proteasome (prosome, macropain) 26S subunit, non-ATPase, 4	1425859_a_at	1.186	5	117	64	UF	UF
PSMD6	proteasome (prosome, macropain) 26S subunit, non-ATPase, 6	1423697_at	1.094	18	146	85	UF	UF
PSMD7	proteasome (prosome, macropain) 26S subunit, non-ATPase, 7	1451056_at	1.294	18	118	71	UF	UF
PSMD11	proteasome (prosome, macropain) 26S subunit, non-ATPase, 11	1429370_a_at	1.367	5	34	20	UF	UF
PSMD12	proteasome (prosome, macropain) 26S subunit, non-ATPase, 12	1448492_a_at	1.118	5	131	80	UF	UF
PSMD14	proteasome (prosome, macropain) 26S subunit, non-ATPase, 14	1421751_a_at	1.248	5	110	71	UF	UF
PSME2	proteasome (prosome, macropain) activator subunit 2 (PA28 beta)	1417189_at	1.155	18	127	78	UF	UF
SKP1/SKP1P2	S-phase kinase-associated protein 1	1423148_at	1.055	22	UF	UF	UF	UF
STUB1	STIP1 homology and U-box containing protein 1, E3 ubiquitin protein ligase	1434412_x_at	-1.504	17	UF	UF	UF	UF
UBE2C	ubiquitin-conjugating enzyme E2C	1452954_at	15.700	22	43	32	UF	UF
UBE2E1	ubiquitin-conjugating enzyme E2E 1	1416943_at	1.196	22	121	75	UF	UF
UBE2G1	ubiquitin-conjugating enzyme E2G 1	1455094_s_at	-1.103	22	UF	UF	UF	UF
UBE2S	ubiquitin-conjugating enzyme E2S	1416726_s_at	2.208	22	59	43	UF	UF
USP14	ubiquitin specific peptidase 14 (tRNA-guanine transglycosylase)	1416208_at	1.174	5	139	83	UF	UF
XIAP	X-linked inhibitor of apoptosis	1437533_at	-1.205	17	UF	UF	UF	UF
				Mean	104	66	127	77

					2d Male		7d Male	
Symbol	Entrez Gene Name	Affymetrix	Fold Change	Net-works	BMD (mg/kg-day)	BMDL (mg/kg-day)	BMD (mg/kg-day)	BMDL (mg/kg-day)
				Median	117	71	127	77
				SD	32	17	13	5
				Count	27		2	2
				UF			37	

[1]UF = unacceptable fit (global goodness of fit p<0.1, BMD > high dose, and/or Hill k flag)

Table B.6. Protein ubiquitination pathway transcriptional benchmark dose summary in female mice at 2 and 7 days

					2d Female		7d Female	
Symbol	Entrez Gene Name	Affymetrix	Fold Change	Net-works	BMD (mg/kg-day)	BMDL (mg/kg-day)	BMD (mg/kg-day)	BMDL (mg/kg-day)
BRCA1	breast cancer 1, early onset	1424629_at	1.584		0.1	0.0	49	24
CDC20	cell division cycle 20 homolog (S. cerevisiae)	1416664_at	21.922	5	76	52	UF[1]	UF
CDC34	cell division cycle 34 homolog (S. cerevisiae)	1434879_at	1.500	22	32	19	106	69
CRYAB	crystallin, alpha B	1434369_a_at	-1.305		20	13	UF	UF
DNAJC9	DnaJ (Hsp40) homolog, subfamily C, member 9	1426473_at	1.567		84	56	UF	UF
HLA-B	major histocompatibility complex, class I, B	1427651_x_at	-2.865		UF	UF	33	20
HSP90AA1	heat shock protein 90kDa alpha (cytosolic), class A member 1	1437497_a_at	1.523	6	28	16	UF	UF
HSPA14	heat shock 70kDa protein 14	1448586_at	1.279		UF	UF	UF	UF
HSPA4L	heat shock 70kDa protein 4-like	1458385_at	2.191		29	17	67	48
HSPE1	heat shock 10kDa protein 1 (chaperonin 10)	1450668_s_at	1.118		30	18	UF	UF
MDM2	Mdm2, p53 E3 ubiquitin protein ligase homolog (mouse)	1427718_a_at	1.673	6	33	19	142	83
NEDD4	neural precursor cell expressed, developmentally down-regulated 4, E3 ubiquitin protein ligase	1450431_a_at	-1.094		UF	UF	UF	UF
NEDD4L	neural precursor cell expressed, developmentally down-regulated 4-like, E3 ubiquitin protein ligase	1441305_at	-1.677		UF	UF	UF	UF
PSMA1	proteasome (prosome, macropain) subunit, alpha type, 1	1415695_at	1.268	3	23	15	UF	UF
PSMA2	proteasome (prosome, macropain) subunit, alpha type, 2	1448206_at	1.191	4	30	18	UF	UF
PSMA3	proteasome (prosome, macropain) subunit, alpha type, 3	1448442_a_at	1.116	4	31	18	UF	UF

					2d Female		7d Female	
Symbol	Entrez Gene Name	Affymetrix	Fold Change	Net-works	BMD (mg/kg-day)	BMDL (mg/kg-day)	BMD (mg/kg-day)	BMDL (mg/kg-day)
PSMA4	proteasome (prosome, macropain) subunit, alpha type, 4	1460339_at	1.146	12	UF	UF	UF	UF
PSMA5	proteasome (prosome, macropain) subunit, alpha type, 5	1424681_a_at	1.172	3	24	15	122	76
PSMA6	proteasome (prosome, macropain) subunit, alpha type, 6	1416506_at	1.050	4	UF	UF	UF	UF
PSMA7	proteasome (prosome, macropain) subunit, alpha type, 7	1423568_at	1.176	3	21	14	95	63
PSMB1	proteasome (prosome, macropain) subunit, beta type, 1	1420053_at	1.068	3	23	15	121	75
PSMB2	proteasome (prosome, macropain) subunit, beta type, 2	1448262_at	1.219	3	35	19	UF	UF
PSMB3	proteasome (prosome, macropain) subunit, beta type, 3	1417052_at	1.203	3	UF	UF	UF	UF
PSMB4	proteasome (prosome, macropain) subunit, beta type, 4	1451205_at	1.173	3	36	20	UF	UF
PSMB5	proteasome (prosome, macropain) subunit, beta type, 5	1415676_a_at	1.236	12	UF	UF	UF	UF
PSMB6	proteasome (prosome, macropain) subunit, beta type, 6	1448822_at	1.163	3	28	17	UF	UF
PSMB7	proteasome (prosome, macropain) subunit, beta type, 7	1416240_at	1.104	3	43	21	UF	UF
PSMC3	proteasome (prosome, macropain) 26S subunit, ATPase, 3	1416282_at	1.236	9	UF	UF	133	80
PSMC4	proteasome (prosome, macropain) 26S subunit, ATPase, 4	1416290_a_at	1.273	12	25	16	130	79
PSMC5	proteasome (prosome, macropain) 26S subunit, ATPase, 5	1415740_at	-1.033	18	34	19	UF	UF
PSMC6	proteasome (prosome,	1417771_a_at	1.133	12	27	17	UF	UF

					2d Female		7d Female	
Symbol	Entrez Gene Name	Affymetrix	Fold Change	Net-works	BMD (mg/kg-day)	BMDL (mg/kg-day)	BMD (mg/kg-day)	BMDL (mg/kg-day)
	macropain) 26S subunit, ATPase, 6							
PSMD1	proteasome (prosome, macropain) 26S subunit, non-ATPase, 1	1429291_at	1.323	9	26	16	122	76
PSMD2	proteasome (prosome, macropain) 26S subunit, non-ATPase, 2	1415831_at	1.176	9	40	20	UF	UF
PSMD3	proteasome (prosome, macropain) 26S subunit, non-ATPase, 3	1448479_at	1.348	9	UF	UF	126	77
PSMD4	proteasome (prosome, macropain) 26S subunit, non-ATPase, 4	1425859_a_at	1.110		UF	UF	UF	UF
PSMD7	proteasome (prosome, macropain) 26S subunit, non-ATPase, 7	1451056_at	1.236	9	UF	UF	UF	UF
PSMD11	proteasome (prosome, macropain) 26S subunit, non-ATPase, 11	1437080_s_at	1.266	9	35	19	UF	UF
PSMD12	proteasome (prosome, macropain) 26S subunit, non-ATPase, 12	1448492_a_at	1.135	9	29	17	UF	UF
PSMD14	proteasome (prosome, macropain) 26S subunit, non-ATPase, 14	1421751_a_at	1.256	9	33	18	UF	UF
PSME1	proteasome (prosome, macropain) activator subunit 1 (PA28 alpha)	1417056_at	1.187	3	26	17	134	80
SKP2	S-phase kinase-associated protein 2, E3 ubiquitin protein ligase	1436000_a_at	3.499	22	82	55	UF	UF
UBE2C	ubiquitin-conjugating enzyme E2C	1452954_at	13.152	22	76	52	UF	UF
UBE2E2	ubiquitin-conjugating enzyme E2E 2	1424358_at	-1.535	22	UF	UF	UF	UF

					2d Female		7d Female	
Symbol	Entrez Gene Name	Affymetrix	Fold Change	Net-works	BMD (mg/kg-day)	BMDL (mg/kg-day)	BMD (mg/kg-day)	BMDL (mg/kg-day)
UBE2L3	ubiquitin-conjugating enzyme E2L 3	1448879_at	1.163	22	27	17	UF	UF
UBE2R2	ubiquitin-conjugating enzyme E2R 2	1415768_a_at	-1.136	22	UF	UF	UF	UF
UBE2S	ubiquitin-conjugating enzyme E2S	1416726_s_at	3.285	22	94	61	UF	UF
UBE2V2	ubiquitin-conjugating enzyme E2 variant 2	1417983_a_at	1.043	22	32	18	UF	UF
USP1	ubiquitin specific peptidase 1	1451080_at	1.280	21	UF	UF	UF	UF
USP10	ubiquitin specific peptidase 10	1448230_at	1.241	21	28	17	UF	UF
USP14	ubiquitin specific peptidase 14 (tRNA-guanine transglycosylase)	1416208_at	1.203	9	40	21	148	86
USP47	ubiquitin specific peptidase 47	1426976_at	1.168	21	UF	UF	129	79
USP48	ubiquitin specific peptidase 48	1419278_at	1.007	21	24	15	129	79
				Mean	36	22	112	68
				Median	30	18	124	77
				SD	20	14	34	20
				Count	36		16	
				UF	16		36	

[1]UF = unacceptable fit (global goodness of fit p<0.1, BMD > high dose, and/or Hill k flag)

Table B.7. Eif2 signaling pathway transcriptional benchmark dose summary in male mice at 2 and 7 days

					2d Male		7d Male	
Symbol	Entrez Gene Name	Affymetrix	Fold Change	Net-works	BMD (mg/kg-day)	BMDL (mg/kg-day)	BMD (mg/kg-day)	BMDL (mg/kg-day)
EIF1AX	eukaryotic translation initiation factor 1A, X-linked	1419736_a_at	1.251	2	93	62	UF[1]	UF
EIF3E	eukaryotic translation initiation factor 3, subunit E	1460432_a_at	1.067	2	UF	UF	UF	UF
MAP2K1	mitogen-activated protein kinase kinase 1	1416351_at	1.339	19	134	81	UF	UF
PPP1CC	protein phosphatase 1, catalytic subunit, gamma isozyme	1452046_a_at	1.945		101	66	UF	UF
RPL3	ribosomal protein L3	1449323_a_at	1.107	2	UF	UF	UF	UF
RPL4	ribosomal protein L4	1425183_a_at	1.118	2	UF	UF	UF	UF
RPL6	ribosomal protein L6	1416546_a_at	1.119	2	UF	UF	UF	UF
RPL7	ribosomal protein L7	1415979_x_at	1.077	2	UF	UF	UF	UF
RPL12	ribosomal protein L12	1416026_a_at	1.314	6	119	74	UF	UF
RPL13	ribosomal protein L13	1450150_a_at	1.153	2	UF	UF	UF	UF
RPL15	ribosomal protein L15	1449255_a_at	1.176	10	UF	UF	UF	UF
RPL17	ribosomal protein L17	1436822_x_at	1.099	2	UF	UF	UF	UF
RPL21	ribosomal protein L21	1455767_x_at	1.074	10	143	84	UF	UF
RPL22	ribosomal protein L22	1448398_s_at	-1.208	2	UF	UF	UF	UF
RPL23	ribosomal protein L23	1454859_a_at	1.126	2	UF	UF	UF	UF
RPL27	ribosomal protein L27	1416099_at	1.100	10	UF	UF	UF	UF
RPL29	ribosomal protein L29	1448846_a_at	1.125	10	UF	UF	UF	UF
RPL30	ribosomal protein L30	1418273_a_at	1.123		UF	UF	UF	UF
RPL35	ribosomal protein L35	1416243_a_at	1.137	2	UF	UF	UF	UF
RPL10A	ribosomal protein L10a	1431177_a_at	1.138	2	UF	UF	UF	UF
RPL13A	ribosomal protein L13a	1433928_a_at	1.218		UF	UF	UF	UF
RPL22L1	ribosomal protein L22-like 1	1417126_a_at	1.374	10	127	78	UF	UF
RPL23A	ribosomal protein L23a	1426660_x_at	1.056		UF	UF	UF	UF

					2d Male		7d Male	
Symbol	Entrez Gene Name	Affymetrix	Fold Change	Net-works	BMD (mg/kg-day)	BMDL (mg/kg-day)	BMD (mg/kg-day)	BMDL (mg/kg-day)
RPLP0	ribosomal protein, large, P0	1419441_at	1.134	10	UF	UF	UF	UF
RPLP2	ribosomal protein, large, P2	1415879_a_at	1.108	6	UF	UF	UF	UF
RPS5	ribosomal protein S5	1416054_at	1.145	10	UF	UF	UF	UF
RPS8	ribosomal protein S8	1455319_x_at	1.159	10	UF	UF	UF	UF
RPS11	ribosomal protein S11	1424000_a_at	1.105	10	UF	UF	UF	UF
RPS12	ribosomal protein S12	1448344_at	1.146	10	UF	UF	UF	UF
RPS13	ribosomal protein S13	1415912_a_at	1.169	10	UF	UF	UF	UF
RPS18	ribosomal protein S18	1455572_x_at	1.162	10	UF	UF	UF	UF
RPS19	ribosomal protein S19	1449243_a_at	1.155	10	UF	UF	UF	UF
RPS21	ribosomal protein S21	1433721_x_at	1.064	10	UF	UF	UF	UF
RPS23	ribosomal protein S23	1460175_at	1.059	10	UF	UF	UF	UF
RPS24	ribosomal protein S24	1428530_x_at	1.095	10	UF	UF	UF	UF
RPS27L	ribosomal protein S27-like	1450925_a_at	1.116	10	UF	UF	UF	UF
RPSA	ribosomal protein SA	1448245_at	1.163	10	UF	UF	UF	UF
				Mean	120	74	NA	
				Median	123	76	NA	
				SD	19	9	NA	
				Count	6		0	
				UF	31		37	

[1]UF = unacceptable fit (global goodness of fit p<0.1, BMD > high dose, and/or Hill k flag)

Table B.8. Eif2 signaling pathway transcriptional benchmark dose summary in female mice at 2 and 7 days

					2d Female		7d Female	
Symbol	Entrez Gene Name	Affymetrix	Fold Change	Net-works	BMD (mg/kg-day)	BMDL (mg/kg-day)	BMD (mg/kg-day)	BMDL (mg/kg-day)
EIF1AX	eukaryotic translation initiation factor 1A, X-linked	1419736_a_at	1.251	2	31	18	UF[1]	UF
EIF3E	eukaryotic translation initiation factor 3, subunit E	1460432_a_at	1.067	2	33	18	UF	UF
MAP2K1	mitogen-activated protein kinase kinase 1	1416351_at	1.339	19	UF	UF	132	80
PPP1CC	protein phosphatase 1, catalytic subunit, gamma isozyme	1452046_a_at	1.945		UF	UF	83	57
RPL3	ribosomal protein L3	1449323_a_at	1.107	2	49	19	UF	UF
RPL4	ribosomal protein L4	1425183_a_at	1.118	2	UF	UF	UF	UF
RPL6	ribosomal protein L6	1416546_a_at	1.119	2	UF	UF	UF	UF
RPL7	ribosomal protein L7	1415979_x_at	1.077	2	UF	UF	UF	UF
RPL12	ribosomal protein L12	1416026_a_at	1.314	6	31	19	UF	UF
RPL13	ribosomal protein L13	1450150_a_at	1.153	2	UF	UF	UF	UF
RPL15	ribosomal protein L15	1449255_a_at	1.176	10	UF	UF	UF	UF
RPL17	ribosomal protein L17	1436822_x_at	1.099	2	36	20	UF	UF
RPL21	ribosomal protein L21	1455767_x_at	1.074	10	34	18	UF	UF
RPL22	ribosomal protein L22	1448398_s_at	-1.208	2	UF	UF	UF	UF
RPL23	ribosomal protein L23	1454859_a_at	1.126	2	37	19	UF	UF
RPL27	ribosomal protein L27	1416099_at	1.100	10	35	20	UF	UF
RPL29	ribosomal protein L29	1448846_a_at	1.125	10	UF	UF	UF	UF
RPL30	ribosomal protein L30	1418273_a_at	1.123		UF	UF	UF	UF
RPL35	ribosomal protein L35	1416243_a_at	1.137	2	UF	UF	UF	UF
RPL10A	ribosomal protein L10a	1431177_a_at	1.138	2	UF	UF	UF	UF
RPL13A	ribosomal protein L13a	1433928_a_at	1.218		40	21	UF	UF
RPL22L1	ribosomal protein L22-like 1	1417126_a_at	1.374	10	33	17	UF	UF
RPL23A	ribosomal protein L23a	1426660_x_at	1.056		UF	UF	UF	UF
RPLP0	ribosomal protein, large, P0	1419441_at	1.134	10	UF	UF	UF	UF
RPLP2	ribosomal protein, large, P2	1415879_a_at	1.108	6	UF	UF	UF	UF

					2d Female		7d Female	
Symbol	Entrez Gene Name	Affymetrix	Fold Change	Net-works	BMD (mg/kg-day)	BMDL (mg/kg-day)	BMD (mg/kg-day)	BMDL (mg/kg-day)
RPS5	ribosomal protein S5	1416054_at	1.145	10	UF	UF	UF	UF
RPS8	ribosomal protein S8	1455319_x_at	1.159	10	34	19	UF	UF
RPS11	ribosomal protein S11	1424000_a_at	1.105	10	28	17	UF	UF
RPS12	ribosomal protein S12	1448344_at	1.146	10	UF	UF	UF	UF
RPS13	ribosomal protein S13	1415912_a_at	1.169	10	37	18	UF	UF
RPS18	ribosomal protein S18	1455572_x_at	1.162	10	UF	UF	UF	UF
RPS19	ribosomal protein S19	1449243_a_at	1.155	10	UF	UF	UF	UF
RPS21	ribosomal protein S21	1433721_x_at	1.064	10	33	19	UF	UF
RPS23	ribosomal protein S23	1460175_at	1.059	10	UF	UF	UF	UF
RPS24	ribosomal protein S24	1428530_x_at	1.095	10	UF	UF	UF	UF
RPS27L	ribosomal protein S27-like	1450925_a_at	1.116	10	UF	UF	UF	UF
RPSA	ribosomal protein SA	1448245_at	1.163	10	UF	UF	UF	UF
				Mean	35	19	108	69
				Median	34	19	108	69
				SD	5.0	1.1	35	16
				Count	14		2	
				UF	22		35	

[1]UF = unacceptable fit (global goodness of fit p<0.1, BMD > high dose, and/or Hill k flag)

Table B.9. Cell-cycle control of chromosomal replication pathway transcriptional benchmark dose summary in male mice at 2 and 7 days

					2d Male		7d Male	
Symbol	Entrez Gene Name	Affymetrix	Fold Change	Net-works	BMD (mg/kg-day)	BMDL (mg/kg-day)	BMD (mg/kg-day)	BMDL (mg/kg-day)
CDC6	cell division cycle 6 homolog (S. cerevisiae)	1417019_a_at	5.790	7	42	32	37	0.1
CDT1	chromatin licensing and DNA replication factor 1	1424143_a_at	3.447	7	48	36	UF[1]	UF
DBF4	DBF4 homolog (S. cerevisiae)	1418334_at	2.974	7	46	34	UF	UF
MCM2	minichromosome maintenance complex component 2	1448777_at	3.786	7	39	30	106	67
MCM3	minichromosome maintenance complex component 3	1449705_x_at	3.821	7	62	45	UF	UF
MCM4	minichromosome maintenance complex component 4	1416214_at	2.730	7	41	31	UF	UF
MCM5	minichromosome maintenance complex component 5	1436808_x_at	6.638	7	27	21	UF	UF
MCM6	minichromosome maintenance complex component 6	1416251_at	3.994	7	35	27	127	76
MCM7	minichromosome maintenance complex component 7	1438320_s_at	1.650	7	63	46	UF	UF
RPA1	replication protein A1, 70kDa	1437309_a_at	1.520	4	78	54	UF	UF
RPA2	replication protein A2, 32kDa	1416433_at	1.834	7	64	46	UF	UF
				Mean	50	37	90	48
				Median	46	34	106	67
				SD	15	10	47	41
				Count	11		3	
				UF	0		8	

[1]UF = unacceptable fit (global goodness of fit p<0.1, BMD > high dose, and/or Hill k flag)

Table B.10. Cell-cycle control of chromosomal replication pathway transcriptional benchmark dose summary in female mice at 2 and 7 days

					2d Female		7d Female	
Symbol	Entrez Gene Name	Affymetrix	Fold Change	Net-works	BMD (mg/kg-day)	BMDL (mg/kg-day)	BMD (mg/kg-day)	BMDL (mg/kg-day)
CDC6	cell division cycle 6 homolog (S. cerevisiae)	1417019_a_at	8.255		48	35	UF[1]	UF
CDT1	chromatin licensing and DNA replication factor 1	1424143_a_at	2.357	15	48	36	UF	UF
DBF4	DBF4 homolog (S. cerevisiae)	1418334_at	4.819	15	85	57	UF	UF
MCM2	minichromosome maintenance complex component 2	1448777_at	5.110	15	46	34	UF	UF
MCM3	minichromosome maintenance complex component 3	1426652_at	6.702	15	56	41	UF	UF
MCM4	minichromosome maintenance complex component 4	1416214_at	2.936	15	48	36	30	18
MCM5	minichromosome maintenance complex component 5	1436808_x_at	6.205	15	40	31	50	24
MCM6	minichromosome maintenance complex component 6	1416251_at	4.698	15	39	29	52	24
MCM7	minichromosome maintenance complex component 7	1439269_x_at	2.304	15	66	47	UF	UF
ORC4	origin recognition complex, subunit 4	1423337_at	1.290	15	15	0.0	138	82
RPA1	replication protein A1, 70kDa	1437309_a_at	1.694	20	18	0.0	127	78
RPA2	replication protein A2, 32kDa	1454011_a_at	2.131	20	29	17	142	84
				Mean	45	30	90	52
				Median	47	35	90	51
				SD	19	17	51	33
				Count	12		6	
				UF	0		6	

[1]UF = unacceptable fit (global goodness of fit p<0.1, BMD > high dose, and/or Hill k flag)

Table B.11. Role of Brca1 in DNA damage response pathway transcriptional benchmark dose summary in male mice at 2 and 7 days

					2d Male		7d Male	
Symbol	Entrez Gene Name	Affymetrix	Fold Change	Net-works	BMD (mg/kg-day)	BMDL (mg/kg-day)	BMD (mg/kg-day)	BMDL (mg/kg-day)
ATF1	activating transcription factor 1	1417296_at	1.189		118	74	UF[1]	UF
ATR	ataxia telangiectasia and Rad3 related	1427197_at	1.709	7	56	41	84	57
CHEK1	checkpoint kinase 1	1450677_at	2.966	17	52	39	34	3.2
GADD45A	growth arrest and DNA-damage-inducible, alpha	1449519_at	8.440		95	64	85	57
PLK1	polo-like kinase 1	1448191_at	9.612		42	32	UF	UF
RAD51	RAD51 homolog (S. cerevisiae)	1418281_at	3.184	17	60	37	88	59
RBBP8	retinoblastoma binding protein 8	1427061_at	1.592		78	55	UF	UF
RBL1	retinoblastoma-like 1 (p107)	1424156_at	1.624	7	59	44	114	71
RFC3	replication factor C (activator 1) 3, 38kDa	1432538_a_at	1.540	4	16	2.7	UF	UF
RFC4	replication factor C (activator 1) 4, 37kDa	1424321_at	1.787	4	48	36	UF	UF
RFC5	replication factor C (activator 1) 5, 36.5kDa	1452917_at	1.475	4	88	60	UF	UF
RPA1	replication protein A1, 70kDa	1437309_a_at	1.520	4	78	54	UF	UF
				Mean	66	45	81	49
				Median	60	43	85	57
				SD	27	18	29	26
				Count	12		5	
				UF	0		7	

[1]UF = unacceptable fit (global goodness of fit p<0.1, BMD > high dose, and/or Hill k flag)

Table B.12. Role of Brca1 in DNA damage response pathway transcriptional benchmark dose summary in female mice at 2 and 7 days

					2d Female		7d Female	
Symbol	Entrez Gene Name	Affymetrix	Fold Change	Net-works	BMD (mg/kg-day)	BMDL (mg/kg-day)	BMD (mg/kg-day)	BMDL (mg/kg-day)
ATF1	activating transcription factor 1	1417296_at	1.142		UF[1]	UF	UF	UF
ATR	ataxia telangiectasia and Rad3 related	1427197_at	1.805	20	42	0.0	UF	UF
BRCA1	breast cancer 1, early onset	1424629_at	1.584		0.1	0.0	49	24
BRCA2	breast cancer 2, early onset	1419076_a_at	1.790		25	3.6	UF	UF
CHEK1	checkpoint kinase 1	1450677_at	4.439		52	38	UF	UF
E2F2	E2F transcription factor 2	1455790_at	6.188	15	69	49	UF	UF
FANCA	Fanconi anemia, complementation group A	1418856_a_at	1.378		32	3.0	UF	UF
GADD45A	growth arrest and DNA-damage-inducible, alpha	1449519_at	3.801		58	42	70	40
MSH6	mutS homolog 6 (E. coli)	1416915_at	1.495	20	33	19	116	73
PLK1	polo-like kinase 1	1448191_at	12.057	4	74	51	UF	UF
RAD51	RAD51 homolog (S. cerevisiae)	1418281_at	6.380	6	53	39	38	21
RBBP8	retinoblastoma binding protein 8	1427061_at	2.342	6	27	17	85	58
RBL1	retinoblastoma-like 1 (p107)	1424156_at	2.297		15	4.4	UF	UF
RFC3	replication factor C (activator 1) 3, 38kDa	1423700_at	1.577	20	34	19	UF	UF
RFC4	replication factor C (activator 1) 4, 37kDa	1424321_at	2.232	20	59	43	UF	UF
RFC5	replication factor C (activator 1) 5, 36.5kDa	1452917_at	1.710	20	118	72	UF	
RPA1	replication protein A1, 70kDa	1437309_a_at	1.694	20	18	0.0	127	78
SMARCD2	SWI/SNF related, matrix associated, actin dependent regulator of chromatin, subfamily d, member 2	1426192_at	2.448		22	14	51	38
				Mean	43	24	77	47
				Median	34	19	70	40
				SD	28	22	34	23
				Count	17		7	
				UF	1		11	

[1]UF = unacceptable fit (global goodness of fit p<0.1, BMD > high dose, and/or Hill k flag)

Table B.13. Cell-cycle: G2/M DNA damage checkpoint regulation pathway transcriptional benchmark dose summary in male mice at 2 and 7 days

					2d Male		7d Male	
Symbol	Entrez Gene Name	Affymetrix	Fold Change	Net-works	BMD (mg/kg-day)	BMDL (mg/kg-day)	BMD (mg/kg-day)	BMDL (mg/kg-day)
ATR	ataxia telangiectasia and Rad3 related	1427197_at	1.709	7	56	41	84	57
CCNB2	cyclin B2	1450920_at	55.019	20	43	33	100	64
CDK1	cyclin-dependent kinase 1	1448314_at	6.560		37	29	UF[1]	UF
CHEK1	checkpoint kinase 1	1450677_at	2.966	17	52	39	34	3.2
CKS2	CDC28 protein kinase regulatory subunit 2	1417457_at	1.211	2	143	84	UF	UF
GADD45A	growth arrest and DNA-damage-inducible, alpha	1449519_at	8.440		95	64	85	57
PLK1	polo-like kinase 1	1448191_at	9.612		42	32	UF	UF
SKP1/SKP1P2	S-phase kinase-associated protein 1	1423148_at	1.055	22	UF	UF	UF	UF
TOP2A	topoisomerase (DNA) II alpha 170kDa	1454694_a_at	5.436		47	35	UF	UF
YWHAH	tyrosine 3-monooxygenase/tryptophan 5-monooxygenase activation protein, eta polypeptide	1416004_at	1.258	6	106	69	UF	UF
YWHAZ	tyrosine 3-monooxygenase/tryptophan 5-monooxygenase activation protein, zeta polypeptide	1436971_x_at	1.101	12	UF	UF	UF	UF
				Mean	69	47	76	45
				Median	52	39	85	57
				SD	37	20	29	28
				Count	9		4	
				UF	2		7	

[1]UF = unacceptable fit (global goodness of fit p<0.1, BMD > high dose, and/or Hill k flag)

Table B.14. Cell-cycle: G2/M DNA damage checkpoint regulation pathway transcriptional benchmark dose summary in female mice at 2 and 7 days

					2d Female		7d Female	
Symbol	Entrez Gene Name	Affymetrix	Fold Change	Net-works	BMD (mg/kg-day)	BMDL (mg/kg-day)	BMD (mg/kg-day)	BMDL (mg/kg-day)
ATR	ataxia telangiectasia and Rad3 related	1427197_at	1.805	20	42	0.0	UF[1]	UF
BRCA1	breast cancer 1, early onset	1424629_at	1.584		0.1	0.0	49	24
CCNB2	cyclin B2	1450920_at	97.608		73	51	UF	UF
CDK1	cyclin-dependent kinase 1	1448314_at	6.669		66	47	UF	UF
CHEK1	checkpoint kinase 1	1450677_at	4.439		52	38	UF	UF
CKS1B	CDC28 protein kinase regulatory subunit 1B	1448441_at	2.353		34	19	109	70
GADD45A	growth arrest and DNA-damage-inducible, alpha	1449519_at	3.801		58	42	70	40
KAT2B	K(lysine) acetyltransferase 2B	1434037_s_at	-1.152		UF		UF	UF
MDM2	Mdm2, p53 E3 ubiquitin protein ligase homolog (mouse)	1427718_a_at	1.673	6	33	19	142	84
PLK1	polo-like kinase 1	1448191_at	12.057	4	74	51	UF	UF
SKP2	S-phase kinase-associated protein 2, E3 ubiquitin protein ligase	1436000_a_at	3.499	22	82	55	UF	UF
TOP2A	topoisomerase (DNA) II alpha 170kDa	1454694_a_at	7.755	19	56	41	UF	
WEE1	WEE1 homolog (S. pombe)	1416773_at	3.128	22	75	51	80	55
YWHAH*	tyrosine 3-monooxygenase/tryptophan 5-monooxygenase activation protein, eta polypeptide	1416004_at	1.408		32	18	138	82
				Mean	52	33	98	59
				Median	56	41	95	63
				SD	23	20	38	24
				Count	13		6	
				UF	1		8	

[1]UF = unacceptable fit (global goodness of fit p<0.1, BMD > high dose, and/or Hill k flag)

Table B.15. Mitotic roles of polo-like kinases pathway transcriptional benchmark dose summary in male mice at 2 and 7 days

					2d Male		7d Male	
Symbol	Entrez Gene Name	Affymetrix	Fold Change	Net-works	BMD (mg/kg-day)	BMDL (mg/kg-day)	BMD (mg/kg-day)	BMDL (mg/kg-day)
ANAPC5	anaphase promoting complex subunit 5	1435177_a_at	1.151	22	UF[1]	UF	UF	UF
CCNB2	cyclin B2	1450920_at	55.019	20	43	33	100	64
Ccnb1/Gm5593	cyclin B1	1419943_s_at	31.196	22	UF	UF	112	70
CDC20	cell division cycle 20 homolog (S. cerevisiae)	1416664_at	40.290	7	48	36	136	80
CDK1	cyclin-dependent kinase 1	1448314_at	6.560		37	29	UF	UF
ESPL1	extra spindle pole bodies homolog 1 (S. cerevisiae)	1433862_at	2.880	20, 22	26	10	UF	UF
HSP90AA1	heat shock protein 90kDa alpha (cytosolic), class A member 1	1426645_at	1.258	13	110	68	UF	UF
KIF11	kinesin family member 11	1435306_a_at	4.363	7	49	37	UF	UF
PLK1	polo-like kinase 1	1448191_at	9.612		42	32	UF	UF
PLK4	polo-like kinase 4	1419838_s_at	3.196		UF	UF	UF	UF
PPP2R5E	protein phosphatase 2, regulatory subunit B', epsilon isoform	1428461_at	-1.263		UF	UF	UF	UF
PRC1	protein regulator of cytokinesis 1	1423775_s_at	3.316	2	51	38	UF	UF
PTTG1	pituitary tumor-transforming 1	1424105_a_at	3.405	22	44	34	UF	UF
				Mean	50	35	116	71
				Median	44	34	112	70
				SD	24	15	18	8
				Count	9		3	
				UF	3		10	

[1]UF = unacceptable fit (global goodness of fit p<0.1, BMD > high dose, and/or Hill k flag)

Table B.16. Mitotic roles of polo-like kinases pathway transcriptional benchmark dose summary in female mice at 2 and 7 days

					2d Female		7d Female	
Symbol	Entrez Gene Name	Affymetrix	Fold Change	Net-works	BMD (mg/kg-day)	BMDL (mg/kg-day)	BMD (mg/kg-day)	BMDL (mg/kg-day)
CCNB2	cyclin B2	1450920_at	97.608		73	51	UF	UF
Ccnb1/Gm5593	cyclin B1	1419943_s_at	53.177		80	54	UF	UF
CDC20	cell division cycle 20 homolog (S. cerevisiae)	1416664_at	21.922	5	76	52	UF	UF
CDC27	cell division cycle 27 homolog (S. cerevisiae)	1454739_at	1.280	22	UF	UF	143	84
CDK1	cyclin-dependent kinase 1	1448314_at	6.669		66	47	UF	UF
ESPL1	extra spindle pole bodies homolog 1 (S. cerevisiae)	1433862_at	4.725	21	93	61	UF	UF
HSP90AA1	heat shock protein 90kDa alpha (cytosolic), class A member 1	1437497_a_at	1.523	6	28	16	UF	UF
KIF11	kinesin family member 11	1435306_a_at	6.807	15	77	53	UF	UF
PLK1	polo-like kinase 1	1448191_at	12.057	4	74	51	UF	UF
PLK4	polo-like kinase 4	1419838_s_at	5.392		53	39	UF	UF
PPP2R5A	protein phosphatase 2, regulatory subunit B', alpha	1423911_at	-1.173		UF	UF	UF	UF
PRC1	protein regulator of cytokinesis 1	1423775_s_at	5.155	5	72	50	UF	UF
PTTG1	pituitary tumor-transforming 1	1424105_a_at	4.274	19	72	50	UF	UF
SMC1A	structural maintenance of chromosomes 1A	1417830_at	1.241	20	UF	UF	UF	UF
WEE1	WEE1 homolog (S. pombe)	1416773_at	3.128	22	75	51	80	55
				Mean	70	48	112	70
				Median	74	51	112	70
				SD	16	11	45	21
				Count	12		2	
				UF	3		13	

[1]UF = unacceptable fit (global goodness of fit p<0.1, BMD > high dose, and/or Hill k flag)

Table B.17. Glutathione-mediated detoxification pathway transcriptional benchmark dose summary in male mice at 2 and 7 days

					2d Male		7d Male	
Symbol	Entrez Gene Name	Affymetrix	Fold Change	Net-works	BMD (mg/kg-day)	BMDL (mg/kg-day)	BMD (mg/kg-day)	BMDL (mg/kg-day)
GSTA3	glutathione S-transferase alpha 3	1423437_at	1.416	15	111	71	UF[1]	UF
Gsta4	glutathione S-transferase, alpha 4	1416368_at	1.472	15	70	50	UF	UF
GSTA5	glutathione S-transferase alpha 5	1421041_s_at	5.719	15	74	50	45	34
GSTK1	glutathione S-transferase kappa 1	1452823_at	-1.220	15	UF	UF	UF	UF
GSTM1	glutathione S-transferase mu 1	1416411_at	3.241	15	30	23	46	35
GSTM3	glutathione S-transferase mu 3 (brain)	1416842_at	1.206	15	UF	UF	UF	UF
Gstm3	glutathione S-transferase, mu 3	1427473_at	13.825	15	49	30	42	25
GSTM4	glutathione S-transferase mu 4	1424835_at	2.852	15	37	29	17	3.3
GSTM5	glutathione S-transferase mu 5	1425626_at	2.132	15	67	48	3.5	0.1
GSTO1	glutathione S-transferase omega 1	1416531_at	-1.136	15	UF	UF	UF	UF
GSTT1	glutathione S-transferase theta 1	1418186_at	1.981	15	76	53	78	54
Gstt3	glutathione S-transferase, theta 3	1423891_at	7.351	15	57	42	23	18
				Mean	63	44	36	24
				Median	67	48	42	25
				SD	24	15	24	19
				Count	9		7	
				UF	3		5	

[1]UF = unacceptable fit (global goodness of fit p<0.1, BMD > high dose, and/or Hill k flag)

Table B.18. Glutathione-mediated detoxification pathway transcriptional benchmark dose summary in female mice at 2 and 7 days

				2d Female		7d Female	
Symbol	Entrez Gene Name	Affymetrix	Fold Change	BMD (mg/kg-day)	BMDL (mg/kg-day)	BMD (mg/kg-day)	BMDL (mg/kg-day)
GSTA3	glutathione S-transferase alpha 3	1423437_at	1.443	UF	UF	120	75
Gsta4	glutathione S-transferase, alpha 4	1416368_at	1.370	46	22	118	74
GSTA5	glutathione S-transferase alpha 5	1421040_a_at	7.363	86	57	49	37
GSTM1	glutathione S-transferase mu 1	1416411_at	2.932	30	18	25	10
Gstm3	glutathione S-transferase, mu 3	1427473_at	11.764	39	30	31	24
GSTM4	glutathione S-transferase mu 4	1424835_at	2.394	24	16	41	32
GSTM5	glutathione S-transferase mu 5	1425626_at	1.882	33	19	59	44
GSTT1	glutathione S-transferase theta 1	1418186_at	1.356	43	21	90	58
Gstt3	glutathione S-transferase, theta 3	1423891_at	2.885	16	11	32	25
GSTT2/GSTT2B	glutathione S-transferase theta 2	1417883_at	1.288	27	17	137	82
GSTZ1	glutathione S-transferase zeta 1	1427552_a_at	-1.104	UF	UF	UF	UF
			Mean	38	23	70	46
			Median	33	19	54	41
			SD	20	14	42	25
			Count	9		10	
			UF	2		1	

[1]UF = unacceptable fit (global goodness of fit p<0.1, BMD > high dose, and/or Hill k flag)

Appendix C: Chapter 3 Supplementary Data

Table C.1. Aryl hydrocarbon receptor (AhR) signaling pathway transcriptional benchmark dose summary in male rat bladder at 20 weeks

Symbol	Entrez Gene Name	Affymetrix	Fold Change	BMD (mg/kg-day)	BMDL (mg/kg-day)
AHRR	aryl-hydrocarbon receptor repressor	1380746_at	2.453	1.8	0.0
ALDH1A1	aldehyde dehydrogenase 1 family, member A1	1387022_at	2.659	64	44
ALDH6A1	aldehyde dehydrogenase 6 family, member A1	1387344_at	-1.667	40	29
ALDH9A1	aldehyde dehydrogenase 9 family, member A1	1387867_at	-1.345	92	58
CCND2	cyclin D2	1370810_at	-1.313	UF[1]	UF
CHEK2	checkpoint kinase 2	1369010_at	1.407	UF	UF
CTSD	cathepsin D	1367651_at	-1.305	106	64
CYP1A1	cytochrome P450, family 1, subfamily A, polypeptide 1	1370269_at	2.274	UF	UF
CYP1B1	cytochrome P450, family 1, subfamily B, polypeptide 1	1368990_at	8.652	4.5	1.2
DCT	dopachrome tautomerase	1383394_at	-7.446	UF	UF
FAS	Fas cell surface death receptor	1384842_s_at	-1.717	UF	UF
GSTA1	glutathione S-transferase alpha 1	1368180_s_at	100.000	50	35
GSTA3	glutathione S-transferase alpha 3	1371089_at	3.465	11	3.5
Gsta3	glutathione S-transferase A3	1367774_at	1.746	28	21
GSTK1	glutathione S-transferase kappa 1	1398378_at	-1.363	42	31
GSTM5	glutathione S-transferase mu 5	1386985_at	1.588	25	19
GSTO1	glutathione S-transferase omega 1	1389832_at	-1.193	32	17
GSTP1	glutathione S-transferase pi 1	1388122_at	1.254	71	47

Symbol	Entrez Gene Name	Affymetrix	Fold Change	BMD (mg/kg-day)	BMDL (mg/kg-day)
HSP90AA1	heat shock protein 90kDa alpha (cytosolic), class A member 1	1388850_at	-1.341	78	51
HSP90B1	heat shock protein 90kDa beta (Grp94), member 1	1388331_at	-1.225	UF	UF
MDM2	MDM2 oncogene, E3 ubiquitin protein ligase	1383288_at	1.055	38	20
MGST3	microsomal glutathione S-transferase 3	1388300_at	1.307	59	41
NFIB	nuclear factor I/B	1388167_at	-2.444	UF	UF
NQO1	NAD(P)H dehydrogenase, quinone 1	1387599_a_at	2.440	59	41
			Mean	47	31
			Median	42	31
			SD	29.6	19.4
			Count	17	
			UF	7	

[1]UF = unacceptable fit (global goodness of fit p<0.1, BMD > high dose, and/or Hill k flag)

Table C.2. Glutathione-mediated detoxification pathway transcriptional benchmark dose summary in male rat bladder at 20 weeks

Symbol	Entrez Gene Name	Affymetrix	Fold Change	BMD (mg/kg-day)	BMDL (mg/kg-day)
ANPEP	alanyl (membrane) aminopeptidase	1386938_at	-2.039	UF[1]	UF
GGH	gamma-glutamyl hydrolase (conjugase, folylpolygammaglutamyl hydrolase)	1368470_at	2.044	31	23
GSTA1	glutathione S-transferase alpha 1	1368180_s_at	100.000	50	35
GSTA3	glutathione S-transferase alpha 3	1371089_at	3.465	11	3.5
Gsta3	glutathione S-transferase A3	1367774_at	1.746	28	21
Gsta4	glutathione S-transferase, alpha 4	1372297_at	2.249	34	25
GSTK1	glutathione S-transferase kappa 1	1398378_at	-1.363	42	31
GSTM5	glutathione S-transferase mu 5	1386985_at	1.588	25	19
GSTO1	glutathione S-transferase omega 1	1389832_at	-1.193	32	17
GSTP1	glutathione S-transferase pi 1	1388122_at	1.254	71	47
MGST3	microsomal glutathione S-transferase 3	1388300_at	1.307	59	41
			Mean	38	26
			Median	33	24
			SD	17.6	12.7
			Count	10	
			UF	1	

[1]UF = unacceptable fit (global goodness of fit p<0.1, BMD > high dose, and/or Hill k flag)

Table C.3. Nrf2-mediated oxidative stress response pathway transcriptional benchmark dose summary in male rat bladder at 20 weeks

Symbol	Entrez Gene Name	Affymetrix	Fold Change	BMD (mg/kg-day)	BMDL (mg/kg-day)
ACTB	actin, beta	1398835_at	-1.136	UF[1]	UF
ACTG2	actin, gamma 2, smooth muscle, enteric	1386869_at	-2.560	UF	UF
CAT	Catalase	1367995_at	-1.331	UF	UF
CBR1	carbonyl reductase 1	1368037_at	-1.450	141	78
CREBBP	CREB binding protein	1380027_at	-2.161	UF	UF
DNAJA4	DnaJ (Hsp40) homolog, subfamily A, member 4	1398343_at	-1.203	UF	UF
DNAJB2	DnaJ (Hsp40) homolog, subfamily B, member 2	1399039_at	-1.275	UF	UF
DNAJC10	DnaJ (Hsp40) homolog, subfamily C, member 10	1373813_at	-1.240	55	38
EPHX1	epoxide hydrolase 1, microsomal (xenobiotic)	1387669_a_at	1.183	26	15
FTH1	ferritin, heavy polypeptide 1	1367565_a_at	-1.087	UF	UF
GCLC	glutamate-cysteine ligase, catalytic subunit	1370688_at	1.840	UF	UF
GSR	glutathione reductase	1369061_at	1.379	UF	UF
GSTA1	glutathione S-transferase alpha 1	1368180_s_at	100.000	50	35
Gsta3	glutathione S-transferase A3	1367774_at	1.746	28	21
GSTA3	glutathione S-transferase alpha 3	1371089_at	3.465	11	3.5
GSTK1	glutathione S-transferase kappa 1	1398378_at	-1.363	42	31
GSTM5	glutathione S-transferase mu 5	1386985_at	1.588	25	19
GSTO1	glutathione S-transferase omega 1	1389832_at	-1.193	32	17
GSTP1	glutathione S-transferase pi 1	1388122_at	1.254	71	47
HSPB8	heat shock 22kDa protein 8	1387282_at	-3.146	UF	UF
MAP2K1	mitogen-activated protein kinase kinase 1	1367760_at	1.158	129	81
MAP2K6	mitogen-activated protein kinase kinase 6	1387809_at	-3.650	UF	UF
MGST3	microsomal glutathione S-transferase 3	1388300_at	1.307	59	41
NQO1	NAD(P)H dehydrogenase, quinone 1	1387599_a_at	2.440	59	41

Symbol	Entrez Gene Name	Affymetrix	Fold Change	BMD (mg/kg-day)	BMDL (mg/kg-day)
PRDX1	peroxiredoxin 1	1367613_at	1.231	62	43
SQSTM1	sequestosome 1	1389381_at	1.243	UF	UF
			Mean	56	37
			Median	53	37
			SD	37.5	22.2
			Count	14	
			UF	12	

[1]UF = unacceptable fit (global goodness of fit p<0.1, BMD > high dose, and/or Hill k flag)

Table C.4. Xenobiotic metabolism pathway transcriptional benchmark dose summary in male rat bladder at 20 weeks

Symbol	Entrez Gene Name	Affymetrix	Fold Change	BMD (mg/kg-day)	BMDL (mg/kg-day)
AHRR	aryl-hydrocarbon receptor repressor	1380746_at	2.453	1.8	0.0
ALDH1A1	aldehyde dehydrogenase 1 family, member A1	1387022_at	2.659	64	44
ALDH6A1	aldehyde dehydrogenase 6 family, member A1	1387344_at	-1.667	40	29
ALDH9A1	aldehyde dehydrogenase 9 family, member A1	1387867_at	-1.345	92	58
CAMK2D	calcium/calmodulin-dependent protein kinase II delta	1368834_at	-1.190	82	53
CAT	catalase	1367995_at	-1.331	UF[1]	UF
CITED2	Cbp/p300-interacting transactivator, with Glu/Asp-rich carboxy-terminal domain, 2	1367601_at	-1.447	46	33
CREBBP	CREB binding protein	1380027_at	-2.161	UF	UF
CYP1A1	cytochrome P450, family 1, subfamily A, polypeptide 1	1370269_at	2.274	UF	UF
CYP1B1	cytochrome P450, family 1, subfamily B, polypeptide 1	1368990_at	8.652	4.5	1.2
ESD	esterase D	1398903_at	-1.280	UF	UF
FMO5	flavin containing monooxygenase 5	1383248_at	1.558	UF	UF
GCLC	glutamate-cysteine ligase, catalytic subunit	1370688_at	1.840	UF	UF
GSTA1	glutathione S-transferase alpha 1	1368180_s_at	100.000	50	35
Gsta3	glutathione S-transferase A3	1367774_at	1.746	28	21
GSTA3	glutathione S-transferase alpha 3	1371089_at	3.465	11	3.5
GSTK1	glutathione S-transferase kappa 1	1398378_at	-1.363	42	31
GSTM5	glutathione S-transferase mu 5	1386985_at	1.588	25	19
GSTO1	glutathione S-transferase omega 1	1389832_at	-1.193	32	17
GSTP1	glutathione S-transferase pi 1	1388122_at	1.254	71	47

Symbol	Entrez Gene Name	Affymetrix	Fold Change	BMD (mg/kg-day)	BMDL (mg/kg-day)
HSP90AA1	heat shock protein 90kDa alpha (cytosolic), class A member 1	1388850_at	-1.341	78	51
HSP90B1	heat shock protein 90kDa beta (Grp94), member 1	1388331_at	-1.225	UF	UF
MAP2K1	mitogen-activated protein kinase kinase 1	1367760_at	1.158	129	81
MAP2K6	mitogen-activated protein kinase kinase 6	1387809_at	-3.650	UF	UF
MGST3	microsomal glutathione S-transferase 3	1388300_at	1.307	59	41
NCOA1	nuclear receptor coactivator 1	1383166_at	-1.167	UF	UF
NQO1	NAD(P)H dehydrogenase, quinone 1	1387599_a_at	2.440	59	41
PPP2R2A	protein phosphatase 2, regulatory subunit B, alpha	1387485_a_at	1.175	UF	UF
PPP2R2B	protein phosphatase 2, regulatory subunit B, beta	1387803_at	-5.296	83	54
UGT1A6	UDP glucuronosyltransferase 1 family, polypeptide A6	1387759_s_at	1.238	2.4	1.1
Ugt1a7c	UDP glucuronosyltransferase 1 family, polypeptide A7C	1370613_s_at	1.091	4.5	1.6
			Mean	48	32
			Median	46	33
			SD	34.3	22.5
			Count	21	
			UF	10	

[1]UF = unacceptable fit (global goodness of fit p<0.1, BMD > high dose, and/or Hill k flag)

Table C.5. CD28 signaling in T-helper cells pathway transcriptional benchmark dose summary in male rat bladder at 20weeks

Symbol	Entrez Gene Name	Affymetrix	Fold Change	BMD (mg/kg-day)	BMDL (mg/kg-day)
ACTR3	ARP3 actin-related protein 3 homolog (yeast)	1395886_at	1.419	UF[1]	UF
ARPC2	actin related protein 2/3 complex, subunit 2, 34kDa	1375137_at	1.401	UF	UF
ARPC1B	actin related protein 2/3 complex, subunit 1B, 41kDa	1386925_at	1.152	UF	UF
Calm1 (includes others)	calmodulin 1	1387772_at	-1.222	73	49
CD86	CD86 molecule	1377943_at	-1.603	UF	UF
CD3G	CD3g molecule, gamma (CD3-TCR complex)	1384787_at	-1.551	UF	UF
CHP1	calcineurin-like EF-hand protein 1	1387388_at	2.077	87	49
HLA-DMB	major histocompatibility complex, class II, DM beta	1370882_at	1.793	4.9	0.8
HLA-DRA	major histocompatibility complex, class II, DR alpha	1370883_at	1.721	3.5	0.3
HLA-DRB1	major histocompatibility complex, class II, DR beta 1	1370383_s_at	1.970	3.6	0.4
ITPR1	inositol 1,4,5-trisphosphate receptor, type 1	1387907_at	-1.345	65	37
MAP2K1	mitogen-activated protein kinase kinase 1	1367760_at	1.158	129	81
PAK1	p21 protein (Cdc42/Rac)-activated kinase 1	1389093_at	-1.890	UF	UF
PPP3CA	protein phosphatase 3, catalytic subunit, alpha isozyme	1368277_at	-1.247	109	66
PTPN11	protein tyrosine phosphatase, non-receptor type 11	1388379_at	-1.154	10	0.2
			Mean	54	32
			Median	65	37
			SD	49.6	31.9
			Count	9	
			UF	6	

[1]UF = unacceptable fit (global goodness of fit p<0.1, BMD > high dose, and/or Hill k flag)

Table C.6. Clathrin mediated endocytosis signaling pathway transcriptional benchmark dose summary in male rat bladder at 20 weeks

Symbol	Entrez Gene Name	Affymetrix	Fold Change	BMD (mg/kg-day)	BMDL (mg/kg-day)
ACTB	actin, beta	1398835_at	-1.136	UF[1]	UF
ACTG2	actin, gamma 2, smooth muscle, enteric	1386869_at	-2.560	UF	UF
ACTR3	ARP3 actin-related protein 3 homolog (yeast)	1395886_at	1.419	UF	UF
AP1B1	adaptor-related protein complex 1, beta 1 subunit	1367872_at	-1.295	UF	UF
AP2A2	adaptor-related protein complex 2, alpha 2 subunit	1369982_at	-1.199	42	30
AP2M1	adaptor-related protein complex 2, mu 1 subunit	1398765_at	-1.155	UF	UF
APOE	apolipoprotein E	1370862_at	-2.810	100	62
ARF6	ADP-ribosylation factor 6	1369998_at	1.226	UF	UF
ARPC2	actin related protein 2/3 complex, subunit 2, 34kDa	1375137_at	1.401	UF	UF
ARPC1B	actin related protein 2/3 complex, subunit 1B, 41kDa	1386925_at	1.152	UF	UF
CHP1	calcineurin-like EF-hand protein 1	1387388_at	2.077	87	49
CLTA	clathrin, light chain A	1386875_a_at	1.100	UF	UF
F2R	coagulation factor II (thrombin) receptor	1367899_at	2.551	87	56
HSPA8	heat shock 70kDa protein 8	1398240_at	-1.134	97	61
ITGB1	integrin, beta 1 (fibronectin receptor, beta polypeptide, antigen CD29 includes MDF2, MSK12)	1368819_at	-1.215	UF	UF
MDM2	MDM2 oncogene, E3 ubiquitin protein ligase	1383288_at	1.055	38	20
PPP3CA	protein phosphatase 3, catalytic subunit, alpha isozyme	1368277_at	-1.247	109	66
RAB4A	RAB4A, member RAS oncogene family	1370181_at	-1.455	UF	UF
RAB5B	RAB5B, member RAS oncogene family	1388823_at	-1.164	61	42
WASL	Wiskott-Aldrich syndrome-like	1373842_at	1.179	72	48
			Mean	77	48
			Median	87	49
			SD	25.4	15.4
			Count	9	
			UF	11	

[1]UF = unacceptable fit (global goodness of fit p<0.1, BMD > high dose, and/or Hill k flag)

Table C.7. LPS/IL-1 mediated inhibition of RXR function pathway transcriptional benchmark dose summary in male rat bladder at 20 weeks

Symbol	Entrez Gene Name	Affymetrix	Fold Change	BMD (mg/kg-day)	BMDL (mg/kg-day)
ACOX1	acyl-CoA oxidase 1, palmitoyl	1367680_at	1.218	42	30
ACSL4	acyl-CoA synthetase long-chain family member 4	1387101_at	-1.407	UF[1]	UF
ALDH1A1	aldehyde dehydrogenase 1 family, member A1	1387022_at	2.659	64	44
ALDH6A1	aldehyde dehydrogenase 6 family, member A1	1387344_at	-1.667	40	29
ALDH9A1	aldehyde dehydrogenase 9 family, member A1	1387867_at	-1.345	92	58
APOE	apolipoprotein E	1370862_at	-2.810	UF	UF
CAT	catalase	1367995_at	-1.331	UF	UF
CPT2	carnitine palmitoyltransferase 2	1386927_at	1.260	43	31
CPT1C	carnitine palmitoyltransferase 1C	1375033_at	4.620	30	22
FMO5	flavin containing monooxygenase 5	1383248_at	1.558	UF	UF
GSTA1	glutathione S-transferase alpha 1	1368180_s_at	100.000	50	35
GSTA3	glutathione S-transferase alpha 3	1371089_at	3.465	11	3.5
Gsta3	glutathione S-transferase A3	1367774_at	1.746	28	21
GSTK1	glutathione S-transferase kappa 1	1398378_at	-1.363	42	31
GSTM5	glutathione S-transferase mu 5	1386985_at	1.588	25	19
GSTO1	glutathione S-transferase omega 1	1389832_at	-1.193	32	17
GSTP1	glutathione S-transferase pi 1	1388122_at	1.254	71	47
HMGCS2	3-hydroxy-3-methylglutaryl-CoA synthase 2 (mitochondrial)	1370310_at	-2.539	UF	UF
IL33	interleukin 33	1373970_at	-2.760	UF	UF
IL1RAP	interleukin 1 receptor accessory protein	1393563_at	-2.528	43	31
MGST3	microsomal glutathione S-transferase 3	1388300_at	1.307	59	41
NCOA1	nuclear receptor coactivator 1	1383166_at	-1.167	UF	UF
			Mean	45	31
			Median	42	31
			SD	20.3	13.5
			Count	15	
			UF	7	

[1]UF = unacceptable fit (global goodness of fit p<0.1, BMD > high dose, and/or Hill k flag)

Table C.8. Calcium-induced T lymphocyte apoptosis pathway transcriptional benchmark dose summary in male rat bladder at 20 weeks

Symbol	Entrez Gene Name	Affymetrix	Fold Change	BMD (mg/kg-day)	BMDL (mg/kg-day)
Calm1 (includes others)	calmodulin 1	1387772_at	-1.222	73	49
CAPN2	calpain 2, (m/II) large subunit	1387860_at	-1.040	UF[1]	UF
CD3G	CD3g molecule, gamma (CD3-TCR complex)	1384787_at	-1.551	UF	UF
CHP1	calcineurin-like EF-hand protein 1	1387388_at	2.077	87	49
HDAC2	histone deacetylase 2	1370908_at	-1.177	79	52
HLA-DMB	major histocompatibility complex, class II, DM beta	1370882_at	1.793	4.9	0.8
HLA-DRA	major histocompatibility complex, class II, DR alpha	1370883_at	1.721	3.5	0.3
HLA-DRB1	major histocompatibility complex, class II, DR beta 1	1370383_s_at	1.970	3.6	0.4
ITPR1	inositol 1,4,5-trisphosphate receptor, type 1	1387907_at	-1.345	65	37
PPP3CA	protein phosphatase 3, catalytic subunit, alpha isozyme	1368277_at	-1.247	109	66
			Mean	53	32
			Median	69	43
			SD	42.6	27.1
			Count	8	
			UF	2	

[1]UF = unacceptable fit (global goodness of fit p<0.1, BMD > high dose, and/or Hill k flag)

Table C.9. Integrin signaling pathway transcriptional benchmark dose summary in male rat bladder at 20 weeks

Symbol	Entrez Gene Name	Affymetrix	Fold Change	BMD (mg/kg-day)	BMDL (mg/kg-day)
ACTB	actin, beta	1398835_at	-1.136	UF[1]	UF
ACTG2	actin, gamma 2, smooth muscle, enteric	1386869_at	-2.560	UF	UF
ACTR3	ARP3 actin-related protein 3 homolog (yeast)	1395886_at	1.419	UF	UF
ARF6	ADP-ribosylation factor 6	1369998_at	1.226	UF	UF
ARPC2	actin related protein 2/3 complex, subunit 2, 34kDa	1375137_at	1.401	UF	UF
ARPC1B	actin related protein 2/3 complex, subunit 1B, 41kDa	1386925_at	1.152	UF	UF
CAPN2	calpain 2, (m/II) large subunit	1387860_at	-1.040	UF	UF
CRK	v-crk avian sarcoma virus CT10 oncogene homolog	1392462_at	1.260	102	58
ITGA6	integrin, alpha 6	1371186_at	1.554	46	33
ITGA7	integrin, alpha 7	1388240_a_at	1.810	3.4	1.8
ITGA11	integrin, alpha 11	1394824_at	4.629	5.1	1.8
ITGB1	integrin, beta 1 (fibronectin receptor, beta polypeptide, antigen CD29 includes MDF2, MSK12)	1368819_at	-1.215	UF	UF
MAP2K1	mitogen-activated protein kinase kinase 1	1367760_at	1.158	129	81
PAK1	p21 protein (Cdc42/Rac)-activated kinase 1	1389093_at	-1.890	UF	
RHOV	ras homolog family member V	1397581_at	-1.539	24	14
SOS2	son of sevenless homolog 2 (Drosophila)	1376489_at	-1.213	UF	UF
TSPAN4	tetraspanin 4	1372752_at	-2.191	UF	UF
TSPAN6	tetraspanin 6	1382146_at	1.850	UF	UF
TSPAN7	tetraspanin 7	1371702_at	1.418	26	16
WASL	Wiskott-Aldrich syndrome-like	1373842_at	1.179	72	48
			Mean	51	32
			Median	36	25
			SD	46	29
			Count	8	
			UF	12	

[1]UF = unacceptable fit (global goodness of fit p<0.1, BMD > high dose, and/or Hill k flag)

Table C.10. Nur77 signaling in T lymphocytes pathway transcriptional benchmark dose summary in male rat bladder at 20 weeks

Symbol	Entrez Gene Name	Affymetrix	Fold Chnage	BMD (mg/kg-day)	BMDL (mg/kg-day)
Calm1 (includes others)	calmodulin 1	1387772_at	-1.222	73	49
CD86	CD86 molecule	1377943_at	-1.603	UF[1]	
CD3G	CD3g molecule, gamma (CD3-TCR complex)	1384787_at	-1.551	UF	
CHP1	calcineurin-like EF-hand protein 1	1387388_at	2.077	87	49
HDAC2	histone deacetylase 2	1370908_at	-1.177	79	52
HLA-DMB	major histocompatibility complex, class II, DM beta	1370882_at	1.793	4.9	0.8
HLA-DRA	major histocompatibility complex, class II, DR alpha	1370883_at	1.721	3.5	0.3
HLA-DRB1	major histocompatibility complex, class II, DR beta 1	1370383_s_at	1.970	3.6	0.4
PPP3CA	protein phosphatase 3, catalytic subunit, alpha isozyme	1368277_at	-1.247	109	66
			Mean	51	31
			Median	73	49
			SD	45.7	29.2
			Count	7	
			UF	2	

[1]UF = unacceptable fit (global goodness of fit p<0.1, BMD > high dose, and/or Hill k flag)

Table C.11. Inhibition of matrix metalloprotease pathway transcriptional benchmark dose summary in male rat bladder at 7 days

Symbol	Entrez Gene Name	Affymetrix	Fold Change	BMD (mg/kg-day)	BMDL (mg/kg-day)
MMP13	matrix metallopeptidase 13 (collagenase 3)	1388204_at	2.526	48	35
MMP14	matrix metallopeptidase 14 (membrane-inserted)	1367860_a_at	-1.594	UF[1]	UF
MMP15	matrix metallopeptidase 15 (membrane-inserted)	1383668_at	1.198	109	71
MMP16	matrix metallopeptidase 16 (membrane-inserted)	1368590_at	-1.303	27	15
MMP2	matrix metallopeptidase 2 (gelatinase A, 72kDa gelatinase, 72kDa type IV collagenase)	1370301_at	-2.015	UF	UF
MMP23B	matrix metallopeptidase 23B	1392265_s_at	-1.379	UF	UF
MMP3	matrix metallopeptidase 3 (stromelysin 1, progelatinase)	1368657_at	2.736	75	53
RECK	reversion-inducing-cysteine-rich protein with kazal motifs	1374448_at	-1.838	UF	UF
SDC1	syndecan 1	1376062_at	-1.114	UF	UF
SDC2	syndecan 2	1370167_at	-1.874	UF	UF
TIMP1	TIMP metallopeptidase inhibitor 1	1367712_at	-3.079	36	18
TIMP2	TIMP metallopeptidase inhibitor 2	1386940_at	-1.572	UF	UF
TIMP3	TIMP metallopeptidase inhibitor 3	1375138_at	-1.624	36	18
			Mean	55	35
			Median	42	27
			SD	31.2	22.8
			Count	6	
			UF	7	

[1]UF = unacceptable fit (global goodness of fit p<0.1, BMD > high dose, and/or Hill k flag)

Table C.12. Nrf2-mediated oxidative stress pathway transcriptional benchmark dose summary in male rat bladder at 7 days

Symbol	Entrez Gene Name	Affymetrix	Fold Change	BMD (mg/kg-day)	BMDL (mg/kg-day)
ABCC1	ATP-binding cassette, sub-family C (CFTR/MRP), member 1	1371005_at	-1.605	UF[1]	UF
ABCC4	ATP-binding cassette, sub-family C (CFTR/MRP), member 4	1379402_at	-1.265	UF	UF
ACTA1	actin, alpha 1, skeletal muscle	1369928_at	-11.783	UF	UF
AKR7A3	aldo-keto reductase family 7, member A3 (aflatoxin aldehyde reductase)	1368121_at	5.600	UF	UF
CAT	catalase	1367995_at	1.218	UF	
CBR1	carbonyl reductase 1	1368037_at	1.170	174	111
CREBBP	CREB binding protein	1385852_at	-1.329	90	61
DNAJB12	DnaJ (Hsp40) homolog, subfamily B, member 12	1374727_at	1.058	UF	UF
FOSL1	FOS-like antigen 1	1368489_at	3.712	UF	UF
FTL	ferritin, light polypeptide	1367559_at	-1.054	UF	UF
GCLC	glutamate-cysteine ligase, catalytic subunit	1370688_at	-1.404	UF	UF
GCLM	glutamate-cysteine ligase, modifier subunit	1370030_at	1.343	141	87
GPX2	glutathione peroxidase 2 (gastrointestinal)	1374070_at	-1.789	UF	UF
GSK3B	glycogen synthase kinase 3 beta	1370267_at	-1.320	170	98
GSR	glutathione reductase	1369061_at	-1.187	UF	UF
Gsta1	glutathione S-transferase alpha 1		-5.871	21	13
Gsta3	glutathione S-transferase alpha 1		-1.254	UF	UF
GSTA3	glutathione S-transferase alpha 3	1371089_at	-1.315	32	17
GSTM3	glutathione S-transferase mu 3 (brain)	1370813_at	-2.402	UF	UF
GSTM5	glutathione S-transferase mu 5	1386985_at	-1.198	25	15
GSTP1	glutathione S-transferase pi 1	1388122_at	-1.124	30	16
HMOX1	heme oxygenase (decycling) 1	1370080_at	-1.528	37	18
KRAS	Kirsten rat sarcoma viral oncogene homolog	1370035_at	-1.363	UF	UF

Symbol	Entrez Gene Name	Affymetrix	Fold Change	BMD (mg/kg-day)	BMDL (mg/kg-day)
MAF	v-maf avian musculoaponeurotic fibrosarcoma oncogene homolog	1387165_at	-2.209	30	16
MAP2K6	mitogen-activated protein kinase kinase 6	1387809_at	1.552	16	10
NQO1	NAD(P)H dehydrogenase, quinone 1	1387599_a_at	-1.392	25	15
PIK3CA	phosphatidylinositol-4,5-bisphosphate 3-kinase, catalytic subunit alpha	1393499_at	1.234	151	91
PPIB	peptidylprolyl isomerase B (cyclophilin B)	1369934_at	-1.132	UF	UF
PRKCH	protein kinase C, eta	1388836_at	1.140	UF	UF
PRKCQ	protein kinase C, theta	1376259_at	1.899	UF	UF
PTPLAD1	protein tyrosine phosphatase-like A domain containing 1	1373469_at	-1.080	27	16
SCARB1	scavenger receptor class B, member 1	1367855_at	-1.375	25	14
SOD3	superoxide dismutase 3, extracellular	1368322_at	-2.607	UF	UF
TXNRD1	thioredoxin reductase 1	1386958_at	-1.397	UF	UF
			Mean	66	40
			Median	30	16
			SD	60.7	37.8
			Count	15	
			UF	19	

[1]UF = unacceptable fit (global goodness of fit p<0.1, BMD > high dose, and/or Hill k flag)

Table C.13. Hepatic fibrosis/stellate cell activation pathway transcriptional benchmark dose summary in male rat bladder at 7 days

Symbol	Entrez Gene Name	Affymetrix	Fold Change	BMD (mg/kg-day)	BMDL (mg/kg-day)
AGT	angiotensinogen (serpin peptidase inhibitor, clade A, member 8)	1387811_at	-15.279	UF[1]	UF
AGTR1	angiotensin II receptor, type 1	1369291_at	-3.418	UF	UF
COL1A1	collagen, type I, alpha 1	1370864_at	-2.308	UF	UF
COL1A2	collagen, type I, alpha 2	1387854_at	-2.041	UF	UF
COL3A1	collagen, type III, alpha 1	1370959_at	-2.162	25	16
CXCL9	chemokine (C-X-C motif) ligand 9	1373544_at	-3.958	3	1
FAS	Fas cell surface death receptor	1384842_s_at	1.338	146	88
FGFR1	fibroblast growth factor receptor 1	1372447_at	-1.708	UF	UF
FIGF	c-fos induced growth factor (vascular endothelial growth factor D)	1373882_at	-6.502	UF	UF
FN1	fibronectin 1	1370234_at	-2.323	27	15
IFNAR1	interferon (alpha, beta and omega) receptor 1	1382769_at	-1.142	UF	UF
IFNGR1	interferon gamma receptor 1	1369956_at	-1.581	194	107
IGF1	insulin-like growth factor 1 (somatomedin C)	1370333_a_at	-6.228	25	15
IGFBP3	insulin-like growth factor binding protein 3	1367652_at	-2.793	UF	UF
IGFBP5	insulin-like growth factor binding protein 5	1387348_at	-1.909	UF	UF
IL1RAP	interleukin 1 receptor accessory protein	1393563_at	1.173	199	109
MMP13	matrix metallopeptidase 13 (collagenase 3)	1388204_at	2.526	48	35
MMP2	matrix metallopeptidase 2 (gelatinase A, 72kDa gelatinase, 72kDa type IV collagenase)	1370301_at	-2.015	UF	UF
MYH14	myosin, heavy chain 14, non-muscle	1384264_at	1.060	UF	UF
MYL1	myosin, light chain 1, alkali; skeletal, fast	1370033_at	-100.000	UF	UF
PDGFRA	platelet-derived growth factor receptor, alpha polypeptide	1370941_at	-2.189	UF	UF
SMAD7	SMAD family member 7	1368896_at	1.499	55	40

Symbol	Entrez Gene Name	Affymetrix	Fold Change	BMD (mg/kg-day)	BMDL (mg/kg-day)
TGFB3	transforming growth factor, beta 3	1367859_at	-2.875	18	11
TIMP1	TIMP metallopeptidase inhibitor 1	1367712_at	-3.079	36	18
TIMP2	TIMP metallopeptidase inhibitor 2	1386940_at	-1.572	UF	UF
TNFRSF11B	tumor necrosis factor receptor superfamily, member 11b	1369407_at	-4.210	UF	UF
TNFRSF1A	tumor necrosis factor receptor superfamily, member 1A	1367715_at	-1.256	UF	UF
VCAM1	vascular cell adhesion molecule 1	1368474_at	-3.746	33	18
			Mean	67	39
			Median	35	18
			SD	70.1	39.0
			Count	12	
			UF	16	

[1]UF = unacceptable fit (global goodness of fit p<0.1, BMD > high dose, and/or Hill k flag)

Table C.14. VDR/RXR activation pathway transcriptional benchmark dose summary in male rat bladder at 7 days

Symbol	Entrez Gene Name	Affymetrix	Fold Change	BMD (mg/kg-day)	BMDL (mg/kg-day)
CCNC	cyclin C	1389101_at	1.322	UF[1]	UF
CDKN1B	cyclin-dependent kinase inhibitor 1B (p27, Kip1)	1373812_at	1.201	UF	UF
CST6	cystatin E/M	1368162_at	-1.171	19	12
HES1	hes family bHLH transcription factor 1	1387036_at	1.584	UF	UF
HSD17B2	hydroxysteroid (17-beta) dehydrogenase 2	1387156_at	1.009	28	16
IGFBP3	insulin-like growth factor binding protein 3	1367652_at	-2.793	UF	UF
IGFBP5	insulin-like growth factor binding protein 5	1387348_at	-1.909	UF	UF
IGFBP6	insulin-like growth factor binding protein 6	1387625_at	-3.476	11	7
KLF4	Kruppel-like factor 4 (gut)	1387260_at	-1.451	UF	UF
MED1	mediator complex subunit 1	1390506_at	-1.539	UF	UF
MXD1	MAX dimerization protein 1	1376077_at	1.692	UF	UF
NCOA3	nuclear receptor coactivator 3	1392385_at	1.130	112	73
NCOR1	nuclear receptor corepressor 1	1372102_at	-1.407	154	92
PRKCH	protein kinase C, eta	1388836_at	1.140	UF	UF
PRKCQ	protein kinase C, theta	1376259_at	1.899	UF	UF
THBD	thrombomodulin	1375951_at	-2.474	28	16
WT1	Wilms tumor 1	1377223_at	-2.533	14	10
YY1	YY1 transcription factor	1381886_at	-1.989	UF	UF
			Mean	52	32
			Median	28	16
			SD	56.8	34.9
			Count	7	
			UF	12	

[1]UF = unacceptable fit (global goodness of fit p<0.1, BMD > high dose, and/or Hill k flag)

Table C.15. Xenobiotic metabolism pathway transcriptional benchmark dose summary in male rat bladder at 7 days

Symbol	Entrez Gene Name	Affymetrix	Fold Change	BMD (mg/kg-day)	BMDL (mg/kg-day)
ABCC3	ATP-binding cassette, sub-family C (CFTR/MRP), member 3	1369698_at	-1.052	UF[1]	UF
AHRR	aryl-hydrocarbon receptor repressor	1380746_at	-1.936	163	96
ALDH1A1	aldehyde dehydrogenase 1 family, member A1	1387022_at	-1.321	38	19
ALDH3A1	aldehyde dehydrogenase 3 family, member A1	1368130_at	-3.460	99	66
ALDH3A2	aldehyde dehydrogenase 3 family, member A2	1368365_at	-1.333	24	14
ALDH6A1	aldehyde dehydrogenase 6 family, member A1	1387344_at	1.193	UF	UF
CAMK2D	calcium/calmodulin-dependent protein kinase II delta	1368834_at	1.159	128	80
CAT	catalase	1367995_at	1.218	UF	UF
Ces1d (Ces3)	carboxylesterase 1D	1370363_at	-4.692	UF	UF
CES5A (Ces7)	carboxylesterase 5A	1396034_at	-2.527	UF	UF
CREBBP	CREB binding protein	1385852_at	-1.329	90	61
CYP1A1	cytochrome P450, family 1, subfamily A, polypeptide 1	1370269_at	-2.498	85	59
CYP1B1	cytochrome P450, family 1, subfamily B, polypeptide 1	1368990_at	-3.888	94	63
FMO2	flavin containing monooxygenase 2 (non-functional)	1377635_at	-3.021	22	13
FMO3	flavin containing monooxygenase 3	1368304_at	-3.916	20	13
FMO5	flavin containing monooxygenase 5	1383248_at	1.081	11	0.0
FTL	ferritin, light polypeptide	1367559_at	-1.054	UF	UF
GCLC	glutamate-cysteine ligase, catalytic subunit	1370688_at	-1.404	UF	UF
GSTA1	glutathione S-transferase alpha 1	1368180_s_at	-5.871	21	13
Gsta3	glutathione S-transferase alpha 1	1367774_at	-1.254	UF	UF
GSTA3	glutathione S-transferase alpha 3	1371089_at	-1.315	32	17
GSTM3	glutathione S-transferase mu 3 (brain)	1370813_at	-2.402	UF	UF
GSTM5	glutathione S-transferase mu 5	1386985_at	-1.198	25	15
GSTP1	glutathione S-transferase pi 1	1388122_at	-1.124	30	16
HDAC5	histone deacetylase 5	1371819_at	1.144	49	21
HMOX1	heme oxygenase (decycling) 1	1370080_at	-1.528	37	18
HS2ST1	heparan sulfate 2-O-sulfotransferase 1	1382101_at	-1.182	UF	UF

Symbol	Entrez Gene Name	Affymetrix	Fold Change	BMD (mg/kg-day)	BMDL (mg/kg-day)
HSP90AB1	heat shock protein 90kDa alpha (cytosolic), class B member 1	1375335_at	-1.300	153	91
HSP90B1	heat shock protein 90kDa beta (Grp94), member 1	1388331_at	-1.194	UF	UF
KRAS	Kirsten rat sarcoma viral oncogene homolog	1370035_at	-1.363	UF	UF
MAF	v-maf avian musculoaponeurotic fibrosarcoma oncogene homolog	1387165_at	-2.209	29	16
MAOA	monoamine oxidase A	1370678_s_at	-1.477	22	13
MAP2K6	mitogen-activated protein kinase kinase 6	1387809_at	1.552	16	10
MAP3K4	mitogen-activated protein kinase kinase kinase 4	1378791_at	1.194	UF	UF
MAP3K8	mitogen-activated protein kinase kinase kinase 8	1369393_at	1.201	UF	UF
MED1	mediator complex subunit 1	1390506_at	-1.539	UF	UF
NQO1	NAD(P)H dehydrogenase, quinone 1	1387599_a_at	-1.392	25	15
PIK3CA	phosphatidylinositol-4,5-bisphosphate 3-kinase, catalytic subunit alpha	1393499_at	1.234	151	91
PNPLA7	patatin-like phospholipase domain containing 7	1377049_at	-1.016	198	108
PPP2R5E	protein phosphatase 2, regulatory subunit B', epsilon isoform	1395826_at	-1.096	UF	UF
PRKCH	protein kinase C, eta	1388836_at	1.140	UF	UF
PRKCQ	protein kinase C, theta	1376259_at	1.899	UF	UF
SOD3	superoxide dismutase 3, extracellular	1368322_at	-2.607	UF	UF
Ugt1a7c	UDP glucuronosyltransferase 1 family, polypeptide A7C	1370613_s_at	-1.078	UF	UF
			Mean	65	39
			Median	35	18
			SD	56.2	34.2
			Count	24	
			UF	21	

[1]UF = unacceptable fit (global goodness of fit p<0.1, BMD > high dose, and/or Hill k flag)

Table C.16. Aryl-hydrocarbon signaling pathway transcriptional benchmark dose summary in male rat bladder at 7 days

Symbol	Entrez Gene Name	Affymetrix	Fold Change	BMD (mg/kg-day)	BMDL (mg/kg-day)
AHRR	aryl-hydrocarbon receptor repressor	1380746_at	-1.936	163	96
ALDH1A1	aldehyde dehydrogenase 1 family, member A1	1387022_at	-1.321	38	19
ALDH3A1	aldehyde dehydrogenase 3 family, member A1	1368130_at	-3.460	99	66
ALDH3A2	aldehyde dehydrogenase 3 family, member A2	1368365_at	-1.333	24	14
ALDH6A1	aldehyde dehydrogenase 6 family, member A1	1387344_at	1.193	UF[1]	UF
CCND2	cyclin D2	1370810_at	-1.449	UF	UF
CDKN1B	cyclin-dependent kinase inhibitor 1B (p27, Kip1)	1373812_at	1.201	UF	UF
CYP1A1	cytochrome P450, family 1, subfamily A, polypeptide 1	1370269_at	-2.498	85	59
CYP1B1	cytochrome P450, family 1, subfamily B, polypeptide 1	1368990_at	-3.888	94	63
DCT	dopachrome tautomerase	1383394_at	2.060	UF	
FAS	Fas cell surface death receptor	1384842_s_at	1.338	146	88
GSTA1	glutathione S-transferase alpha 1	1368180_s_at	-5.871	21	13
Gsta3	glutathione S-transferase alpha 1	1367774_at	-1.254	32	17
GSTA3	glutathione S-transferase alpha 3	1371089_at	-1.315	UF	UF
GSTM3	glutathione S-transferase mu 3 (brain)	1370813_at	-2.402	UF	UF
GSTM5	glutathione S-transferase mu 5	1386985_at	-1.198	25	15
GSTP1	glutathione S-transferase pi 1	1388122_at	-1.124	30	16
HSP90AB1	heat shock protein 90kDa alpha (cytosolic), class B member 1	1375335_at	-1.300	153	91
HSP90B1	heat shock protein 90kDa beta (Grp94), member 1	1388331_at	-1.194	UF	UF
MED1	mediator complex subunit 1	1390506_at	-1.539	UF	
NCOA3	nuclear receptor coactivator 3	1392385_at	1.130	112	73
NFIB	nuclear factor I/B	1371202_a_at	-1.439	21	13
NFIX	nuclear factor I/X (CCAAT-binding transcription factor)	1370946_at	-1.678	34	18

Symbol	Entrez Gene Name	Affymetrix	Fold Change	BMD (mg/kg-day)	BMDL (mg/kg-day)
NQO1	NAD(P)H dehydrogenase, quinone 1	1387599_a_at	-1.392	25	15
TGFB3	transforming growth factor, beta 3	1367859_at	-2.875	18	11
			Mean	66	40
			Median	34	18
			SD	52.1	32.5
			Count	17	
			UF	8	

[1]UF = unacceptable fit (global goodness of fit p<0.1, BMD > high dose, and/or Hill k flag)

Table C.17. Leukocyte extravasation pathway transcriptional benchmark dose summary in male rat bladder at 7 days

Symbol	Entrez Gene Name	Affymetrix	Fold Change	BMD (mg/kg-day)	BMDL (mg/kg-day)
ACTA1	actin, alpha 1, skeletal muscle	1369928_at	-11.783	UF[1]	UF
ARHGAP1	Rho GTPase activating protein 1	1371994_at	1.065	135	84
ARHGAP12	Rho GTPase activating protein 12	1391101_at	1.119	UF	UF
ARHGAP5	Rho GTPase activating protein 5	1392864_at	-1.379	25	15
CLDN1	claudin 1	1383946_at	-1.064	UF	UF
CLDN11	claudin 11	1376711_at	-1.466	UF	UF
CLDN7	claudin 7	1370894_at	-1.103	UF	UF
CXCR4	chemokine (C-X-C motif) receptor 4	1370097_a_at	-1.097	UF	UF
CYBA	cytochrome b-245, alpha polypeptide	1370219_at	-1.144	UF	UF
GNAI2	guanine nucleotide binding protein (G protein), alpha inhibiting activity polypeptide 2	1367844_at	-1.239	UF	UF
GNAI3	guanine nucleotide binding protein (G protein), alpha inhibiting activity polypeptide 3	1368030_at	-1.707	UF	UF
MAP3K4	mitogen-activated protein kinase kinase kinase 4	1378791_at	1.194	UF	UF
MMP13	matrix metallopeptidase 13 (collagenase 3)	1388204_at	2.526	48	35
MMP14	matrix metallopeptidase 14 (membrane-inserted)	1367860_a_at	-1.594	UF	UF
MMP15	matrix metallopeptidase 15 (membrane-inserted)	1383668_at	1.198	109	71
MMP16	matrix metallopeptidase 16 (membrane-inserted)	1368590_at	-1.303	27	15
MMP2	matrix metallopeptidase 2 (gelatinase A, 72kDa gelatinase, 72kDa type IV collagenase)	1370301_at	-2.015	UF	UF
MMP23B	matrix metallopeptidase 23B	1392265_s_at	-1.379	UF	UF
MMP3	matrix metallopeptidase 3 (stromelysin 1, progelatinase)	1368657_at	2.736	75	53

Symbol	Entrez Gene Name	Affymetrix	Fold Change	BMD (mg/kg-day)	BMDL (mg/kg-day)
PIK3CA	phosphatidylinositol-4,5-bisphosphate 3-kinase, catalytic subunit alpha	1393499_at	1.234	151	91
PRKCH	protein kinase C, eta	1388836_at	1.140	UF	UF
PRKCQ	protein kinase C, theta	1376259_at	1.899	UF	UF
PXN	paxillin	1371664_at	-1.100	UF	UF
RAP1A	RAP1A, member of RAS oncogene family	1388615_at	1.054	UF	UF
RAP1GAP	RAP1 GTPase activating protein	1373631_at	1.196	6.8	0.0
RDX	radixin	1396207_at	-2.078	24	14
TIMP1	TIMP metallopeptidase inhibitor 1	1367712_at	-3.079	36	18
TIMP2	TIMP metallopeptidase inhibitor 2	1386940_at	-1.572	UF	UF
TIMP3	TIMP metallopeptidase inhibitor 3	1375138_at	-1.624	36	18
VAV2	vav 2 guanine nucleotide exchange factor	1384169_a_at	1.172	131	82
VCAM1	vascular cell adhesion molecule 1	1368474_at	-3.746	33	18
WASL	Wiskott-Aldrich syndrome-like	1391625_at	-1.180	36	18
			Mean	62	38
			Median	36	18
			SD	48.5	31.5
			Count	14	
			UF	18	

[1]UF = unacceptable fit (global goodness of fit p<0.1, BMD > high dose, and/or Hill k flag)

Table C.18. Acute phase response signaling pathway transcriptional benchmark dose summary in male rat bladder at 7 days

Symbol	Entrez Gene Name	Affymetrix	Fold Change	BMD (mg/kg-day)	BMDL (mg/kg-day)
AGT	angiotensinogen (serpin peptidase inhibitor, clade A, member 8)	1387811_at	-15.279	UF[1]	UF
C1R	complement component 1, r subcomponent	1383241_at	-2.774	UF	UF
C1S	complement component 1, s subcomponent	1387893_at	-2.131	26	15
C2	complement component 2	1383392_at	-2.981	UF	UF
C4A/C4B	complement component 4B (Chido blood group)	1370892_at	-6.764	UF	UF
CFB	complement factor B	1389470_at	-3.211	12	8
CP	ceruloplasmin (ferroxidase)	1368419_at	-2.836	27	16
FGG	fibrinogen gamma chain	1370086_at	-1.906	8	6
FN1	fibronectin 1	1370234_at	-2.323	27	15
FTL	ferritin, light polypeptide	1367559_at	-1.054	UF	UF
HMOX1	heme oxygenase (decycling) 1	1370080_at	-1.528	37	18
IL1RAP	interleukin 1 receptor accessory protein	1393563_at	1.173	199	109
IL33	interleukin 33	1389581_at	-3.303	13	9
IL36RN	interleukin 36 receptor antagonist	1381288_at	1.835	UF	UF
IL6ST	interleukin 6 signal transducer (gp130, oncostatin M receptor)	1370957_at	-1.391	UF	UF
IRAK1	interleukin-1 receptor-associated kinase 1	1373379_at	-1.053	UF	UF
KRAS	Kirsten rat sarcoma viral oncogene homolog	1370035_at	-1.363	UF	UF
MAP2K6	mitogen-activated protein kinase kinase 6	1387809_at	1.552	16	10
PIK3CA	phosphatidylinositol-4,5-bisphosphate 3-kinase, catalytic subunit alpha	1393499_at	1.234	151	91
RBP4	retinol binding protein 4, plasma	1371762_at	-2.433	20	12
RBP7	retinol binding protein 7, cellular	1374863_at	1.324	UF	UF
SERPINA3	serpin peptidase inhibitor, clade A (alpha-	1368224_at	-7.506	32	17

Symbol	Entrez Gene Name	Affymetrix	Fold Change	BMD (mg/kg-day)	BMDL (mg/kg-day)
	1 antiproteinase, antitrypsin), member 3				
SERPINF1	serpin peptidase inhibitor, clade F (alpha-2 antiplasmin, pigment epithelium derived factor), member 1	1388569_at	-4.109	UF	UF
SERPING1	serpin peptidase inhibitor, clade G (C1 inhibitor), member 1	1372254_at	-3.545	UF	UF
TF	transferrin	1370228_at	-1.742	UF	UF
TNFRSF11B	tumor necrosis factor receptor superfamily, member 11b	1369407_at	-4.210	UF	UF
TNFRSF1A	tumor necrosis factor receptor superfamily, member 1A	1367715_at	-1.256	UF	UF
TTR	transthyretin	1367598_at	-1.252	UF	UF
			Mean	47	27
			Median	27	15
			SD	61.1	34.4
			Count	12	
			UF	16	

Table C.19. LPS/IL-1-mediated inhibition of RXR function pathway transcriptional benchmark dose summary in male rat bladder at 7 days

Symbol	Entrez Gene Name	Affymetrix	Fold Change	BMD (mg/kg-day)	BMDL (mg/kg-day)
ABCC3	ATP-binding cassette, sub-family C (CFTR/MRP), member 3	1369698_at	-1.052	UF[1]	UF
ABCC4	ATP-binding cassette, sub-family C (CFTR/MRP), member 4	1379402_at	-1.265	UF	UF
ACOX1	acyl-CoA oxidase 1, palmitoyl	1367680_at	-1.008	UF	UF
ACSL1	acyl-CoA synthetase long-chain family member 1	1388153_at	-4.686	UF	UF
ACSL5	acyl-CoA synthetase long-chain family member 5	1397375_at	-1.187	UF	UF
ALDH1A1	aldehyde dehydrogenase 1 family, member A1	1387022_at	-1.321	38	19
ALDH3A1	aldehyde dehydrogenase 3 family, member A1	1368130_at	-3.460	99	66
ALDH3A2	aldehyde dehydrogenase 3 family, member A2	1368365_at	-1.333	24	14
ALDH6A1	aldehyde dehydrogenase 6 family, member A1	1387344_at	1.193	UF	UF
APOE	apolipoprotein E	1370862_at	-1.105	18	11
CAT	catalase	1367995_at	1.218	UF	UF
FMO2	flavin containing monooxygenase 2 (non-functional)	1377635_at	-3.021	22	13
FMO3	flavin containing monooxygenase 3	1368304_at	-3.916	20	13
FMO5	flavin containing monooxygenase 5	1383248_at	1.081	11	0
GSTA1	glutathione S-transferase alpha 1	1368180_s_at	-5.871	21	13
Gsta3	glutathione S-transferase alpha 1	1367774_at	-1.254	UF	UF
GSTA3	glutathione S-transferase alpha 3	1371089_at	-1.315	32	17
GSTM3	glutathione S-transferase mu 3 (brain)	1370813_at	-2.402	UF	UF
GSTM5	glutathione S-transferase mu 5	1386985_at	-1.198	25	15
GSTP1	glutathione S-transferase pi 1	1388122_at	-1.124	30	16
HS2ST1	heparan sulfate 2-O-sulfotransferase 1	1382101_at	-1.182	UF	UF

Symbol	Entrez Gene Name	Affymetrix	Fold Change	BMD (mg/kg-day)	BMDL (mg/kg-day)
IL1RAP	interleukin 1 receptor accessory protein	1393563_at	1.173	199	109
IL33	interleukin 33	1389581_at	-3.303	13	9
IL36RN	interleukin 36 receptor antagonist	1381288_at	1.835	UF	UF
IRAK1	interleukin-1 receptor-associated kinase 1	1373379_at	-1.053	UF	UF
MAOA	monoamine oxidase A	1370678_s_at	-1.477	22	13
PAPSS2	3'-phosphoadenosine 5'-phosphosulfate synthase 2	1395721_at	-2.929	UF	UF
PLTP	phospholipid transfer protein	1391435_at	-2.980	UF	UF
SCARB1	scavenger receptor class B, member 1	1367855_at	-1.375	25	14
SLC27A4	solute carrier family 27 (fatty acid transporter), member 4	1377123_at	-1.037	UF	UF
SLCO1A2	solute carrier organic anion transporter family, member 1A2	1368606_at	1.491	195	97
SOD3	superoxide dismutase 3, extracellular	1368322_at	-2.607	UF	UF
TNFRSF11B	tumor necrosis factor receptor superfamily, member 11b	1369407_at	-4.210	UF	UF
TNFRSF1A	tumor necrosis factor receptor superfamily, member 1A	1367715_at	-1.256	UF	UF
			Mean	50	27
			Median	25	14
			SD	60.9	32.7
			Count	16	
			UF	18	

[1]UF = unacceptable fit (global goodness of fit p<0.1, BMD > high dose, and/or Hill k flag)

Table C.20. Atherosclerosis signaling pathway transcriptional benchmark dose summary in male rat bladder at 7 days

Symbol	Entrez Gene Name	Affymetrix	Fold Change	BMD (mg/kg-day)	BMDL (mg/kg-day)
ALOX12	arachidonate 12-lipoxygenase	1380636_at	1.216	21	13
APOD	apolipoprotein D	1398258_at	-3.612	UF[1]	UF
APOE	apolipoprotein E	1370862_at	-1.105	18	11
CD36	CD36 molecule (thrombospondin receptor)	1386901_at	-3.601	28	16
COL1A1	collagen, type I, alpha 1	1370864_at	-2.308	UF	UF
COL1A2	collagen, type I, alpha 2	1387854_at	-2.041	UF	UF
COL3A1	collagen, type III, alpha 1	1370959_at	-2.162	25	16
COL5A3	collagen, type V, alpha 3	1368347_at	-3.711	UF	UF
CXCR4	chemokine (C-X-C motif) receptor 4	1370097_a_at	-1.097	UF	UF
F3	coagulation factor III (thromboplastin, tissue factor)	1369182_at	-1.786	24	14
IL33	interleukin 33	1389581_at	-3.303	13	8.9
IL36RN	interleukin 36 receptor antagonist	1381288_at	1.835	UF	UF
LPL	lipoprotein lipase	1386965_at	-2.420	21	13
MMP13	matrix metallopeptidase 13 (collagenase 3)	1388204_at	2.526	48	35
MMP3	matrix metallopeptidase 3 (stromelysin 1, progelatinase)	1368657_at	2.736	75	53
PCYOX1	prenylcysteine oxidase 1	1370407_at	1.294	UF	UF
PLA2G16	phospholipase A2, group XVI	1370202_at	-1.157	UF	UF
PLA2G4A	phospholipase A2, group IVA (cytosolic, calcium-dependent)	1387566_at	1.042	UF	UF
PNPLA8	patatin-like phospholipase domain containing 8	1372733_at	1.091	UF	UF
RBP4	retinol binding protein 4, plasma	1371762_at	-2.433	20	12
VCAM1	vascular cell adhesion molecule 1	1368474_at	-3.746	33	18
			Mean	30	19
			Median	24	14
			SD	17.7	13.2
			Count	11	
			UF	10	

[1]UF = unacceptable fit (global goodness of fit p<0.1, BMD > high dose, and/or Hill k flag)

Table C.21. Glutathione-mediated detoxification pathway transcriptional benchmark dose summary in male rat bladder at 7 days

Symbol	Entrez Gene Name	Affymetrix	Fold Change	BMD (mg/kg-day)	BMDL (mg/kg-day)
ANPEP	alanyl (membrane) aminopeptidase	1386938_at	-2.085	UF[1]	UF
GSTA1	glutathione S-transferase alpha 1	1368180_s_at	-5.871	21	13
GSTA3	glutathione S-transferase alpha 3	1371089_at	-1.315	UF	UF
Gsta3	glutathione S-transferase alpha 1	1367774_at	-1.254	32	17
Gsta4	glutathione S-transferase, alpha 4	1372297_at	-1.321	31	17
GSTM3	glutathione S-transferase mu 3 (brain)	1370813_at	-2.402	UF	UF
GSTM5	glutathione S-transferase mu 5	1386985_at	-1.198	25	15
GSTP1	glutathione S-transferase pi 1	1388122_at	-1.124	30	16
			Mean	28	16
			Median	30	16
			SD	4.7	1.7
			Count	5	
			UF	3	

[1]UF = unacceptable fit (global goodness of fit p<0.1, BMD > high dose, and/or Hill k flag)